

Immobilization mechanisms of
lead(II) and zinc(II) ions in fly ash
based geopolymers depending on the
Na/Al and Si/Al ratio

Dissertation

zur Erlangung des
Doktorgrades der Naturwissenschaften (Dr. rer. nat.)

der

Naturwissenschaftlichen Fakultät III
Agrar -und Ernährungswissenschaften,
Geowissenschaften und Informatik

der Martin-Luther-Universität Halle-Wittenberg

vorgelegt von

Eva Kränzlein

geb. am: 16.07.1989 in Nürnberg

Gutachterin bzw. Gutachter:

1. Prof. Dr. Dr. Pöllmann, Prof. Dr. Kremer
2. Prof. Dr. Bier

Verteidigt am: 30.01.2019 Halle (Saale)

*The whole is more than the
sum of its parts*

(Aristotle)

Acknowledgments

Many people and institutions have helped to make this thesis possible.

First of all, I would like to thank my supervisor at the University of Halle–Wittenberg Professor Dr. Dr. Pöllmann for the opportunity to work with his group and his support throughout the years. Moreover, I would like to thank my supervisor at Technische Hochschule Nürnberg Professor Dr. Krcmar who gave me the opportunity to work in his research group and to use the obtained experimental data in my thesis. Additionally my thanks go to every Professor and research assistant at Nuremberg Tech who always helped me to fix my problems using various analytical instruments.

Thank you also to my former colleagues at Energie Campus Nürnberg for their friendship and help, especially Christian Allar, Nelli Wedel and Andreas Geber, and my former students, Anja Tusch, Johannes Neuweg and Jessica Harmel, who worked in this project. And thanks to the whole research group of Geology at the University Halle–Wittenberg who were always happy to help with problems.

Funding for this research project was given by Forschungszentrum Jülich.

I would also like to thank my family and friends without whom it would not have been possible for me to finish this thesis. Especially my sister and my dad who always support me.

Abstract

In this thesis we deal with the analysis of immobilization mechanisms of metal ions in geopolymers. We chose to use black coal fly ash as a starting material and not metakaoline, due to the fact that fly ash is considered to be industrial waste. As fly ash is not homogenous, we firstly analyze our used fly ash (considered a class F ash) using X-ray diffraction (XRD), Fourier transformation infrared spectroscopy (FTIR) and leaching experiments which eluates were analyzed by inductive coupled plasma optical emission spectroscopy (ICP-OES). After a thorough understanding of the starting material is gained, this thesis is separated in three different parts dealing with different geopolymer systems which each had a slightly different focus. However, the examined geopolymer samples in the first part, lay the foundation for the second and third part.

As a first step, we investigated geopolymers with a varying Na/Al ratio. In these samples, the Na/Al varied between 0.4 and 0.8 calculated with the reactive, amorphous amounts of aluminum. In this part of the research no heavy metals were added to the samples because only the finding of the ideal Na/Al ratio, and therefore the most stable geopolymer sample, was the aim of this experimental setup. The found Na/Al ratio of 0.6 was kept during the next set of experiments. In this work we focus on the use of metal powders as foaming agents and their impact on the structure of geopolymers. The impact of the porosity onto the structure will be examined using different spectroscopic measurement techniques.

In the second part of this thesis samples with the ideal Na/Al ratio of 0.6 were used as reference sample. PbO, ZnO, Pb(NO₃)₂ and Zn(NO₃)₂ were added in varying percentages to our reference geopolymer slurry. We used a wide spectrum from 0,0 to 5,0 wt% addition of metal powders to our samples. Most research is focused on the addition of lesser amounts but our goal was to see how geopolymers react when larger amounts were added to the mix. In a second step, we analyzed the immobilization behavior depending on the porosity of the samples. In this step, we added foaming agents to the geopolymer slurry. As in our previous research, we focused on aluminum powder as foaming agent. Two different percentages (0,1 wt% and 0,2 wt%) were added to the slurry. All samples were leached in water, sulfuric acid (10 %) and hydrochloric acid (3 M) and the weight loss was calculated. The aim of this part of the research was to investigate first of all the influence of the added metal ions and secondly the influence of the porosity onto the immobilization behavior.

The third part of this thesis deals with the influence of the Si/Al ratio onto the immobilization abilities of geopolymers. We used samples with a Na/Al ratio of 0.6 and added zinc and lead nitrates in a percentage of 5 wt%. The Si/Al ratio was varied

between 2.0 and 3.0, which corresponds approximately to the total possible range for geopolymer production. All samples were leached in sulfuric acid (10%) and hydrochloric acid (3 M) and characterized using the mentioned analytical techniques.

In this thesis, we gain a thorough understanding of the behavior of our geopolymer system and analyze conclusively the different factors influencing geopolymer synthesis. Moreover, we investigate the immobilization mechanisms of Pb^{2+} and Zn^{2+} which can both be bound in the amorphous matrix of the geopolymers. Therefore, the bonds are quite stable against acidic attack. Moreover, we show the connection of the Si/Al ratio onto the acidic resistance of geopolymers. In conclusion, we provide with this thesis a foundation for further research using geopolymers as cementitious systems in industry.

Zusammenfassung

In dieser Dissertation werden die Immobilisierungsmechanismen von Metallionen in Geopolymeren analysiert. Als Rohstoff wird Steinkohle Flugasche eingesetzt, die im Gegensatz zu Metakaolin, als ein Nebenprodukt bei der Steinkohle Verbrennung anfällt. Da Flugasche nicht homogen ist und keine wohldefinierten Eigenschaften besitzt, wird die verwendete Flugasche zunächst charakterisiert. Die eingesetzten Analysemethoden sind: Röntgendiffraktometrie (XRD), Fourier Transformations Infrarotpektroskopie (FTIR) und Laugungsexperimente, deren Eluate mittels Optischer Emissionsspektroskopie (ICP-OES) analysiert werden. Nachdem eine gründliche Charakterisierung erfolgte, ist diese Arbeit in drei Teile gegliedert, die sich je mit einem unterschiedlichen Geopolymer-System befassen. Jeder dieser drei Teile legt den Fokus auf unterschiedliche Eigenschaften im Geopolymer. Allerdings bauen der zweite und der dritte Teil entscheidend auf dem ersten System auf.

Im ersten Teil werden Geopolymere hergestellt, die ein variierendes Na/Al Verhältnis aufweisen. Dieses Verhältnis wird zwischen 0,4 und 0,8 variiert, wobei die Berechnung der Verhältnisse sich nur auf den reaktiven, amorphen Anteil von Aluminium im Gesamtsystem bezieht. In diesem Teil werden noch keine Schwermetallsalze zugegeben, da das beste Na/Al Verhältnis von 0,6 in den folgenden Experimenten stets beibehalten wurde. Es wird sich auf den Einfluss von Metallpulvern (Zink und Aluminium) auf die Struktur in den Geopolymeren fokussiert. Dieser Einfluss der Porosität wird zusätzlich zu den bereits erwähnten Analysemiteln auch mittels Quecksilberporosimetrie und Rasterelektronenmikroskopie (SEM) analysiert.

Zweitens werden Proben mit dem vorher optimierten Na/Al Verhältnis von 0,6 hergestellt und als Referenzproben verwendet. Außerdem werden Proben mit Zusatz von Blei -und Zinksalzen (PbO , ZnO , $\text{Pb}(\text{NO}_3)_2$ and $\text{Zn}(\text{NO}_3)_2$) in Mengen von 1–5m%, bezogen auf Flugasche, hergestellt. Ein Großteil der vorhandenen Literatur beschäftigt sich mit deutlich geringeren Mengen an Metallsalz Zusätzen, jedoch wird hier bewusst eine höhere Menge gewählt, da der Einfluss oft erst bei größeren Mengen nachweisbar wird. In einem zweiten Schritt wurden wiederum Metallpulver (Aluminiumpulver) eingesetzt um eine höhere Porosität in den Proben zu erzeugen. Aluminiumpulver wurde in 0,1m% und 0,2m% zugesetzt. Mit allen Proben wurden Elutionsversuche in Wasser, Schwefelsäure (10 %ig) und Salzsäure (3 M) durchgeführt. Mit diesem experimentellen Setup wird der Einfluss von wasserunlöslichen und wasserlöslichen Metallsalzen auf die Struktur der Geopolymere und deren Fähigkeit der Immobilisierung analysiert. Des Weiteren wird untersucht inwiefern sich eine höhere Porosität auf die Immobilisierungseigenschaften auswirkt.

Im dritten Teil schließlich, wird der Einfluss des Si/Al Verhältnisses auf die Immobilisierungsfähigkeit der Geopolymere untersucht. Wiederum basieren die Proben

auf einem Na/Al Verhältnis von 0,6, variieren aber zwischen 2,0 und 3,0 im Si/Al Verhältnis. Zusätzlich werden Zink -und Bleinitratsalze in einer Menge von 5 m% bezogen auf Flugasche zugegeben. Alle Proben werden eluiert und mit den bereits erwähnten Analysemethoden (REM, FTIR, XRD, ICP-OES) untersucht.

In dieser Arbeit wird ein logischer, gründlicher Ansatz einer kompletten Charakterisierung eines Geopolymer Systems verfolgt. Es werden schlüssig Faktoren untersucht, die die Geopolymer Herstellung und insbesondere deren Struktur beeinflussen. Außerdem werden die Immobilisierungsmechanismen von Pb^{2+} und Zn^{2+} analysiert und es wird festgestellt, dass beide in den amorphen Teil der Matrix eingebunden werden können. Aus diesem Grund sind die entstehenden Bindungen relativ stabil gegen Säureattacken und weisen einen chemischen Charakter auf. Des Weiteren wird auch der starke Einfluss des Si/Al Verhältnisses auf die Säureresistenz von Geopolymeren aufgezeigt. Zusammenfassend lässt sich sagen, dass mit dieser Arbeit ein Grundstein für die weitere Erforschung von Geopolymeren insbesondere zur Anwendung in der Industrie gelegt wird.

Acronyms and Abbreviations

Al	Aluminum
cm	Centimeter
°C	Degree Celsius
edx	Energy dispersive X-ray
IR	Infrared Spectroscopy
ICP-OES	Inductive Coupled Plasma Optical Emission Spectroscopy
LOI	Loss On Ignition
μm	Micrometer
MIP	Mercury Intrusion Porosimetry
Na	Sodium
OPC	Ordinary Portland Cement
Pb	Lead
SEM	Scanning Electron Microscopy
Si	Silicon
TCLP	Toxic Characteristic Leaching Procedure
XRD	X-ray Diffraction Spectroscopy
XRF	X-ray Fluorescence Spectroscopy
Zn	Zinc

Contents

Acknowledgments	iv
Abstract	v
Zusammenfassung	vii
Acronyms and Abbreviations	viii
1 Objective	1
2 Theoretical Background	2
2.1 Structure and reaction mechanism	3
2.2 Heavy metals in geopolymers	5
2.2.1 Leaching experiments	7
2.3 Resistance of geopolymers against acidic attack	8
2.3.1 Quantitative determination of reaction products in geopolymers using acidic resistance	11
2.4 Structural analysis of geopolymers using FTIR spectroscopy	13
2.5 Foaming agents in geopolymer synthesis	18
3 Experimental Procedure	20
3.1 Analysis	20
3.1.1 Fourier Transformation Infrared Spectroscopy (IR Spectroscopy)	20
3.1.2 X-ray Diffraction Spectroscopy (XRD)	20
3.1.3 Inductive Coupled Plasma Optical Emission Spectroscopy (ICP-OES)	21
3.1.4 Scanning electron microscopy (SEM)	21
3.1.5 Mercury intrusion porosimetry (MIP)	21
3.1.6 Compressive strength testing	22
3.1.7 Leaching tests and mass loss	22
3.2 Synthesis of geopolymers	22
3.2.1 Geopolymer synthesis	22
3.2.2 Activating Solution	23
3.2.3 Used chemicals	24
4 Characterization of the used fly ash Microsit 10	25
4.1 Chemical Composition	25
4.2 Structural Characterization	26
4.2.1 X-ray diffraction	26
4.2.2 FTIR spectroscopy	27
4.3 Leaching behavior	28
5 Variation of the Na/Al ratio with addition of metal powders	31
5.1 Experimental Procedure	31
5.1.1 Geopolymer Synthesis	31

5.2	Results and Discussion	32
5.2.1	Material properties	32
5.2.2	Microscopy	34
5.2.3	IR spectroscopy	36
5.2.4	X-ray diffraction spectroscopy	39
5.2.5	Porosity	40
5.3	Conclusion	42
6	Addition of PbO, Pb(NO₃)₂, ZnO and Zn(NO₃)₂	43
6.1	Experimental Procedure	43
6.1.1	Geopolymer Synthesis	43
6.2	Results	45
6.2.1	Scanning electron microscopy	45
6.2.2	IR spectroscopy	50
6.2.3	X-ray diffraction spectroscopy	55
6.2.4	Porosity	59
6.2.5	Leaching tests: Loss of weight	61
6.2.6	Leaching test: ICP-OES analysis	63
6.3	Discussion	67
6.3.1	Structural analysis	67
6.3.2	Leaching behavior	68
6.4	Conclusion	71
7	Variation of the Si/Al ratio and addition of Pb²⁺ and Zn²⁺	73
7.1	Materials and Methods	73
7.2	Results and Discussion	74
7.2.1	Structural analysis	74
7.2.2	Leaching tests	80
7.3	Conclusion	85
8	Summary and Conclusion	87
9	Appendix	98
9.1	Chapter 5: Metal powders as foaming agents and their impact on the structure depending on the Na/Al ratio	98
9.1.1	IR spectroscopy	98
9.1.2	XRD	99
9.1.3	MIP	99
9.2	Chapter 6: Addition of PbO, Pb(NO ₃) ₂ , ZnO and Zn(NO ₃) ₂	99
9.2.1	IR spectroscopy	99
9.2.2	XRD	102
9.2.3	MIP	104
9.2.4	Compressive strength	106
9.3	Chapter 7: Variation of the Si/Al ratio and addition of Pb ²⁺ and Zn ²⁺	106
9.3.1	IR spectroscopy	106
9.3.2	XRD	107
	Declaration	110
	Curriculum Vitae	111

1 Objective

In the European Union a CO₂ emission reduction of 80 % below the values of 1990 until 2050 is a goal set by a European Committee for Carbon footprint reduction.¹ As cement production is one of the main industries in the building sector responsible for a high CO₂ emission, research is focused on reduction of emissions during the production and the development of alternative materials. Already, a reduction of the needed energy could be achieved. Per kilogram cement, nowadays only 2900 kJ are needed, in contrast to beforehand double of that amount.² Furthermore, research is conducted investigating new, cement-like materials which can be used as alternatives in the building sector.

One of these cement-like materials are geopolymers. Geopolymers are alkali activated pozzolan cements in which synthesis, fly ash, metakaoline, slag etc. can be used as starting materials.³ Especially fly ash and slag are interesting starting materials as they itself are produced as a waste material during industrial processes. Therefore, we focus on the usage of fly ash as starting material in our geopolymers, which are investigated in this thesis.

The aim of this thesis is to gain a thorough understanding of geopolymers regarding the influences of the Na/Al and the Si/Al ratio. Moreover, we investigated the ability of geopolymers to immobilize zinc and lead ions and their resistance against acidic attacks. We also use foaming agents to maximize the porosity of the geopolymers and therefore enhance the surface which can be attacked by acids. The changes made by the introduction of heavy metal ions (water soluble and not water soluble) are analyzed and conclusions as to how these metals are bound in the geopolymers can be drawn. For these reasons, the main part of this work is separated in four different parts.

2 Theoretical Background

The search for alternatives to OPC (ordinary portland cement) started as soon as the 1930th with Kuhl experimenting using KOH and slag. In 1940, Glukhovsky started investigating alkali activated binding systems and introduced two different classes: $\text{Me}_2\text{-Al}_2\text{O}_3\text{-SiO}_2\text{-H}_2\text{O}$ and $\text{Me}_2\text{-MO-Al}_2\text{O}_3\text{-SiO}_2\text{-H}_2\text{O}$ (with $\text{Me} = \text{Na}, \text{K}, \dots$; $\text{M} = \text{Ca}, \text{Mg}, \dots$).⁴ Our research, as many other, is focused on the first class which includes five categories of alkali activated cements:

1. alkali activated slag-based cements
2. alkali activated pozzolan cements
3. alkali activated lime-pozzolan/slag cements
4. alkali activated calcium aluminate blended cements
5. alkali activated Portland blended cements (hybrid cements)

As our research focuses on the secondly mentioned alkali activated pozzolan cements, we only describe the chemistry involved in these materials. These category of binders is called by different terms: "soil cements" (Glukhovsky⁵), "geocements" (Krivenko⁶), "inorganic polymers" (van Deventer⁷), "zeocements" (Palomo⁸) and geopolymers (Davidovits⁹).

Geopolymers, or alkali activated cementitious systems can be synthesized using a variety of aluminum and silicate sources, eg. metakaolinite, kaolinite, slag and fly ash (brown coal fly ash and black coal fly ash).³ The alumino silicates, either natural occurring, like kaolinite or industrial wastes like fly ash and slag, are activated by an alkaline solution, sometimes called geopolymer liquor¹⁰, consisting of an alkali hydroxide solution and a sodium (or potassium) silicate solution.

In this thesis the term "geopolymer" is used. This category includes the following systems which are differentiated by their used raw materials:⁴

1. alkali activated fly ash cements
2. alkali activated natural pozzolan cement
3. alkali activated metakaoline cement

4. alkali activated soda lime glass cement

Of these cementitious systems, metakaoline and fly ash systems were investigated extensively over the last couple of years. In this thesis fly ash is used exclusively as a raw material.

2.1 Structure and reaction mechanism

Geopolymers are inorganic, X-ray amorphous polymers composed of linked tetrahedrons with silicon or aluminum ions as centers. The 4 \times -coordinated Al³⁺-ions show a negative charge in the tetrahedrons which is balanced by the introduced Na⁺-ions.^{7,9,11} A schematic description is given in figure 2.1.

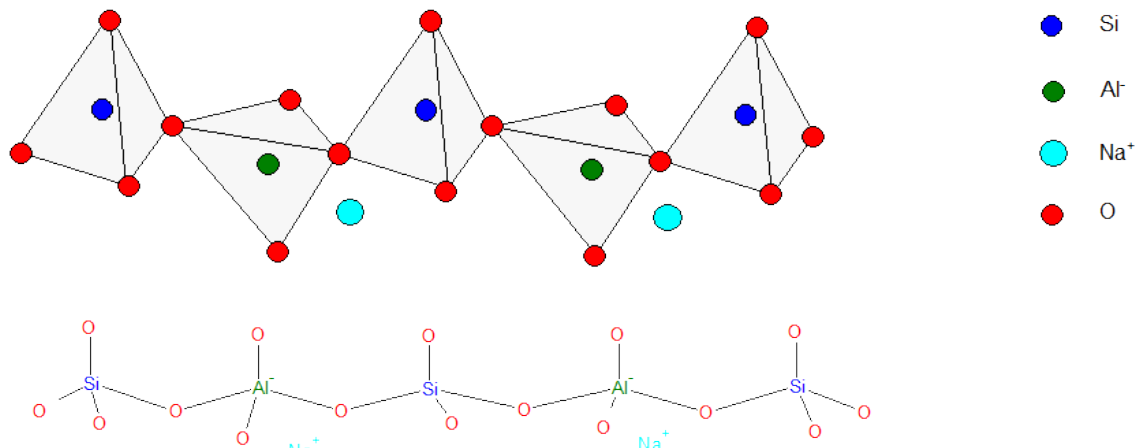


Figure 2.1: Schematic illustration of a geopolymer structure

Davidovits described three different polysialates which can be formed during the reaction: PS (polysialate), PSS (Poly(sialate-siloxo)) and PSDS (Poly(sialate-disiloxo)).⁹ The chemical formula of the monomeres are:

- PS: -Si-O-Al-O-
- PSS: -Si-O-Al-O-Si-O-
- PSDS: -Si-O-Al-O-Si-O-Si-O-

Which monomer is formed, is dependent on the Si/Al ratio in the precursors. Davidovits reported that the overall Si/Al ratio should vary between 1,6 – 2,3 to form stable geopolymers.^{8,12,13}

Six steps in the geopolymer reaction mechanisms were, based on a zeolitic reaction model, suggested by A. Fernández-Jiménez, A. Palomo, M.M. Alonso¹⁴.⁴ These steps are shown in the following figure 2.2.

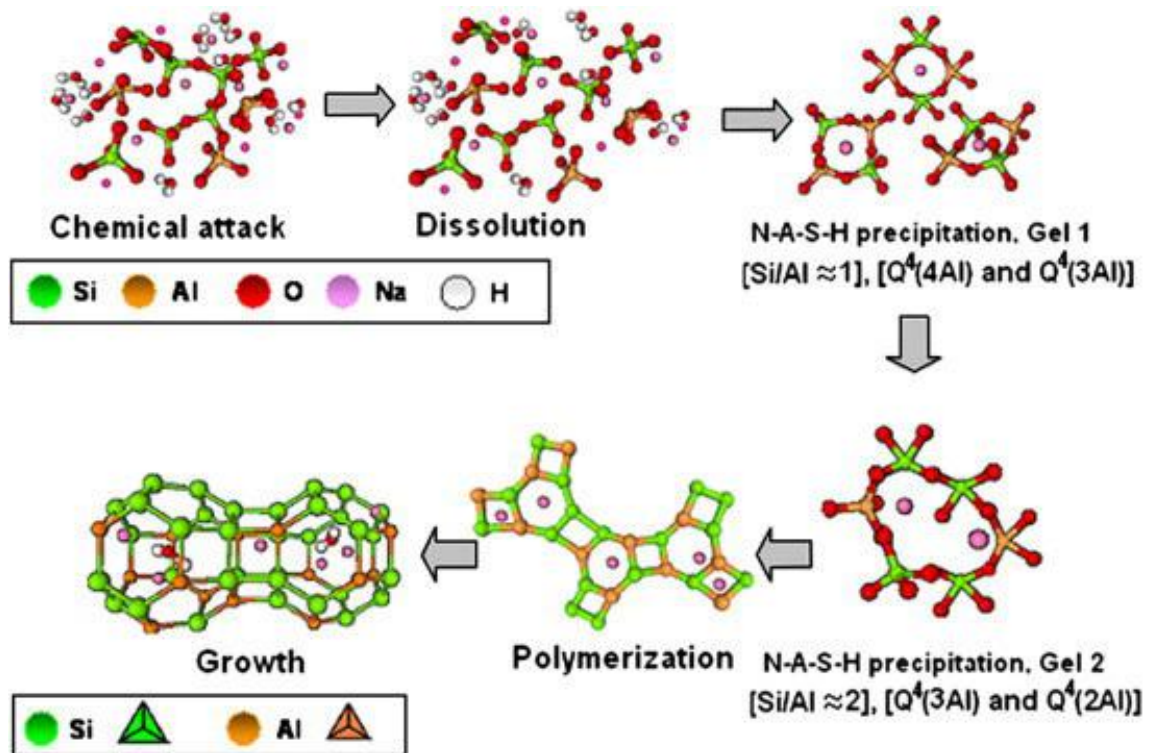


Figure 2.2: The six steps to form a geopolymer network

In the first step, the chemical attack of the highly alkaline activator onto the solid component, eg. fly ash, the bonds between Si-O-Si, Al-O-Al, Al-O-Si and Me-O are severed. This leads directly to the second step, the dissolution. During these steps, a change in the electronic densities around the silicon atoms occurs and therefore the Si-O-Si bonds are attacked. The alkaline metal cations neutralize these anions, building Si-O⁻Na⁺, thereby preventing the reverse reaction. The attacked and severed Al-O-Si bonds form aluminates which are stabilized by the hydroxy groups and form complexes like: Al(OH)₄⁻ or Al(OH)₆³⁻. Which complexes are formed, is dependent on the pH of the solution.^{4,15}

These monomers agglomerate to form an aluminum rich gel 1 which consists of alternating silicon and aluminum tetrahedral units. This structure was confirmed by NMR and FTIR data and is a metastable form during the reaction. One suggested reason why an aluminum rich gel is formed is that the Al-O bonds, which are weaker than the Si-O bonds, are severed firstly and to a higher amount. This leads to a higher concentration of Al³⁺ in the medium at the beginning of the reaction.^{4,16,17}

This metastable gel 1 transforms into a gel 2 which has a Si/Al ratio of about two. This change in ratio comes from the fact that during the reaction, more Si-O groups dissolve. The change into a Si rich gel was proven by NMR study which provided the evidence of the formation of a Q⁴(3Al) and Q⁴(2Al) signal.¹⁸ The exact mechanisms of the formation of the N-A-S-H gels 1 and 2 were studied firstly by Iler¹⁹ and were later on thoroughly investigated by Ikeda et al.¹⁰. Hereby they

synthesized gels similar to these observed in alkali activated metakaoline and fly ash at different pH levels. At a $\text{pH} \geq 7$ they found that polymerization is the main mechanism and which reaction rate increases with an increasing pH. Due to Ostwald ripening, colloids are generated which form cross-links and thereby generate 3D structures.^{4,19,20}

Polymerization is the fifth step during the alkali activation of aluminosilicates at a pH of about 12.5 which also leads to growth of the colloid particles and therefore to a three dimensional network.^{4,21}

A description of the chemical reactions during the polycondensation step was already proposed by Joseph Davidovits¹¹ and is depicted in figure 2.3.

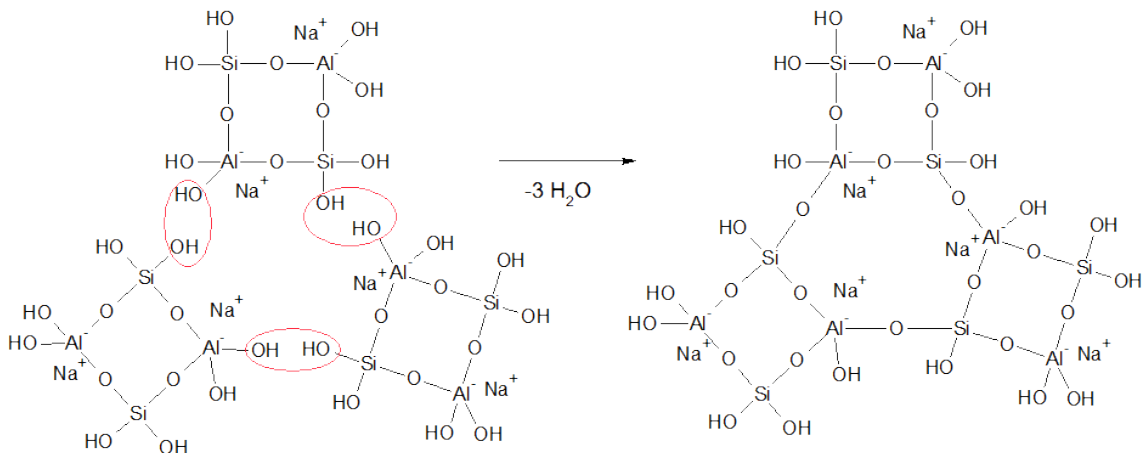


Figure 2.3: Polycondensation reaction involved in geopolymer reaction mechanism

2.2 Heavy metals in geopolymers

Due to the binding mechanisms during the formation of this amorphous network and the similarity to zeolitic materials, it was expected that geopolymers have a great potential in immobilizing heavy metals.^{13,22,23} Many authors have investigated the possibility to use fly ash and metakaoline based geopolymers to immobilize heavy metals, however the mechanism for each element is different and depending on many variables.^{13,24} Breck²⁵ suggested a replacement of Na^+ or K^+ by heavy metal ions in aluminosilicate materials which was later on included in other research articles.

A. Palomo²⁶ investigated the stabilization of boron, chromium and lead in fly ash based alkali activated cementitious materials.^{26,27} Boron, as a non metal element was investigated due to its appearance in nature and therefore in the used materials. It was shown that boron may form sodium borates like $\text{NaB}(\text{OH})_4$ to partially fill pores, holes etc. in the geopolymer matrix. Of a higher interest is the second study which focuses on the immobilization of chromium and lead. It is believed that the solidification of lead is a combination of physical encapsulation and chemical

bonding.¹³ In their research lead was used as a water soluble nitrate salt ($\text{Pb}(\text{NO}_3)_2$, 3.125 %) and Cr^{6+} was added as CrO_3 at 2,60 %. It was observed that the in water dissolved salt did not, in contrast to OPC samples, change the setting behavior of the geopolymer samples. The samples were studied using leaching tests in water, FTIR and XRD analysis. XRD results showed a newly formed phase, namely Pb_3SiO_5 and a formation of a herschelite type zeolite was also observed. Leaching tests resulted in a leaching rate of 12.5 – 13.0 which concludes a matrix with a high efficiency of confining lead ions. The found lead silicate is supposed to show the same low solubility as other lead silicates (Pb_5SiO_7 , PbSiO_3).

Zhang et al.²⁸ investigated the immobilization of Cr^{6+} , Pb^{2+} and Cd^{2+} . In case of the lead contamination (0.5 %) a slight increase in compressive strength was noticed. In the XRD diffractograms of their study, a small peak at $33^\circ 2\theta$ which may correspond to a lead silicate phase was determined to be not conclusive. Nevertheless, they concluded that lead ions participate to some extent in the geopolymer reaction and are therefore chemically bound into the network. Their analysis using energy dispersive X-ray microanalysis showed that lead was well dispersed in the binder but appears to be concentrated in areas of a diameter of less than one micron. Some spots in the micrographs however show higher amounts of lead (about 30 %) which is about the same concentration which would be expected in a Pb_3SiO_5 phase. The leaching experiments, which were also conducted by Zhang et al.²⁸, are discussed later on.

Zheng et al.²² investigated the immobilization of Cu^{2+} , Zn^{2+} , Pb^{2+} and Cd^{2+} in geopolymers. In his research he used up to 0.8 % of metal nitrate adding it to metakaoline based geopolymers. Moreover, Na_2SiO_3 was added in varying amounts to increase the Si/Al ratio in the geopolymers. This increased Si/Al ratio increased the strength of the Si-O-Si bonds which resulted in higher Cu^{2+} immobilization efficiency. However, no crystalline phase containing any metal phase was found in the XRD diffractograms, which, according to the authors, proves that metal ions are immobilized in the amorphous phase of the geopolymer.

Other researchers investigated the ability of mechanically activated fly ash for immobilizing lead ions.²³ No indication of lead silicate phases in XRD spectra were found, suggesting no chemical bonds were formed. However, only 1 % of lead nitrate was added to the fly ash and according to previous research, at least 3 % are needed to see signals in the XRD diffractogram.²⁷ Mechanical activation of fly ash, however, proved to be a successful way in improving the immobilization of lead. This may be due to the increase in surface area through activation and therefore a higher reactivity of fly ash. Moreover, the porosity in the geopolymer was decreased.²³

Much more research has been conducted regarding the immobilization of metal

ions, especially using lead as heavy metal. Perera et al.²⁹ found a connection of increased porosity and lead nitrate addition in geopolymers. He also focused his work on the use of static leaching experiments, using TCLP method. Martina Minaříková³⁰ investigated the use of brown coal fly ash as a starting material and its ability to immobilize Cu^{2+} , Zn^{2+} , Pb^{2+} , Cd^{2+} and Cr^{3+} . In accordance to previous research, they did not find any new crystalline phases but that the heavy metals are distributed evenly throughout the matrix. The best results were achieved for zinc inclusion. Furthermore, the effect of the Al source (kaolinite, metakaolinite, K-feldspar and fly ash) was analyzed by Phair et al.³¹. Lead and copper nitrate were added in a weight percentage of 0.5%. Fly ash showed to be the most effective Al source in immobilizing lead, followed by kaolinite, K-feldspar and metakaolinite.³¹

2.2.1 Leaching experiments

Static and dynamic leaching experiments are both used in the investigation of immobilization mechanisms of heavy metals in geopolymer synthesis. Guo et al.³² studied two different forms of leaching. As a static leaching the TCLP method (toxicity characteristic leaching procedure) was applied, as dynamic leaching was conducted according to the tank leaching method (ANSI/ANS-16.1-2003). In the TCLP method, acetic acid solution of 0.1 mol/l is used as a leachate. The crushed specimens are submersed with a liquid:solid ratio of 20:1 and shaken for 18 h. The leachate was then analyzed using ICP-AES. In dynamic leaching, deionized water was used a $20 \times$ volume to the specimen volume. The leachate was replaced after a certain amount of time (2, 8, 24, 48, 72, 102, 168 and 384 hours). Again, the leachate was analyzed using ICP-AES. Their study revealed that lead was probably fixed in the geopolymer by replacing the cations calcium and sodium. Moreover, both leaching experimental setups revealed a high ability of geopolymers to immobilize heavy metals, dynamic leaching experiments giving long term stability.³²

As mentioned before, Zhang et al.²⁸ used leaching experiments to determine the immobilization effectiveness in geopolymers. They used sulfuric acid (pH = 1.0), MgSO_4 solution (5%) and Na_2CO_3 solution (5%) to approximate conditions geopolymers might be exposed to. He concludes geopolymers are highly capable of immobilizing lead with the highest concentration measured being less than 0.5% after 90 days of leaching in sulfuric acid. The leaching rate in the other media being significantly lower than in sulfuric acid. Moreover, he added 1% pure lead powder which resulted in a lower leaching concentration than the concentration measured using a lead nitrate salt.

2.3 Resistance of geopolymers against acidic attack

Bakharev²⁴ did a thorough investigation of the resistance of geopolymers to acidic attack. He used fly ash based geopolymers and leached the dried samples in 5 % solutions of acetic and sulfuric acid for 150 days. He found a weight gain of 3.8 % in samples activated by sodium silicate solution leached in acetic solution and a weight loss of 2.5 % when leached in sulfuric acid. The compressive strength of the samples decreased overtime, probably due to the breakdown of geopolymer components and the migration of alkali cations into the acidic environment. The residues after leaching were analyzed using XRD technique and showed only small changes in case of the samples leached in acetic acid. Using sulfuric acid as leaching medium however, new phases of chabazite and gismondine zeolites were found in the diffractograms. SEM micrographs revealed a porous structure after leaching in acetic acid. IR spectroscopy recorded a shift in wavelength due to leaching. The stretching vibrations of Si-O-T (with T = Si, Al) all shifted to higher wavenumbers due to an increase of Si/Al ratio. Moreover, the concentration of ring silicates significantly increased after exposure to sulfuric acid. To sum it up, Bakharev²⁴ found a dealumination process taking place when fly ash based, sodium silicate activated geopolymers are exposed to acidic attack. This goes hand in hand with a liberation of silicic acid, the replacement of sodium cations by hydrogen or hydronium and therefore a geopolymerisation of the aluminosilicate structure.

Further research regarding the stability of geopolymers against sulfuric acid was conducted by X. J. Song, M. Marosszky, M. Brungs, R. Munn³³ who used 10 % sulfuric acid. They exposed samples of alkaline activated fly ash to acidic treatment up to 56 days. A 10 % sulfuric acid was chosen due to the fact that it was used in LA county to test the resistance of products against acidic attack.³⁴ Mass change was determined and resulted in a mass loss of almost 3 % after leaching time and the compressive strength decrease from almost 55 MPa to 30 MPa.

Ali Allahverdi³⁵ investigated the behavior of geopolymers which were exposed to nitric acid. He therefore, exposed alkali activated fly ash/ slag for 90 days to nitric acid, pH = 1 and pH = 2. In their study, the residue was examined using ²⁹Si MAS NMR and ²⁷Al MAS NMR as well as FTIR spectroscopy. The NMR study revealed a dealumination process changing Si(4Al), Si(3Al), Si(2Al) and Si(1Al) structural units to Si(0Al) with the vacancies filled by Si atoms. IR spectroscopy underlines these results through shifts in wavenumbers. Furthermore, internal and external linkage of the TO₄ tetrahedra (T = Si, Al) remains intact, which leads to the conclusion that the network is not completely destroyed by the acidic attack.

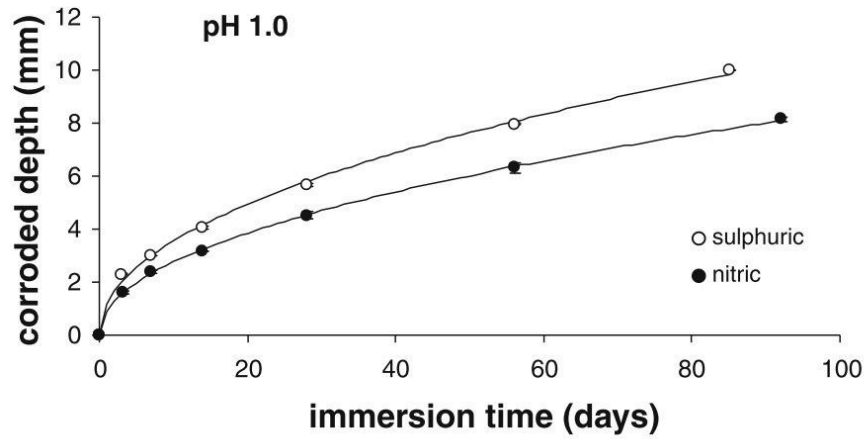
The form of the IR bands in the spectra remain mostly broad, which suggests a highly amorphous structure. Two steps were proposed in destroying the framework:

1. Leaching process in which Na^+ or Ca^{2+} are substituted by H^+ or H_3O^+ and an electrophilic attack, resulting in dealumination
2. Vacancies are re-occupied by Si atoms resulting in an imperfect highly siliceous network

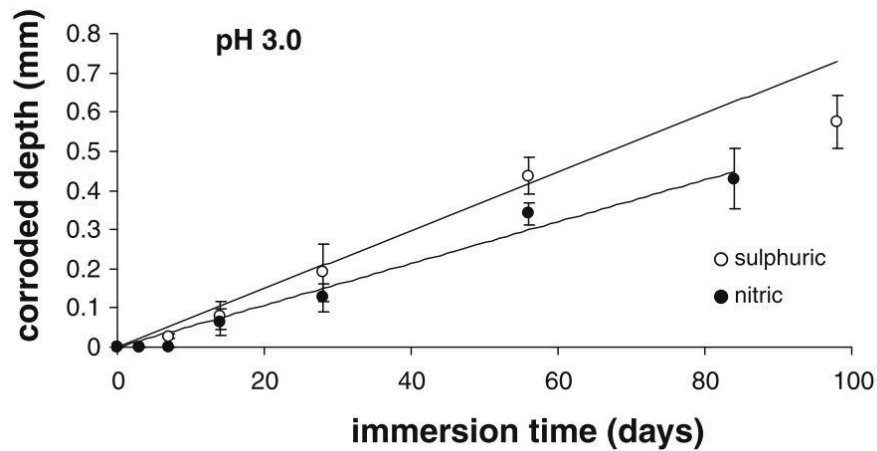
Arioz et al.³⁶ used this method to examine the immobilization of heavy metals in geopolymers which are already present in fly ash. In this study, especially arsenic and mercury showed a high percentage of immobilization whereas lead, zinc and cadmium were found in a even higher percentage than from leached fly ash.

Lloyd et al.³⁷ investigated the stability of alkali activated binders to acidic treatment. Nitric acid and sulfuric acid were used at a pH of 1.0, 2.0 and 3.0 and samples were exposed to the acid up to 100 days with the pH held constant throughout the experiment. The exposure to sulfuric acid mirrors the conditions in sewer systems or acid rain. Not only is the mass loss analyzed in this study but also a corrosion depth is measured. In this experimental setup only one surface of the sample is exposed to the acidic media and then the corroded area is smoothed down, leaving only intact binder. This depth was recorded and analyzed as the authors claim that mass loss analysis is not exact in comparing different samples as different degrading mechanisms occur. It was found that in the beginning a linear correlation between corrosion depth and the immersion time exists which then turns into a saturation curve. This leads to the conclusion that during the first days, corrosion is governed by a chemical reaction which then turns into a diffusion mechanism. The chemical reaction is due to the attack of H_3O^+ ions which dissolve the Si-O-Si bonds. This also explains why samples in sulfuric acid showed higher corrosion rates than samples in nitric acid. Interestingly, the solutions with a pH = 3.0 only show corrosion caused by a chemical reaction mechanism. The curves of the samples of pH = 1.0 and pH = 3.0 are shown in figure 2.4.

The change of the mechanisms taking place is probably due to the formation of a corroded but not completely dissolved product layer which acts as a protective coat. The authors also analyzed several other changes in the network, eg. the existence of soluble silicate during synthesis. It was found that sodium silicate solution provides binder systems which show a higher stability towards acidic attack. The same results were found when the concentration of sodium was enhanced during synthesis. Both variables lead to a higher availability of silica which leads to a tighter amorphous network. However, if no soluble silicate is provided and activation only occurs via addition of sodium, less strength is measured due to a higher crystalline product.



Corrosion rate at pH = 1.0



Corrosion rate at pH = 3.0

Figure 2.4: Corrosion rates of samples exposed to nitric and sulfuric acid³⁷

Recent research, undertaken by Mehta and Siddique³⁸ analyzed the acidic resistance strength of fly ash based geopolymer concrete with and without the addition of OPC to the binder. The samples were exposed to 2% sulfuric acid solution with a constant pH of 1.0 for 365 days. In the first month a weight gain was observed, probably due to the filling of pores by the solution. Further on, a weight loss of 13% was noticed in samples without addition of OPC, almost 35% for samples with the addition of 30% OPC. After 365 days, the compressive strength of the samples without OPC was 48.2% of the original measured strength. The reduction of the compressive strength values was a result of the breakage of alumina-silicate bonds in the geopolymer network. However, the observed microstructure in specimens with no OPC remained mostly unchanged under the SEM investigation. XRD analysis revealed C-A-S-H phases in the geopolymers, which in the original samples appear at $67^{\circ}2\theta$ and at $45^{\circ}2\theta$ in the corroded samples. The study proved a dealumination process taking place due to acidic attack during the exposure of geopolymer cement to sulfuric acid.

A comparison of geopolymers leached in acidic and alkaline environment was undertaken by Temuujin et al.³⁹ who used calcined and as-prepared fly ash based geopolymers in their study. Samples were subjected to 18 % HCl solution and 14 M NaOH solution. These high concentrations were chosen because products which are highly stable against these attacks are very attractive in industrial uses. Samples were immersed in the leaching solutions for 1–5 days and then analyzed. Calcined samples showed a high resistance against alkaline attack, whereas as-prepared geopolymers showed a low resistance as the leaching solution became "muddy" from the start on. Samples immersed in HCl did not show any outwardly change in appearance, however ICP results show a high concentration of leached Al, Fe and Ca ions increasing with time. This leads to the assumption that amorphous phases react preferentially when exposed to HCl treatment. In the calcined samples, the leaching concentration of Al and Na dropped significantly compared to the concentrations found in the as-prepared samples. When as-prepared samples are exposed to alkaline solution, the levels of Si leaching are very high. In spite of the results of the leaching experiments, compressive strength measurements show higher values for the as-prepared geopolymer samples than for the calcined specimens. This leads to the conclusion that calcination influences the structure of geopolymer samples to a higher extent than the acidic and alkaline treatment which produces a slightly higher porosity.

2.3.1 Quantitative determination of reaction products in geopolymers using acidic resistance

The use of acidic treatment of geopolymer samples to quantify the amorphous phase in geopolymers and fly ash as starting material was firstly investigated by Granizo et al.⁴⁰ who used a 1:9 attack of acidic acid. Fernández-Jiménez et al.⁴¹ applied this method to quantify the vitreous phase in fly ash, as this is proposed to be the reactive phase during the geopolymerisation reaction.^{41,42} In this research paper an acidic attack of 1 % HF is used to dissolve only the vitreous phase in fly ash with the crystalline phase remaining intact.

Other methods of selective dissolution are summarized in the following table (table 2.1).⁴³

Further on, we focus on the use of HCl as acid for selective chemical attack, since it is optimized for alkali activated fly ash based cementitious systems. Palomo et al.⁴⁹ used the method introduced by Granizo et al.⁴⁰ and optimized it. In this research paper, Palomo used the selective chemical attack of 1:20 HCl to determine the percentage of reaction product of alkali activated fly ash. A reaction rate varying between 25 % and 52 % depending on curing conditions was found.

Method	Starting material	Chemicals needed / 1 g sample	References
Salicylic acid	Hydrated fly ash $\text{CaSO}_4 \cdot x\text{H}_2\text{O}$ $\text{Ca}(\text{OH})_2$	6 g salicylic acid 40 ml methanol methanol*	Ohsawa et al. ⁴⁴
Hydrochloric acid and salicylic acid	Portland fly ash cements	5 g salicylic acid 4.2 ml HCl fill to 100 ml with methanol ethanol*	Suprenant and Papadopoulos ⁴⁵
Hydrochloric acid	Alkali activated fly ash	250 ml (1:20) HCl distilled water*	Fernández-Jiménez et al. ⁴²
EDTA/DEA	OPC blended with slag	25 ml triethanolamine 9.3 g disodium $\text{EDTA} \cdot 2\text{H}_2\text{O}$ 17.3 ml DEA fill to 100 ml with distilled water 1600 ml distilled water distilled water*	Lumley et al. ⁴⁶
EDTA/NaOH	Hydrated blast furnace slag cements	500 ml disodium $\text{EDTA} \cdot 2\text{H}_2\text{O}$ (0.05 M) in NaOH (0.1 M) 500 ml distilled water 50 ml (1:1) triethanolamine:water 125 ml NaOH (1 M) to adjust pH distilled water and ethanol*	Luke and Glasser ⁴⁷
Picric acid	Hydrated cements or $\text{Ca}(\text{OH})_2$ with fly ash or silica fume	11 g picric acid 60 ml methanol 40 ml distilled water methanol* 500 ml distilled water at 40 °C*	Li et al. ⁴⁸

Table 2.1: Methods of selective chemical dissolution of fly ash based cementitious systems;
*Rinse solution

Fernández-Jiménez et al.⁴² used this 1:20 selective chemical attack to determine the percentage of reaction in their samples of alkali activated fly ash. The resulting percentages were about 65% reacted material. It is assumed that through the chemical attack, the alkaline aluminosilicate gel and formed zeolites are dissolved, leaving only not reacted fly ash particles and not reacted crystalline phases (mullite and quartz).

2.4 Structural analysis of geopolymers using FTIR spectroscopy

FTIR spectroscopy (*fourier transformation infrared spectroscopy*) is an important and well documented tool in the structural analysis of geopolymers. Many researchers have investigated the correlations between differences in the structure and shifts of IR bands.

Bell and Dean⁵⁰ investigated the atomic vibrations in vitreous silica and therefore laid the foundation for further research. The authors found a rough division of the known bands into three regions. Stretching vibrations at 1100 cm^{-1} , deformation vibrations at 800 cm^{-1} and rocking vibrations at 500 cm^{-1} .

Other signals detected in the IR spectra, at 3250 cm^{-1} and 2350 cm^{-1} are due to -OH and CO_2 vibrations.^{51,52} The observed signals can be matched to stretching bending vibrations of Si-O-Si and Si-O-Al. The assignment, according to Lee and Van Deventer, J. S. J.⁵³ is shown in table 2.2.

wavelength [cm^{-1}]	group	type of vibration	intensity
1120	Si-O-Si	ν_{as}	sh / w
1030	Si-O-T	ν_{as}	s
880	NBO	ν	sh
777	Si-O-T	ν_s	w
695	Si-O-T	ν_s	w
622	Si-O-T	ν_s	w
560	Si-O-Al	ν_s	w
455	Si-O-Si	δ_s	m

Table 2.2: Overview of IR active vibrations in geopolymers⁵³; T = Si, Al; sh: shoulder, s: strong, m: medium, w: weak

This overview of most signals in geopolymers is used as a base for the assignment in all following spectra. NBO stands for non-bridging-oxygens which form during the reaction of silicates (or aluminosilicates) with alkaline solutions. The possibly formed functional groups are: Si-OH, $\text{Si-O}^- \text{Na}^+$, Al-OH. Most NBOs are located

at the silicon atom and are deprotonated due to the high pH. However, it has been shown that even at this high pH Al-OH groups exist (as $\text{Al}(\text{OH})_4^-$).⁵⁴ As the vibrational modes of aluminosilicates are closely related to the vibrations in vitreous silica, conclusions from these investigations can be drawn.

Plinio Innocenzi⁵⁵ analyzed this silicate network and concluded that changes to the length and angle of the Si-O-T bonds change the position of the asymmetric stretching band.^{55,56} These changes can be caused by presence of NBOs due to Al inclusion into the network or by stress, porosity, temperature change etc. Moreover, it was found that larger T-O bond length correlate with smaller T-O bond angles.⁵⁷

Tuddenham and Lyon⁵⁸ analyzed the substitution of Si ions by Al ions and were able to develop a quantitative relationship, in their system, which could be calculated from IR spectra alone. The authors found the absorption band between 1100–950 cm^{-1} varied with Al substitution and split up to three different signals. A linear correlation between this band and the Al substitution was determined.

Stubičan and Roy⁵⁹ introduced Al^{3+} into a silicate network, thereby introducing an ion with a different charge replacing the Si^{4+} in the network. The authors found an increase in the shoulder at 880 cm^{-1} (vibration caused by NBOs) and new bands appearing between 800 – 850 cm^{-1} . Moreover, the main stretching band at 1000 cm^{-1} shifted towards lower wavenumbers due to the increase in the T-O bond length and the increased ionic character of the bond. However, no band in this region was assigned to an only Al-O vibration. Other authors assigned the Al-O in plane stretching mode to a band at 828 cm^{-1} and the Al-O out of plane mode at 909 cm^{-1} .⁶⁰

Tarte⁶¹ investigated inorganic aluminates (AlO_4 and AlO_6) and their vibrations in IR spectroscopy. He differentiated between "isolated" and "condensed" tetrahedra for AlO_4 as the surroundings influence the vibrational modes. In geopolymers, mostly condensed tetrahedra are apparent as a polymeric network is formed. He assigned the region between 900–750 cm^{-1} to AlO_4 lattice vibrations.

As geopolymers show partly zeolitic behavior, it is worth looking at the IR bands in zeolites. Flanigen et al.⁶² found that zeolites show two classes of vibrations, connected internal vibrations of tetrahedral TO_4 and external linkage of the tetrahedrons. The external linkages are caused by different arrangements of the TO_4 structures. The observed bands are:³⁵

Internal Tetrahedra:

- Asymmetric stretch: 1250 – 9850 cm^{-1}
- Symmetric stretch: 720 – 650 cm^{-1}

- T-O bend: 500 – 420 cm^{-1}

External Linkages:

- Double ring: 650 – 500 cm^{-1}
- Pore opening: 420 – 300 cm^{-1}
- Symmetric stretch: 820 – 750 cm^{-1}
- Asymmetric stretch: 1150-1050 cm^{-1}

Moreover, Ali Allahverdi³⁵ mentions that the broadness of the bands in their geopolymers leads to the conclusion of a not well ordered crystalline structure but an, in varying degrees, disordered amorphous structure.

Faujastite zeolites were also investigated by Shigemoto et al.⁶³ who found a linear relationship between Al content and the main band. Furthermore, the authors studied the amorphous precursors of the zeolites and IR spectra of the precursor and the final zeolite are displayed in figure 2.5.

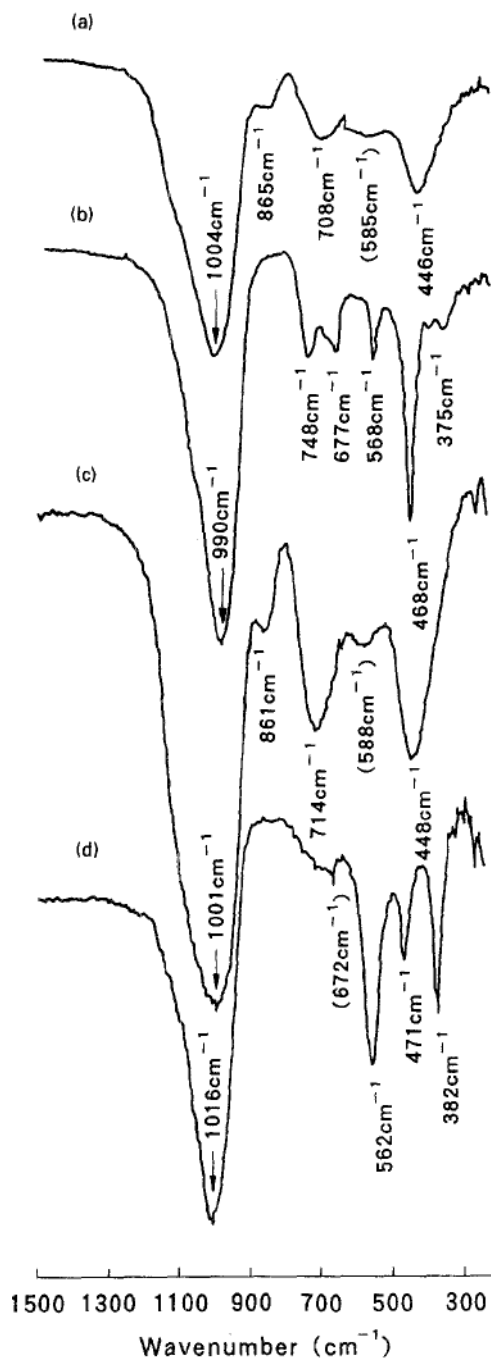


Figure 2.5: IR spectra of Na X (b), Na A zeolite (d) and their amorphous precursors ((a) for Na-X, (c) for Na-A).⁶³

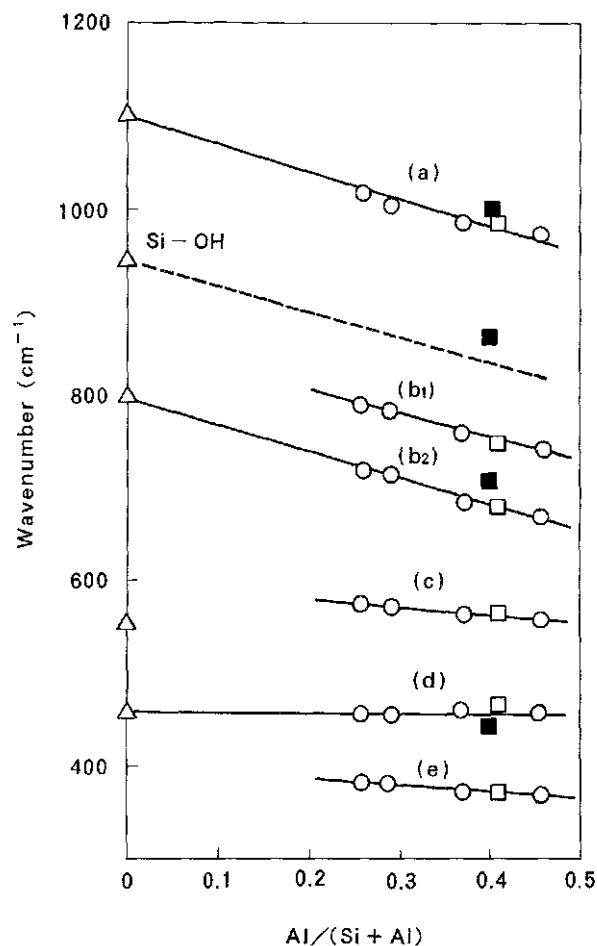


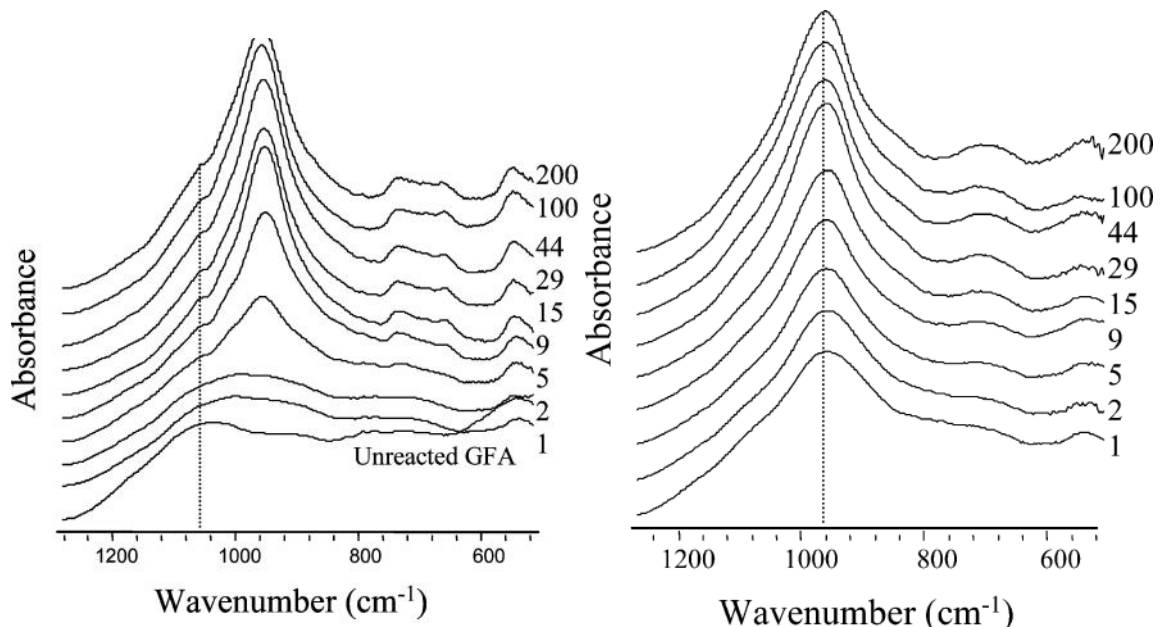
Figure 2.6: Shift in position of aluminosilicates with different Al contents. (a) asymmetric stretch T-O bonds, (b) symmetric stretch of Si-O-T, (c) double 6-ring vibrations, (d) T-O bending, (e) pore opening.⁶³

The formation of the, for zeolites typical external linkages, can be clearly seen in comparing the IR spectra. Pore opening (382 cm^{-1} (d), 375 cm^{-1} (b)) and double six ring bands (562 cm^{-1} (d), 568 cm^{-1} (b)) only form in final zeolites. Asymmetric stretching (990 cm^{-1}), symmetric stretching (748 cm^{-1} , 677 cm^{-1}) and bending (468 cm^{-1}) vibrations are apparent beforehand (1004 cm^{-1} , 708 cm^{-1} , 446 cm^{-1} resp.). Moreover, T-OH (or NBO) are found as a shoulder at 865 cm^{-1} .

Furthermore, the influence of sodium ions in aluminosilicates was investigated by

several authors. Sweet and White⁶⁴ observed a shift in the main band to lower wavenumbers with increasing Na^+ content.

Rees et al.⁶⁵ investigated the formation of geopolymers over 200 days with focus on gel formation stages during the early stages of the reaction. Therefore, mostly ATR-FTIR spectroscopy was used as it is a non-destructive technique and can be performed during the reaction without the need of drying of the geopolymer gel. The authors used a class F fly ash (CaO content $\leq 10\%$) as raw material and different Na/Al ratios in the geopolymers. Moreover, different concentrations of silicate were used in the activating solutions. It was found that if the activation occurs only by sodium ions, a significant change in the appearance of the IR spectra is seen between 2–5 days. After this time, the IR spectra show only small changes. However in geopolymers activated by silicate solution only small changes during the 200 day period are observed. The IR spectra can be seen in figure 2.7.



a) Geopolymer development of a sample with Na/Al = 0.5 and $[\text{SiO}_2] = 0 \text{ M}$ b) Geopolymer development of a sample with Na/Al = 0.5 and $[\text{SiO}_2] = 2.5 \text{ M}$

Figure 2.7: FTIR spectra showing geopolymer development over 200 days⁶⁵

Moreover, the authors used a definition of geopolymer which includes stability in water and found that in their systems, only samples which show a final wavenumber lower than 995 cm^{-1} of the asymmetric stretching band meet this premise. Samples which were synthesized with a high silicate concentration but a low Na/Al ratio, showed signals with higher wavenumbers. The authors suggested this is because only monomeric species in the alkali activator will take part in the reaction. In solutions with a high $\text{SiO}_2/\text{Na}_2\text{O}$ ratio however, the silicates will be present in ring and cage species as well as colloids. Furthermore, the authors found that in samples with a high silicate ratio (3.5–4.5 M) in the activating solution, no zeolites formed

during the reaction. This behavior was found to be independent from the NaOH concentration.

2.5 Foaming agents in geopolymer synthesis

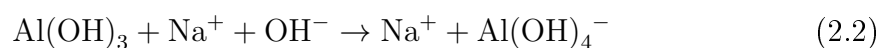
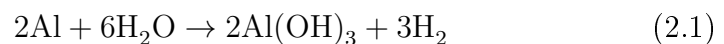
In principle, two ways of foaming exist for cementitious products. The first one being a pre-foaming method and the second one a mixed-foaming method.^{66,67} In the pre-foaming method, a foam is generated, for example by use of water and superplasticizer, and then added to the geopolymer slurry.⁶⁷ The mixed-foaming method, which is applied in this thesis, used foaming agents which are brought directly into the geopolymer slurry.

The usage of foaming agents, like metal powders, surfactants, hydrogen peroxide or NaOCl provides lightweight, fire resistant building materials.⁶⁷⁻⁷⁰

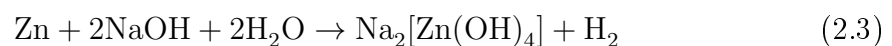
Foaming agents react in different ways as to how the geopolymer or alkali activated slag is foamed. One method is to distribute air in the system via quick stirring and using a surfactant for stabilization of the foamed material.⁷¹ Another method is to use the well known decomposition of hydrogen peroxides in alkaline solutions which are the main medium in most geopolymer syntheses.⁶⁸

Metal powders, like Zn or Al powders, react in sodium hydroxide solution into their oxidized state, releasing hydrogen in the process. The reaction equations are as following:

Reaction of Al-powder



Reaction of Zn-powder



Aluminum powder is a very fast reacting foaming agent.⁷² As can be seen in the reaction equations, the same molar amount of Zn-powder sets free 50 % less hydrogen than Al-powder. For this reason, Zn-powder reacts slower and less vigorous than Al-powder.

Hajimohammadi et al.⁷³ investigated the influence of aluminum powder onto the geopolymer structure during a setting time of 28 days. The authors used 1 % of Al-powder which was added to the geopolymer solid components before it was mixed

with NaOH solution. A thorough investigation over time was done using IR spectroscopy. It was found that the sample without the addition of aluminum powder showed a steady increase in intensity of the Si-O-T band over time. Sample A in which aluminum powder was added, showed a stronger increase in intensity of this Si-O-T band, especially over the first few hours of the reaction. According to the authors, this behavior can be explained by the higher concentration of aluminium hydroxides which are not only produced by the attack of Al-O bonds by sodium ions but also by the reaction of aluminum in alkaline media. The final intensity of the Si-O-T band (at 940 cm^{-1}) is higher in the sample with added aluminum suggesting more gel formation. However, the signal correlating to original fly ash decreases stronger in samples without addition of aluminum. Furthermore, a shift in wavelength was noticed in the main signal at 940 cm^{-1} which is shown in figure 2.8.

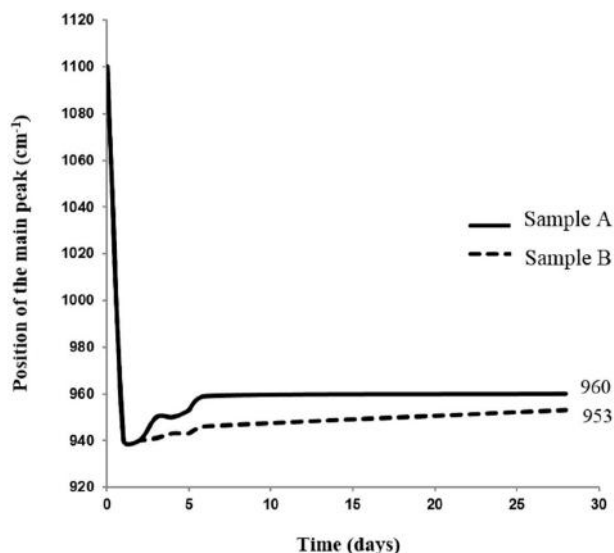


Figure 2.8: Shift in the position of main Si-O-T asymmetric stretch bond in the FTIR spectra of sample A (with added aluminum) and Sample B (no added aluminum).⁷³

As mentioned earlier, a shift towards higher wavenumbers is usually connected to a higher amount of Si participating in the gel formation. In contrast, a shift to lower wavenumbers correlates to a gel with a higher amount of Al coordinated tetrahedrons. This leads to the conclusion that in samples with aluminum addition a higher Si content is achieved which is critical for the gel hardening stage. Interestingly, density values of both samples are nearly identical.

When the foaming agent is added to the mixture and the container kept closed, the pore size is inversely proportional to the developed pressure in the container.⁷² This behavior is described by the Young-Laplace equation.⁷⁴

3 Experimental Procedure

As the procedure of sample preparation varied in each experimental setup, detailed descriptions are given in the beginning of the relevant chapter. However, analytical methods were always conducted in the same way and on the same instruments, therefore they are described in the following chapter. All measurements were conducted after a period of 28 days setting time.

3.1 Analysis

3.1.1 Fourier Transformation Infrared Spectroscopy (IR Spectroscopy)

FTIR spectroscopy was used as a analytical technique to determine small changes in the geopolymer matrix. In this work, the KBr pellet technique was used. Therefore, the dried samples were crushed and mixed with KBr (2.0 mg sample and 200.0 mg KBr). The pellets were pressed for 5 min with a pressure of 9 tn. The measurements were conducted on a Bruker Tensor 27 spectrometer.

Analysis was carried out using OriginPro 2017, no signals were diminished, however the baseline in the spectra was corrected.

3.1.2 X-ray Diffraction Spectroscopy (XRD)

XRD was conducted on a Bruker D8 using a $\text{Cu} - \text{K}\alpha$ X-ray tube and a divergence slit of 1/2. The samples were ground into a fine powder using a Mixer Mill and then, using the back-load method, put into the sample holders.

Qualitative determination of the phases was done using a variable slit whereas measurements for quantification were conducted using a fixed slit. For quantification, the dried, ground sample was blended with 20 % of rutile. For measurements a step size of 0,0131 was chosen.

Analysis was conducted using the HighScorePlus Software. As reference cards, only cards fit for Rietveld refinement of Star quality cards were accepted. Rietveld refinement was carried out with the Chebyshev I baseline.

3.1.3 Inductive Coupled Plasma Optical Emission Spectroscopy (ICP-OES)

For quantification of leached ions, ICP-OES was used as an analytical tool. Samples were diluted (1/50) with bidistilled water and a drop of HNO₃ was added to the liquid. Two measurements were taken of each sample with the prepared method taking three individual measurements each time of each sample carrier. Therefore, the here presented values are calculated from six individual values.

The prepared method was compiled using a multi-element standard (standard VIII) with HNO₃ as matrix supplied by VWR Chemicals. The calibration reference line was established using six different dilutions of the standard (1:1000–1), therefore ensuring a wide range of measurable concentrations.

3.1.4 Scanning electron microscopy (SEM)

The SEM technique can be used to gain topographic images of a surface, up to a magnification of 50.000 ×.

A small piece of the sample was broken off the block and glued onto a carbon pad. The sample was coated using a physical vapor deposition (PVD) technique with either gold or carbon. A carbon coating was used at the ZWL in Lauf for edx (energy dispersive X-ray) analysis.

SEM images were taken using a Zeiss EVO MA. Supplementary to the topographic images, element mappings were taken as well. Furthermore, on some samples edx measurements were conducted.

3.1.5 Mercury intrusion porosimetry (MIP)

Mercury porosimetry can be used to determine pores in between 3 nm and 950 μm⁷⁵. However due to experimental reasons the starting pressure was set at the option "contact +0,1" and the final pressure at 50000 *psi* which results in a bandwidth between 0,01 μm and 100 μm. For smaller pores gas adsorption measurement need to be used. Mercury porosimetry determines the pore size by filling the measurement cell with mercury and then applying pressure correlating the intruded mercury to the pore size by the Washburn equation.⁷⁶ Thereby a cylindrical pore geometry is assumed although it is known that hardly any pores show this structure. Thus the measured pore size is, to be exact, a determination of the pore's neck size and might result in incorrect results regarding the pore size.⁷⁷ Moreover, the appearing hysteresis is still a problem not fully understood. In literature, three possible reasons are given, however none of them is fit to explain the phenomena completely.⁷⁶ Hence,

in the experimental data set in this work mercury intrusion porosimetry is used only as a comparative measurement tool.

Samples were dried and then about three small pieces were put into the measurement cell. The sample weight was about 1.1 g for not foamed samples, for foamed samples, the sample weight was about 0.5 g. The measurement cells were shut tight and firstly put into the low pressure compartment, afterward filled with oil and put into the high pressure chamber.

3.1.6 Compressive strength testing

For compressive strength testing, the geopolymer slurry was filled into $40 \times 40 \times 40$ mm cubes. At least three different cubes of one sample were used to gain a dependable average value. Testing was conducted according to DIN EN 196-1.

3.1.7 Leaching tests and mass loss

In this work, a static leaching procedure was conducted. The samples were, after 28 days of setting time subjected to acidic resistance analysis. For this procedure, 1g of each sample was put into a plastic container. A beforehand prepared acidic solution was added to the sample with a ratio 1/100. The used solutions were:

- bidestilled water
- hydrochloric acid (3 mol/l)
- sulfuric acid (1 mol/l).

The acidic solutions were diluted from concentrated solutions supplied by VWR.

The containers were kept closed to minimize evaporation and contamination by the atmosphere. No further adjustments, eg. of the pH were made. After 28 days, the samples were filtered using a vacuum filter flask and then the residue was dried at 50 °C and stored for further analysis. The filtrate was saved, put into plastic containers and kept for analysis using ICP-OES.

Mass loss of the dried residues was determined by weighting the residues and the filter.

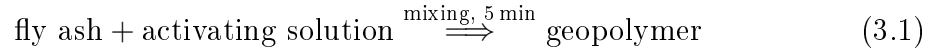
3.2 Synthesis of geopolymers

3.2.1 Geopolymer synthesis

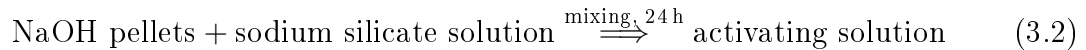
As mentioned before, the exact amounts of each synthesis vary and are given in the relevant chapter. However, here an overview of the main steps involved in

geopolymer synthesis are given.

Basically geopolymer synthesis consists of the addition of activating solution to the dry starting materials.



The activating solution consists of NaOH pellets and sodium silicate solution.



In some experimental setups in this thesis additional components were used. These were:

- Dry sodium silicate (SIKALON)
- Foaming agents (Al and Zn powder)
- Metal salts
 - PbO
 - Pb(NO₃)₂
 - ZnO
 - Zn(NO₃)₂·6 H₂O

Foaming agents and metals salts were added to the already mixed geopolymer slurry and the suspension was again mixed for about 2 min. Dry sodium silicate was added as dry material to fly ash in the beginning of the production process. After the final mixing was complete, the suspension was filled into the desired forms, covered with foil to diminish water evaporation and therefore, cracks in the samples, and left to set for 28 days.

3.2.2 Activating Solution

The activating solutions were prepared using sodium silicate solution (39T) supplied by Woellner GmbH & Co.KG, Germany. The specific properties of the sodium silicate solution are shown in table 3.1.

The exact amounts of sodium silicate solution and dried sodium silicate are given in the relevant chapter.

Name	SiO ₂ /Na ₂ O weight ratio	SiO ₂ [%]	Na ₂ O [%]	H ₂ O [%]
39T	3,3	27,63	8,37	64,0
SIKALON	2,04	56,33	27,67	16,0

Table 3.1: Specifications of sodium silicate solution

3.2.3 Used chemicals

Chemical compound	Supplier	Specification
Argon	Westfalen AG	4.8 Spektro
Betol 39 T	Woellner GmbH	
Hydrochloric acid	Fluka Analytical	TraceSelect, 34–37 %
KBr	Merck KGaA	Uvasol
Lead II-oxide	Merck KGaA	Emplura
Lead II-nitrate	Thermo Fischer GmbH	99.0 % min
Mercury	GMR mbH	> 99.9995 %
Microsit 10	BauMineral GmbH	
Multi Element Standard VIII	Merck KGaA	
NaOH pellets	Merck KGaA	EMPROVE
Rutile	Kronos Titan GmbH	Kronos 2900
Sikalon A	Woellner GmbH	
Sulfuric acid	Merck KGaA	EMSURE, 95–97 %
Water (bidistilled)	Panreac AppliChem	technical
Zinc II-oxide	VWR Chemicals	NORMAPURE
Zinc II-nitrate hexahydrate	Thermo Fischer GmbH	98.0 %

Table 3.2: Used Chemicals

4 Characterization of the used fly ash Microsit 10

In this research fly ash, provided by BauMineral, was used as raw material. The exact name of this fly ash is Microsit 10 which has a maximum in grain size of $10\ \mu\text{m}$ and according to the data sheet, the specific surface area is $7.300\ \text{cm}^2/\text{g}$.⁷⁸ A SEM image can be seen in figure 4.1.

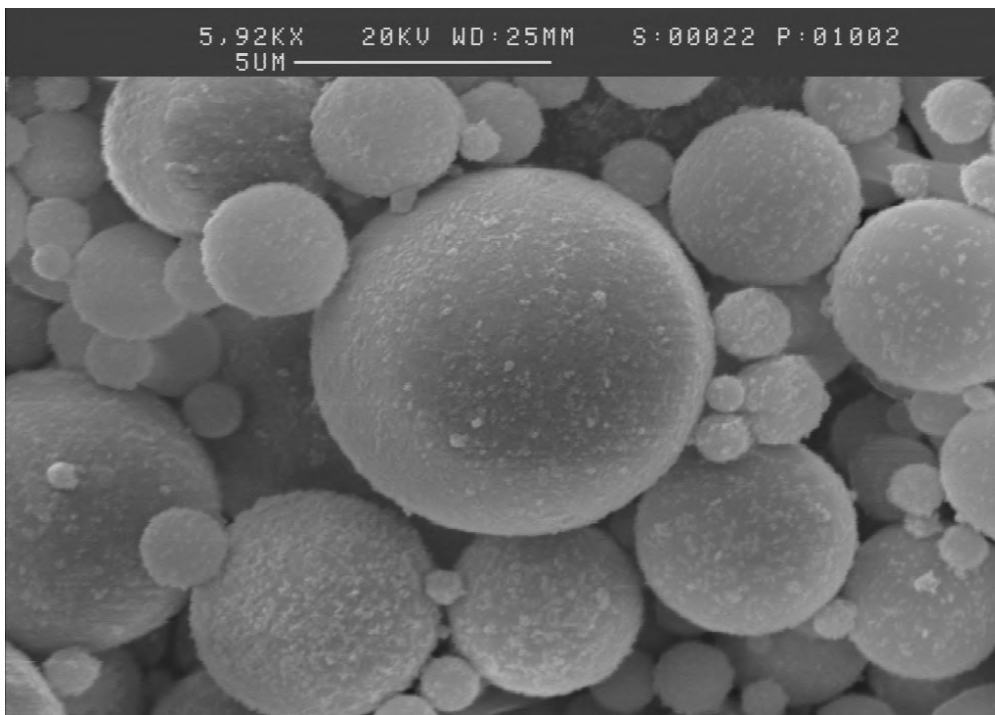


Figure 4.1: SEM image of Microsit 10; Magnification of $5,92\ \text{kx}$ ⁷⁸

For a better experimental setup, we analyzed the chemical composition (XRF and acid fusion) and the mineralogical and structural composition (XRD and IR). Moreover, we used the raw material in our leaching experiments to gain knowledge as to how raw fly ash behaves when subjected to acidic treatment.

4.1 Chemical Composition

XRF spectroscopy shows the main contents of the materials, whereas the ICP-OES results of the acid fusion of the materials show trace elements, like heavy metals.

The data of the XRF analysis can be seen in table 4.1 and the material showing a LOI of 3,09 %. With a calcium percentage of about 5 % this fly ash can be classified as class F fly ash.¹¹

SiO ₂	Al ₂ O ₃	Fe ₂ O ₃	CaO	MgO	K ₂ O	Na ₂ O	LOI
52.07	27.38	5.12	4.29	1.87	2.04	0.77	3.09

Table 4.1: XRF Analysis of Composition; in %

For the acid fusion, 250 mg of the raw material were submitted into a microwave container. Then 3,0 ml of concentrated HNO₃, 3 ml of concentrated HF and 1 ml of concentrated HCl were added. The container was shut and carefully put into the Microwave. The power was raised in 10 min to the desired 800 W and held for 45 min to achieve a complete fusion. After cooling down, leftover HF was annihilated by 20 ml of boric acid. The resulting solution was diluted 1/10 and analyzed by ICP-OES, which results can be seen in table 4.2.

As	Ba	Be	Bi	Co	Cr	Cu	Ga	Li	Mn
69	1005	11	190	55	117	127	128	140	326
Mo	Ni	Pb	Se	Sr	Te	U	V	Zn	
14	116	71	0	654	0	103	255	232	

Table 4.2: ICP-OES analysis of acid fusion; in ppm

4.2 Structural Characterization

For structural characterization we used X-ray diffraction to determine the different phases in our fly ash as well as to calculate the amount of crystalline phases and the leftover amorphous phase. Calculations were based on Rietveld refinement. Infrared spectroscopy was used to determine the Si-O and Al-O vibrations in fly ash.

4.2.1 X-ray diffraction

For X-ray diffraction, first a qualitative measurement was taken, to determine all phases apparent in fly ash. The detected phases were mullite, quartz, anhydrite, magnetite and hematite. An overview of the taken spectra is shown in the following figure (4.2).

As reference cards ICSD 98-008-0125 (mullite), 98-005-4664 (quartz low), 98-004-1057 (hematite), 98-011-2702 (magnetite) and 98-000-5295 (anhydrite) were used.

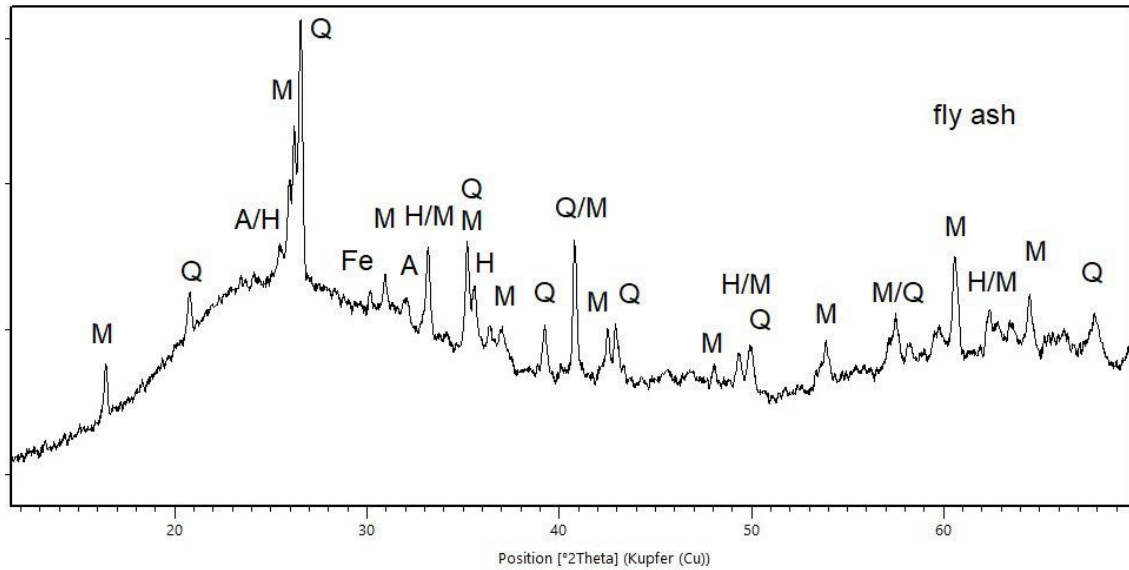


Figure 4.2: XRD diffractogram of fly ash; M: mullite, Q: quartz, A: anhydrite, H: hematite, Fe: magnetite

To determine the phases quantitatively, 20 % rutile was added as internal standard. The calculated amounts are shown in table 4.3.

Phase	mullite	quartz	hematite/magnetite	anhydrite	amorphous
Percentage	16	3	1	1	79

Table 4.3: Quantification of determined phases in fly ash by Rietveld refinement

As the crystalline phase consists mostly of mullite and quartz in which silicon-ions and aluminum-ions are bound, calculations to the overall reactive, amorphous amounts of aluminum and silicon can be made. In fly ash, the percentage of crystalline silicon is, according to our calculations, 3.2 %, of crystalline aluminum 6.4 % of the silicon and aluminum present. About 10 % of oxygen is bound in crystalline phases as well. This leaves an amorphous phase in which 97 % of the total amount of silicon and 93.6 % of aluminum are present.

4.2.2 FTIR spectroscopy

Fly ash was subjected to infrared spectroscopy using the KBr pellet technique. A complete spectra of raw fly ash can be seen in figure 4.3.

The bands at 3500 cm^{-1} and 1620 cm^{-1} show -OH vibrations which either come from moisture in the fly ash itself or from the KBr which is very hydrophilic. The original fly ash shows a main signal at 1170 cm^{-1} which correlates to the Si-O-Si vibrations in fly ash. Moreover, the band at 1434 cm^{-1} is connected to sodium carbonate and the second largest peak at 474 cm^{-1} can be assigned to the symmetrical deformation vibrations of Si-O-Si (δ_s Si-O-Si).

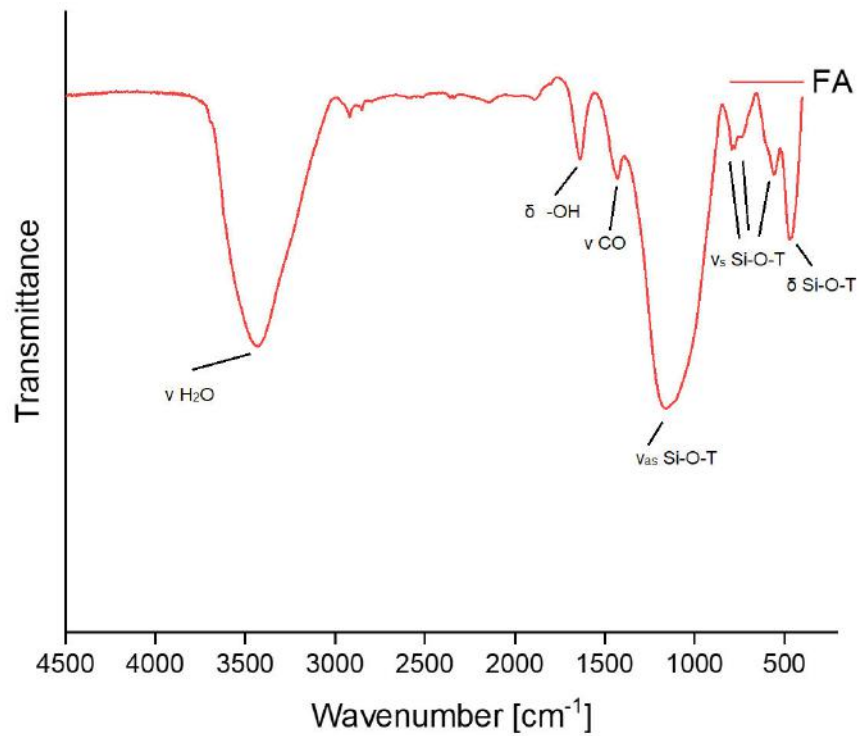


Figure 4.3: IR spectra of fly ash Microsit 10

4.3 Leaching behavior

Fly ash was subjected to the same leaching conditions as later on the geopolymer samples. Bidestilled water, sulfuric acid and hydrochloric acid were used as eluates for 28 days. The remaining solid material was weighted, filtered, dried and analyzed using XRD and FTIR spectroscopy. The mass loss was determined and is shown in table 4.4

Leaching solution	H ₂ O	H ₂ SO ₄	HCl
Percentage	4	17	21

Table 4.4: Mass loss of fly ash after leaching experiments

Fly ash submersed in water does hardly show any mass loss, in sulfuric acid a larger percentage is lost, however in hydrochloric acid over 1/5th of the original mass is lost. The resulting diffractograms of the residues are shown in figure 4.4.

The crystalline phases of mullite and quartz remain unchanged, not depending on the leaching solution. However, the signals of anhydrite and hematite disappear in sulfuric acid and hydrochloric acid completely. In water, a remaining residue of these signals can be detected.

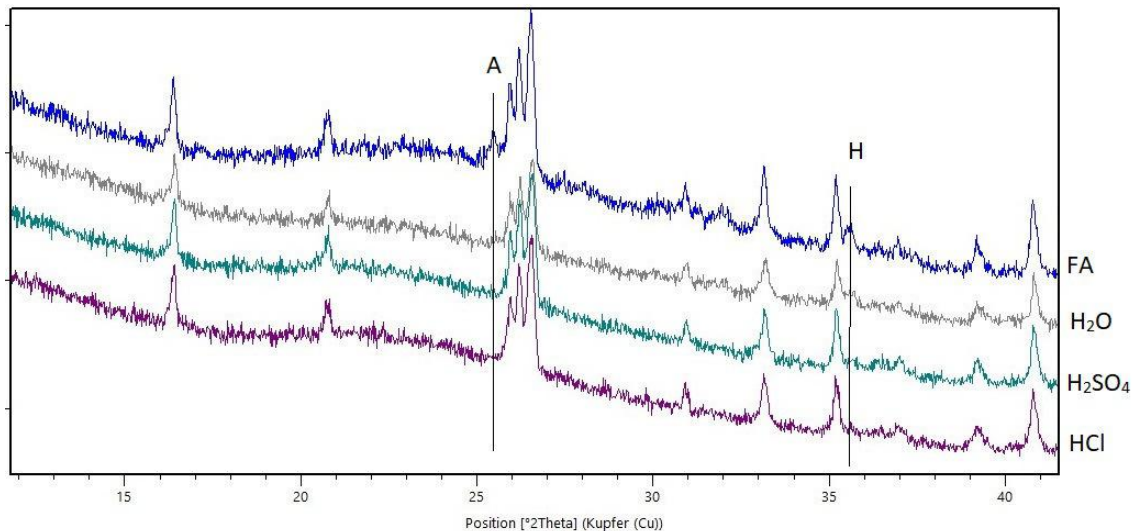


Figure 4.4: Comparison of fly ash (FA), fly ash leached in water (H_2O), in sulfuric acid (H_2SO_4) and hydrochloric acid (HCl); A: anhydrite, H: hematite

Looking at a comparison of the IR spectra of fly ash (original and leached, see figure 4.5), a shift in wavenumbers can be detected.

Fly ash which was eluted in water shows a shift in the asymmetrical stretching vibrations of Si-O-Si from 1170 cm^{-1} to 1200 cm^{-1} . Furthermore, it is noticed that the carbonate band disappears and a small peak at 1384 cm^{-1} appears. In the sample leached in sulfuric acid, a shift to 1191 cm^{-1} for the ν_{as} Si-O-T vibration is seen, however the appearance of this shift changes and a second shoulder is visible at 1110 cm^{-1} . This shoulder appears even stronger, as second peak, in the sample leached in hydrochloric acid. There a signal at 1100 cm^{-1} is found. We correlated this signal to the asymmetrical stretching vibrations of Si-O-Al. The deformation vibrations show no change at all, however the symmetrical stretching vibration of Si-O-T at 796 cm^{-1} increases in intensity and looks sharper, therefore more crystalline, than before.

We can conclude, that mostly the amorphous phase of fly ash is attacked during the acidic leaching process.

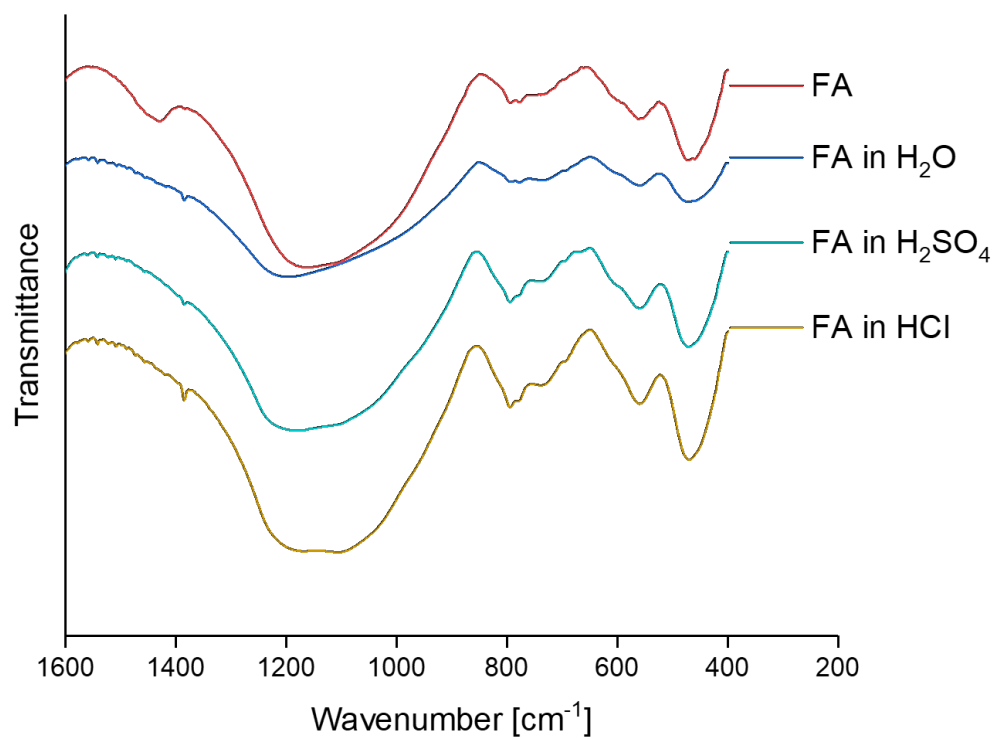


Figure 4.5: Comparison of IR spectra of leached and not leached fly ash; 1800 – 250 cm^{-1}

5 Variation of the Na/Al ratio with addition of metal powders

As mentioned in the introduction, we first of all investigated the influence of the Na/Al ratio in geopolymers. Therefore, we synthesized six different samples with a ratio varying between 0.4–0.8. Higher ratios as well as lower ratios did not produce solid, dry samples, therefore this range was used. In theory, an amount of 1.0 would be expected to produce geopolymers with the best properties. However, this theoretical amount suggest all aluminum apparent in fly ash (in the amorphous phase, not bound in mullite), is used in the reaction. However, in chemistry, we hardly have reactions which show a turnover rate of 100 % therefore, the lower amounts of sodium are quite as expected.

Furthermore, we investigated the possibilities to foam geopolymers using metal powders as foaming agents. This knowledge was considered to be useful in the later on investigation of heavy metal inclusion and the investigation of acidic resistance, depending on the porosity of samples. Only aluminum and zinc powder were used as foaming agents, as we focused on the chemical reaction producing hydrogen via oxidation of the used metals.

5.1 Experimental Procedure

5.1.1 Geopolymer Synthesis

The geopolymers were synthesized by mixing all dry materials and then adding the activating solution in the desired amount. The exact composition can be seen in table 5.1.

Foamed Geopolymers

Using the same ratios as in the not foamed samples, foamed geopolymers were prepared using different foaming methods. Aluminum powder was added to the slurry in an amount of 0.005, 0.1 and 0.2 % of the solid raw materials. Zinc powder was added in 1.0 % of the solid raw materials. The powder was added to the geopolymer

Name	SiO ₂ /Al ₂ O ₃	Na/Al	l/s	NaOH [g/l _{39T}]
F04	4,0	0.4	0.51	106
F05	4,0	0.5	0.51	169
F06	4,0	0.6	0.51	233
F07	4,0	0.7	0.51	297
F08	4,0	0.8	0.51	361

Table 5.1: Composition of Geopolymers

slurry and stirred for another 3 to 4 minutes before the mixture was molded into the desired forms, covered with foil and set for 28 days.

5.2 Results and Discussion

5.2.1 Material properties

First of all, the compressive strength of the reference samples F04–F08 was tested. The resulting average values of at least three measurements with the standard deviation can be seen in figure 5.1.

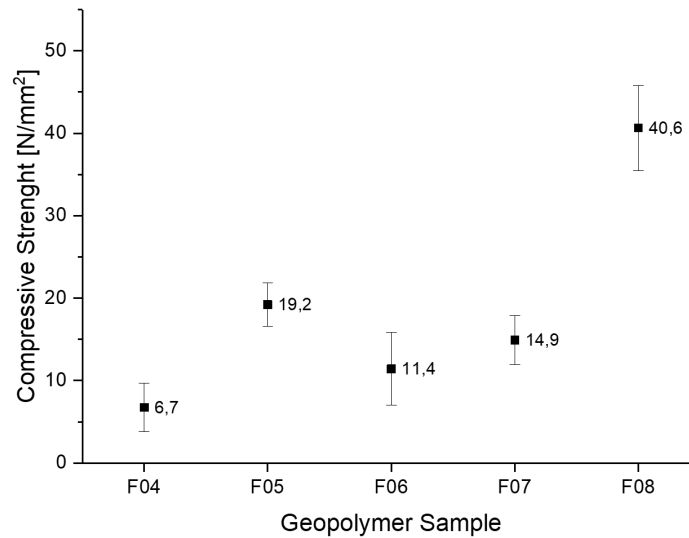


Figure 5.1: Compressive strength values of samples F04–F08

F08 shows the highest average value with 40 N/mm², followed by sample F05. No definite correlation between an increasing Na concentration and increasing compressive strength value could be found. For foamed samples, however the results are clearer. Additionally to compressive strength, thermoconductivity and density were determined. The results are shown in figure 5.2.

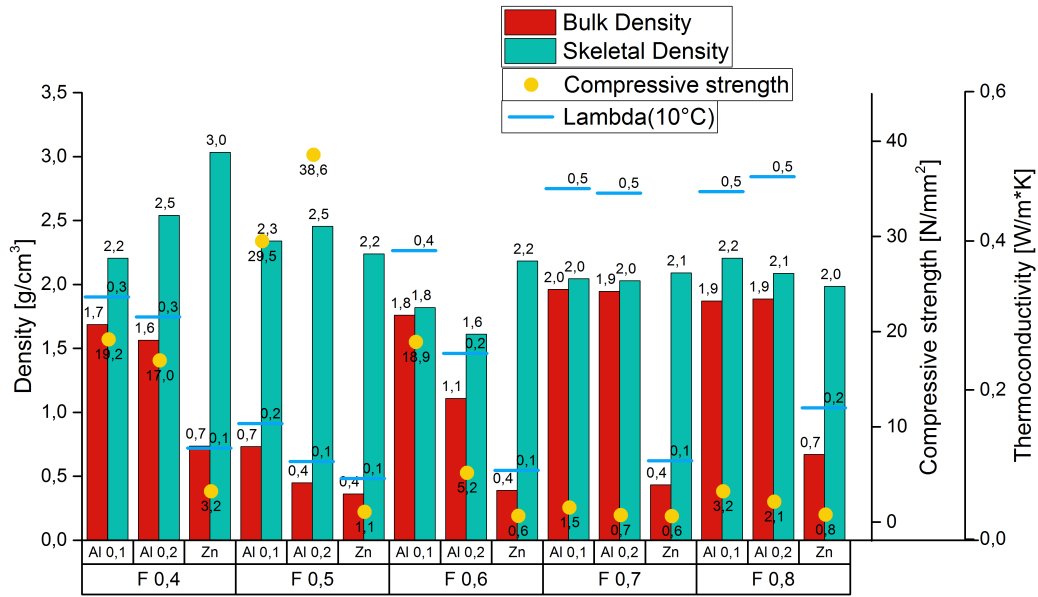


Figure 5.2: Material properties (thermoconductivity, density, compressive strength) of foamed samples F04–F08

The skeletal densities show a slight decrease for the samples F06, F07 and F08 in the order of Al 0,1 – Al 0,2 – Zn. Samples of F04 show an increase of the skeletal density. However the decrease in the bulk density is more pronounced. It shows that Zn-powder is, independently on the ratio of Na/Al, the most efficient material to produce foamed geopolymers. The compressive strength in the Zn – samples is mostly lower than in the Al – samples, however, it is still a measurable strength, which shows the geopolymers are stable enough to be handled. The lowest thermoconductivity could be found for F05 with a value of 0.08 W/m*K and a compressive strength of 1.06 N/mm².

Furthermore, samples were leached in hydrochloric and sulfuric acid to investigate the acidic resistance in dependency of the Na/Al ratio. The resulting mass loss percentages are given in figure 5.3.

In some research articles, it is reported that hydrochloric acid destroys the reaction products of the geopolymer reaction, therefore leaving only not reacted fly ash particles as well as the crystalline phases mullite and quartz.^{40,42,49} We observe a mass loss of up to 55% for sample F08. However, this mass loss was recorded for leaching in sulfuric acid. The highest mass loss in hydrochloric acid was observed for sample F07 with a percentage of 50%. F06 shows the lowest mass loss percentages in hydrochloric and sulfuric acid and is considered, therefore the sample with the most stable ratio.

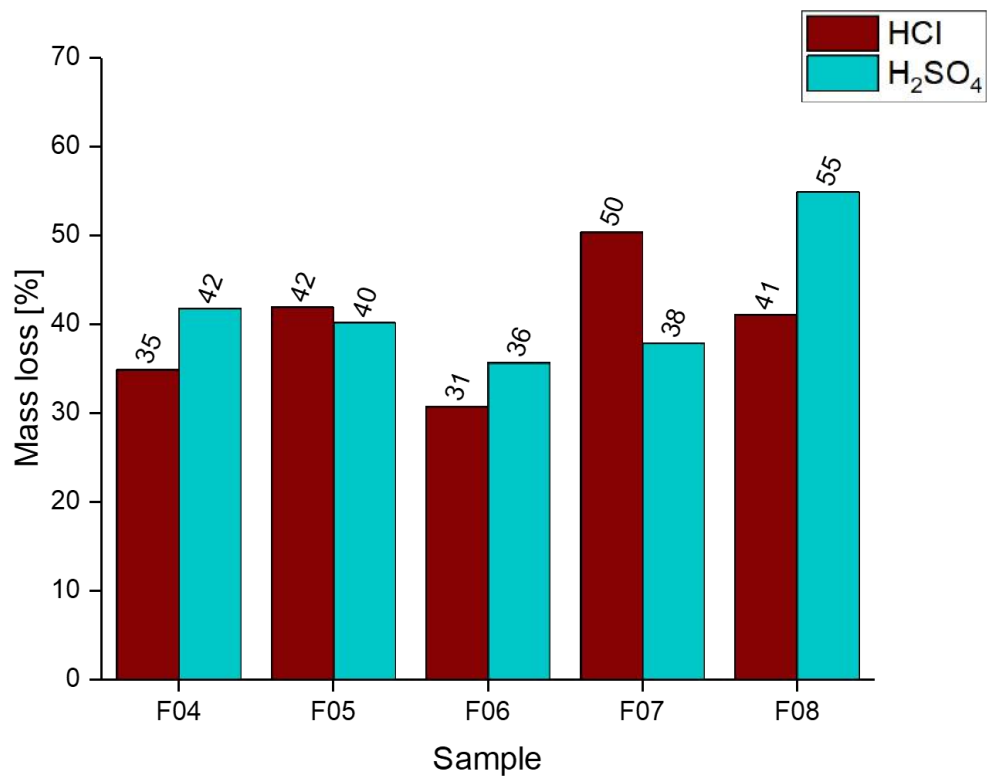


Figure 5.3: Mass loss determined in hydrochloric and sulfuric acid of geopolymer samples F04–F08

5.2.2 Microscopy

Optical Microscopy

Geopolymer samples were examined using an optical microscope. The porous structure and the differences between the foaming methods can be observed clearly. In figure 5.4 samples of F08 with all three foaming methods are displayed. The images show that Zn-powder generates a highly porous structure, resulting in pores up to $500\ \mu\text{m}$.

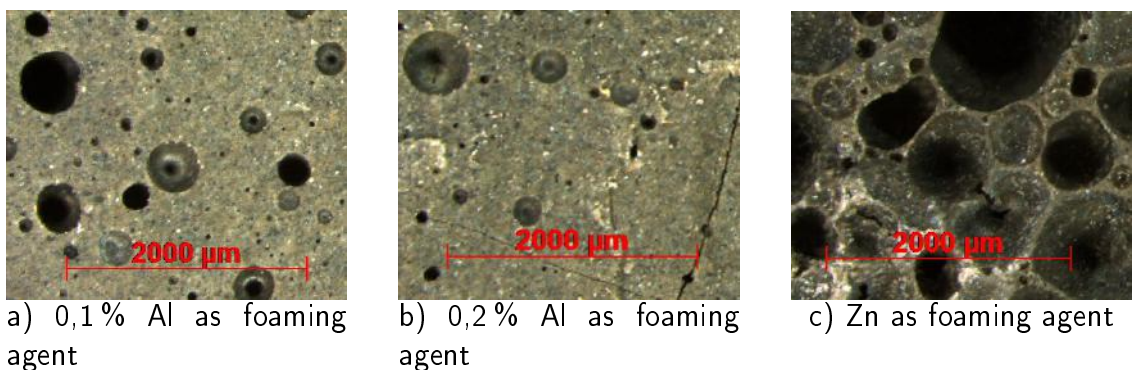


Figure 5.4: Microscopy images of geopolymers F08 using different foaming agents

Scanning electron microscopy

In addition to optical microscopy, SEM was used to gain a deeper insight into the geopolymer phases. Firstly, optical images were attained to obtain a clearer morphological image of the different phases (unreacted fly ash particles, amorphous matrix and crystalline phases). Furthermore, the influence of the different amounts and kinds of metallic powder could be analyzed. Here, an exemplary image of F06 with 0,1% of Al-powder in a magnification of 150 times is shown, figure 5.5. The size of the formed pores using this amount is about $200\ \mu\text{m}$. If the material in between the pores is examined more carefully and a higher resolution is used, more information about the phases can be obtained.

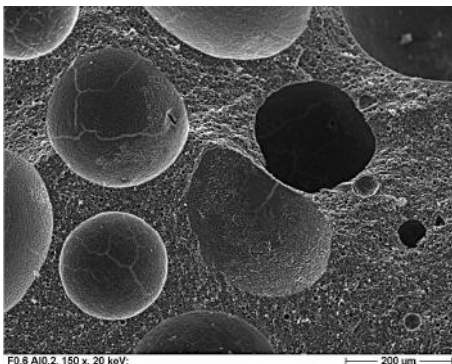


Figure 5.5: SEM image of F06 foamed with 0,2% Al-powder; Magnification: 1 kx

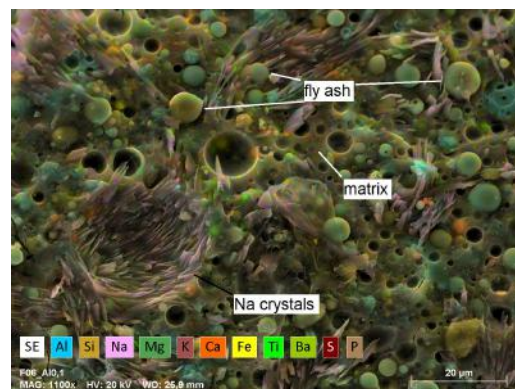


Figure 5.6: Element mapping of F06 foamed with 0,1% Al-powder showing Na crystals, fly ash spheres and geopolymer matrix; Magnification: 1 kx

In figure 5.7, SEM images of geopolymer samples with Na/Al ratio from 0.4–0.8 are displayed. A magnification of around $6000\times$ was used to enhance the structure in the μm area. It can be seen that, with increasing Na/Al ratio (from 0.4–0.6, a–c) the crystalline phase grows from in the beginning small infrequent crystals to bigger ones, which are partially connected. Figure 5.7d and e show the formation of a glassy phase which covers other particles in the matrix. In figure 5.7f a sample of a foamed geopolymer is shown. In this case a comparison with the not foamed samples (figure 5.7 c), indicates lesser crystal growth which is probably due to the interference of the pore building with the crystal growth. This leads again to the generation of an almost glassy overcoat in the sample. The increasing crystal growth due to higher concentrations of sodium ions is well established in literature.^{7,79} However, the formation of a glassy sphere covering the particles at a higher concentration of sodium ions is not well known. Moreover, little is known about the influences of metal powders introduced into the matrix as foaming agents.

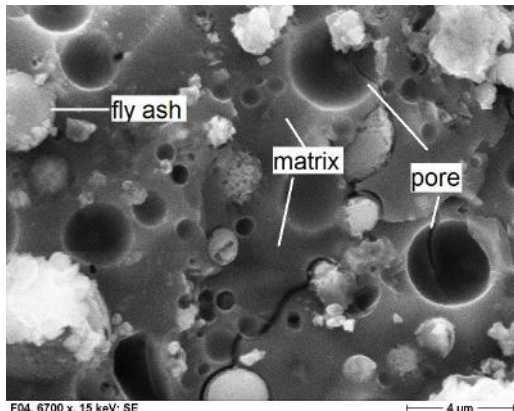
Supplementary to the optical images, element mappings were taken. These mappings show the distribution of elements in a specific area which leads to a deeper knowledge of the different phases and their composition in the materials. Figure 5.6 shows a mapping of the sample F06 with 0,1% added Al-powder. It displays the area in between the pores. The geopolymer matrix in this area is exemplary for all other samples. The needle shaped crystals show a higher amount of Na^+ -ions than the rest of the matrix. Moreover, unreacted fly ash spheres are clearly visible. The element distribution of the gel phase in the geopolymers shows the development of an (C,N)-ASH gel with a ratio Ca/Si lower than 0,3.⁴ The ratio Si/Al of the measured points in the gel decreases in the order: F04–F05–F06–F07 from 3.1 to 1.3. F08 shows a slightly higher ratio of 1.9.

5.2.3 IR spectroscopy

The IR spectrum of geopolymers can be separated in different parts (figure 5.8). The signals at ca. 3000 cm^{-1} and 1620 cm^{-1} are due to H_2O which is either leftover in the geopolymer paste or, probably the higher part, due to H_2O in the KBr pellet. The band at 1425 cm^{-1} can be attributed to the formation of NaCO_3 which is more pronounced in samples with a higher Na^+ amount.³ The signals which are due to Si-O-T (Si-O-Si and Si-O-Al) bonds can be differentiated into three parts: $\approx 1000\text{ cm}^{-1}$ ν_{as} asymmetric stretching vibration, $\approx 700\text{ cm}^{-1}$ ν_s : symmetric stretching vibration, 500 cm^{-1} δ deformation vibration.^{50,80}

In figure 5.8b the region between 250 and 1600 cm^{-1} is displayed. This part of the spectrum is chosen because it shows the vibrations of the Si-O-T bond. The, in comparison to the raw material fly ash, new developed bands at 1000 cm^{-1} are due to the Si-O-T bonds in the formed geopolymers. The signal at 1100 cm^{-1} can be attributed to the Si-O-Si bonds in the geopolymer. Moreover, a shift to lower wavelengths can be observed correlating with a higher ratio of Na/Al. This suggests a better inclusion of Al^{3+} in the geopolymer network.⁵⁰ A formation of NBOs (non-bridging-oxygens) is also observed at higher amounts of Na^+ . This shoulder at 880 cm^{-1} is more pronounced in geopolymers with higher Na^+ concentration, due to stretching vibrations of $\text{Si}-\text{O}^-\text{Na}^+$ and is also connected with the inclusion of Al^{3+} in the tetrahedral network.^{81,82} According to Lee and Van Deventer, J. S. J.⁵³ a fully polymerized tetrahedral network would depolymerize with increasing concentration of Na^+ -ions, which can be seen in the increase of the absorption at 880 cm^{-1} .⁵³ Due to the smaller molecular vibration constants, which result from the more ionic bonds of T-O, also explains the shift to lower wavelength of the absorption at 1000 cm^{-1} .

A comparison between the shift of the asymmetric stretching vibrations of the Si-O-T bond of foamed and not-foamed geopolymers can be seen in graph 5.8 d). The



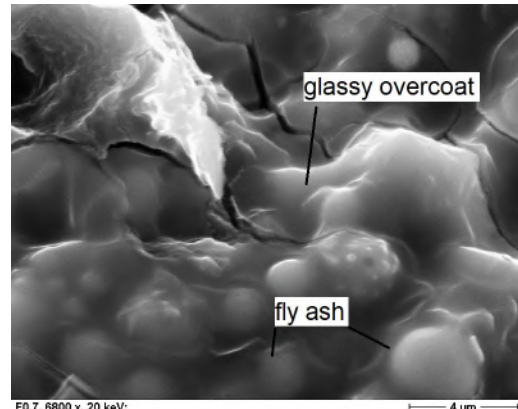
a) F04 showing fly ash particles, matrix and pores



b) F05 showing crystalline material and a fly ash sphere



c) F06 showing small fly ash spheres and growing crystalline material



d) F07 showing fly ash particles and a beginning glassy overcoat

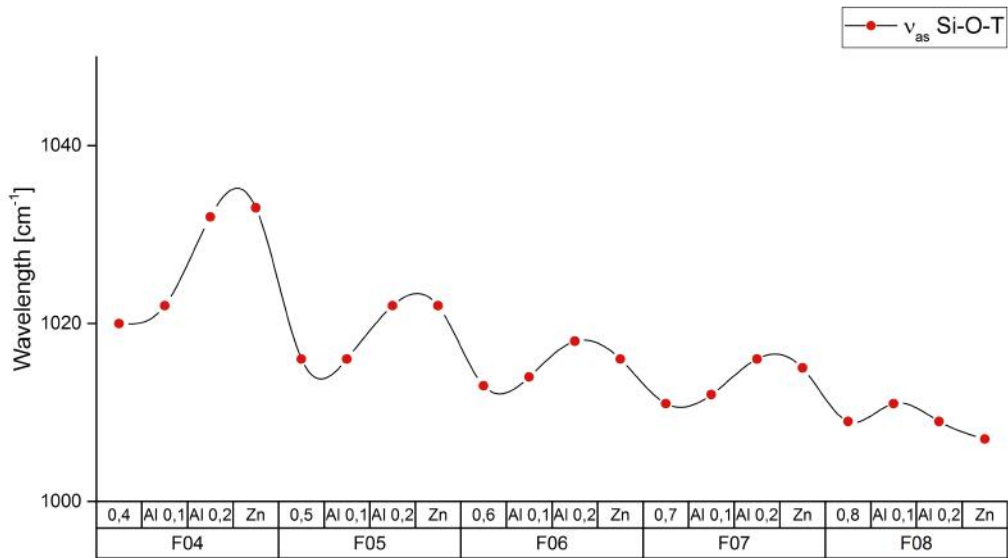
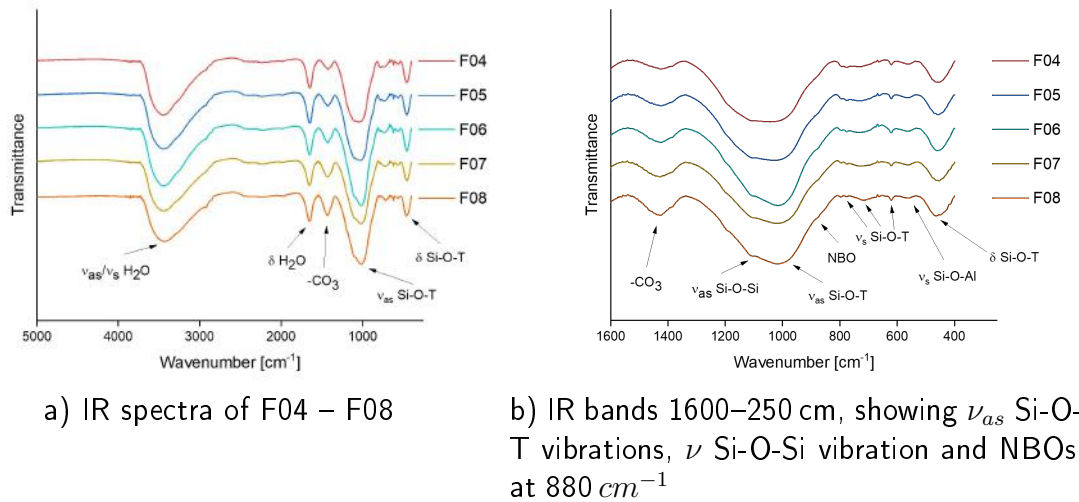


e) F08 showing a glassy overcoat over the sample and fly ash spheres



f) F06 Al 0,1 showing pores and fly ash residues

Figure 5.7: High resolution (6 kx) SEM images of samples with different Na/Al ratio.



d) Shift of wavelengths of ν_{as} Si-O-T vibrations in foamed geopolymers
 Figure 5.8: IR spectra of geopolymers; a) IR spectra of F04–F08, b) IR bands 1600–250 cm, c) Shift of wavelength of Si-O-T bond, d) Shift of wavelengths of ν_{as} Si-O-T vibrations in foamed geopolymers

shift of the signals towards lower frequencies due to the amount of Na^+ inclusion has been discussed earlier. Although the samples were ground during the preparation for IR measurements, the porosity of the samples is mirrored by a shift in frequency. In the samples F04 – F07 the wavelength between not foamed samples and samples foamed with Al 0,1 % hardly any shift is observed. The samples with Al 0,2% and Zn-powder show a shift towards higher frequencies but only slight differences in between these two foaming methods. Moreover, the shift is less pronounced in the samples with a higher amount of alkali metal ions. According to Roy⁵¹ porosity is an important aspect in interpreting IR spectra because the porosity influences the

bond length and therefore the force constant between the alternating elements.⁵¹ By grinding the geopolymer samples, bigger pores are destroyed, however smaller pores (about $1\ \mu\text{m}$, according to mercury porosimeter, see section 5.2.5) are still existent in the sample. In shifting to higher wavenumbers, the vibrational force constant increases which indicates a shorter bond length.

5.2.4 X-ray diffraction spectroscopy

As mentioned earlier, section 5.1, the used fly ash was analyzed using XRD spectroscopy. The quantitative Rietveld refinement showed a value of 79 % of amorphous material. Depending on this value, the amounts of Na-ions were calculated. The geopolymers (F04 – F08) were also investigated using diffraction spectroscopy. A qualitative comparison of the different geopolymers can be seen in graph 5.9. This representation was chosen to show the different qualitative phases of the geopolymers. The quantitative data is represented in table 5.2 and table 5.3.

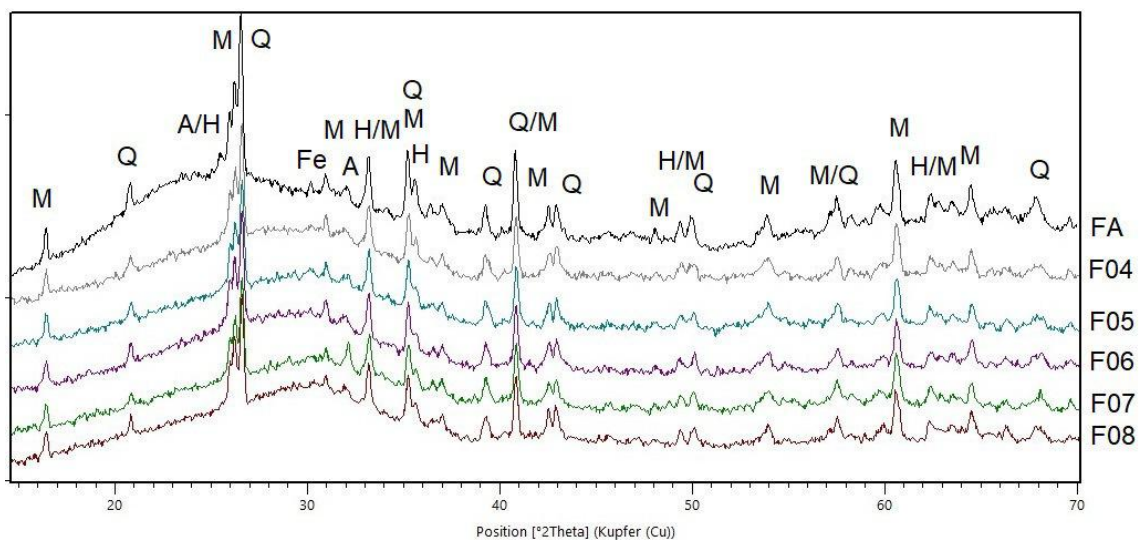


Figure 5.9: Qualitative XRD spectra of geopolymers F04-F08; Q: quartz; M: mullite; A: anhydrite, H: hematite, Fe: magnetite

Phase	F04	F05	F06	F07	F08
Mullite	12	8.5	4.5	9.2	2.4
Quartz	4.1	2.2	6.5	2.5	5.5
Amorphous	83.6	89.2	89.0	88.4	92.1

Table 5.2: Quantitative data obtained from XRD measurements; [ω in %]

Qualitative analysis of the geopolymer samples results in the detection of four phases: Quartz, mullite, anhydrite, hematite and magnetite. This conclusion is coherent with the analysis of Zhang et al.²⁸, although he attributed the signal at $30^\circ 2\theta$

Phase	F06	F06 Al0,005	F06 Al0,1	F06 Al0,2	F06 Zn
Amorphous	89.0	85.9	83.4	86.5	80.1

Table 5.3: Quantitative data obtained from XRD measurements, a comparison of foamed samples; [ω in %]

in fly ash to calcite and not to magnetite and the signal at $33^\circ 2\theta$ to hematite as it is the case here.²⁸ However, these signals are hardly detectable in the geopolymer samples. Mullite and quartz are the main components, iron oxides are detectable only in small amounts. The amorphous phase accounts for about 90 % of the geopolymer which explains the big amorphous "hump" in the XRD diffractograms and the bad resolution. Moreover, if 20 % of rutile are added to the samples to gain a quantitative result, only the phases mullite and quartz are detectable.

It can be observed that the amorphous amount in the geopolymer increases with higher Na^+ -ratio up to almost 92%. However, in the foamed samples, this amount decreases with higher porosity, samples foamed with Zn powder showing only an amount of 80 % amorphous phase.

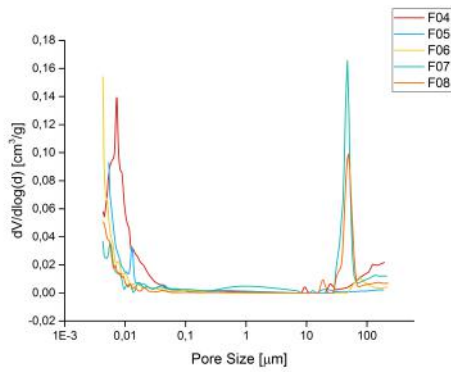
5.2.5 Porosity

In graph 5.10a comparison of the not foamed geopolymers F04 – F08 and an overview of the intruded volume of all samples can be seen.

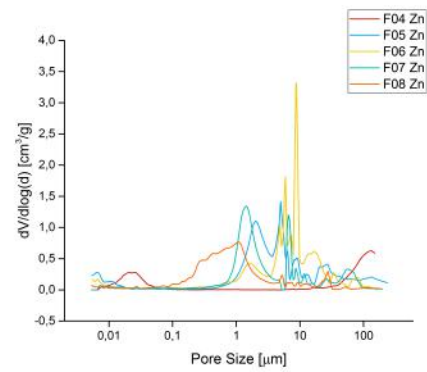
The samples without any addition of foaming agent show pores at $0,01 \mu\text{m}$ (F04, F05, F06) and at $90 \mu\text{m}$ (F07 and F08). According to this observation, the porous structure changes with the ratio of Na/Al. A lower ratio promotes smaller pores, whereas a higher ratio facilitates larger pores. This might be connected to the setting time of the geopolymers as the samples with a higher ratio harden faster than the samples with the lower ratio. In fact, if the ratio in our system is lower than 0.4, samples do not harden completely within 28 days.

The intruded volume graph (graph 5.11) shows clearly that the most porous material is the geopolymer foamed with Zn-powder. The highest amount of mercury intruded for all different ratios was determined at a pore size between $1 \mu\text{m}$ and $10 \mu\text{m}$ (see figure 5.10). Part c of figure 5.10 displays the sample F06 as an example for the different foaming agents. Zn-powder shows the highest values for the pore volume distribution, followed by Al powder in higher concentration. The addition of Al in 0,2 % shows a formation of pores with a diameter of $0.01\text{--}0.1 \mu\text{m}$, whereas the addition of Al 0,1 % results in pores with a smaller diameter than $0.01 \mu\text{m}$. The pores from the original framework are, to a lower extent, traceable in the foamed geopolymers.

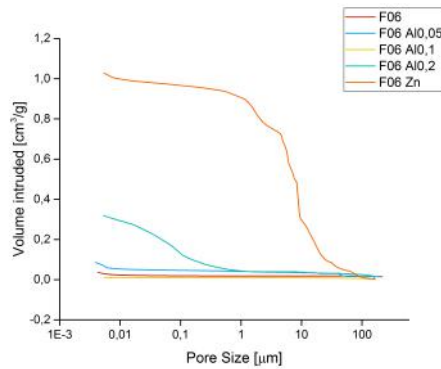
In contradiction to the data of Masi et al.⁶⁸, we found that pores with an addition



a) Overview of all not foamed geopolymer



b) Comparison of geopolymers foamed using Zn-powder



c) Comparison of F06 using all foaming agents

Figure 5.10: Mercury Intrusion porosimetry of samples F04–F08: a) Overview of all not foamed geopolymers, b) Comparison of geopolymers foamed using Zn-powder, c) Comparison of F06 using all foaming agents

higher than 0.01 % of Al-powder do not collapse but our system is stable up to the addition of 0,2 % of Al-powder. The amount of collapsed pores is depending on the ratio Na/Al with an ideal ratio of 0.6 for stabilization of the built pores. The intruded volume of the samples foamed using Al-powder is higher in the samples with a lower Na/Al ratio (F04, F05 and F06). Masi et al.⁶⁸ states that the reaction with higher amounts of Al-powder is very fast and therefore the pores collapses. Although we could observe a very fast foaming reaction, the pores were stable enough throughout the setting time.⁶⁸ The samples with a higher ratio (F07 and F08) developed a firm structure faster than the samples with a lower ratio. This would suggest that the collapse of the pores is depending on other factors than the time the geopolymers need to build up a solid structure.

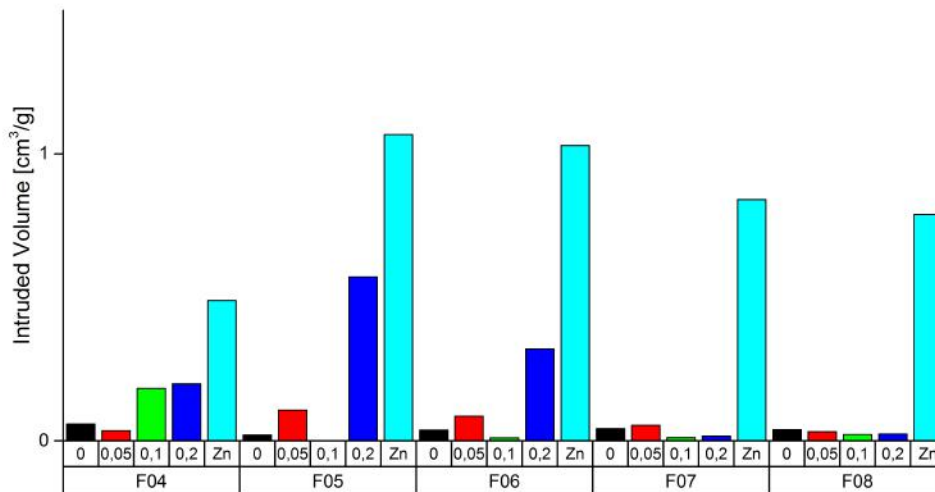


Figure 5.11: Intruded volume, recorded by MIP, of samples F04–F08

5.3 Conclusion

We showed in our work that it is possible to use metal powder as foaming agents during geopolymer synthesis and build lightweight building materials. Different pore volumes and pore sizes, depending on the foaming agent and amount of metal powder, were synthesized. Using Zn-powder, the highest porosity was achieved. Moreover, the influence of the foaming agent and therefore of the porosity to the structure of the geopolymer was analyzed on a sample with a Na/Al ratio of about 0.6. Sodium ions stabilize the geopolymer structure and therefore the introduced pores. The most stable ratio against acidic attack was found to be 0.6. Moreover, it was observed that with a higher amount of Na⁺-ions, the generation of crystalline phases was preferred compared to the geopolymers synthesized with a lower amount of sodium ions. The formed crystals show a needle shaped structure and were preferably build inside pores with an diameter higher than 20 μm .

6 Addition of PbO, Pb(NO₃)₂, ZnO and Zn(NO₃)₂

In this experimental setup, metal salts in varying amounts were added to a reference sample. The reference sample was produced, according to the amounts given in chapter 5 for the mixture F06. Lead and zinc were chosen as metal ions and added in the water soluble form of lead nitrate and zinc nitrate. Moreover, the not water soluble form lead oxide and zinc oxides were chosen. These "nonreactive" components were added to see a mainly physical encapsulation of metal ions and the ability of geopolymers to immobilize these salts. Metal nitrates were added in a dissolved form, to gain knowledge of metals salts which could be reactive and participate in the geopolymer reaction. Furthermore, this way it was possible to see the difference of probable physical and chemical encapsulation.

Samples were foamed to enhance the surface of the geopolymers especially to see the influence of the porosity onto the acidic resistance. Samples with a high surface and water soluble metal nitrates are added can be expected to show the highest possible leaching values.

6.1 Experimental Procedure

6.1.1 Geopolymer Synthesis

The main synthesis procedure is given in section 3. As a reference sample F 06 was chosen due to the experimental data gained in the previous chapter (chapter 5). This sample has a Na/Si ratio of 0.6 and a Si/Al ratio of 1.7.

PbO and ZnO samples

The metal oxides were added to the slurry in the amounts of 1 – 5 % depending on the fly ash amount. An overview of the prepared samples is shown in the following table (6.1).

The setting time was 28 days based on cement production. After this time the geopolymers were used for further analysis (IR spectroscopy and XRD spectroscopy,

Name	PbO [ω in %]	ZnO [ω in %]
"PbO" 1	1	0
"PbO" 2	2	0
"PbO" 3	3	0
"PbO" 4	4	0
"PbO" 5	5	0
"ZnO" 1	0	1
"ZnO" 2	0	2
"ZnO" 3	0	3
"ZnO" 4	0	4
"ZnO" 5	0	5

Table 6.1: Composition of geopolymers with metal oxide addition

microscopy and porosimetry). Leaching tests were also done after this setting time

$Pb(NO_3)_2$ and $Zn(NO_3)_2$

In the samples with nitrate addition, the same Al/Si ratio was used. However, as the nitrates are water soluble, they were added to the geopolymer slurry in their dissolved form. For this the needed amount of metal nitrate was dissolved in 100 ml water. For keeping the same ratios as in table 5.1 described, especially the same l/s ratio, a few adjustments had to be made. As 100 ml less activating solution were used, the needed amount of silica was added in form of dried silica powder and the extra NaOH was added to the activating solution. As not water free zinc nitrate was used, the actual percentages of added zinc nitrate are between 0.6 and 3.2%. An overview of the prepared samples is shown in table 6.2.

Name	$Pb(NO_3)_2$ [ω in %]	$Zn(NO_3)_2$ [ω in %]
"PbNO" 1	1	0
"PbNO" 2	2	0
"PbNO" 3	3	0
"PbNO" 4	4	0
"PbNO" 5	5	0
"ZnNO" 1	0	0.6
"ZnNO" 2	0	1.3
"ZnNO" 3	0	1.9
"ZnNO" 4	0	2.6
"ZnNO" 5	0	3.2

Table 6.2: Composition of geopolymers with metal nitrate addition

Activating Solution

The activating solutions were prepared using sodium silicate solution (39T) supplied by Woellner GmbH & Co.KG, Germany. Moreover, SIKALON was used as a dry silica source in the preparation of the nitrate samples.

The activating solutions were prepared using 39T and 233 g NaOH pellets for preparation of 1 l activating solution. For the preparation of the metal nitrate samples, 44,47 g of NaOH pellets were added extra in 1 l activating solution. The NaOH pellets were dissolved in 39T solution and stirred for 24 h.

Foamed geopolymers

Foamed geopolymers were synthesized using aluminum powder as foaming agent. After preparing the slurry, 0,1 % or 0,2 % of Al-powder were added to the slurry. The percentage is correlated to the amount of fly ash. The further preparation of the geopolymers was not changed.

6.2 Results

6.2.1 Scanning electron microscopy

Topographic SEM images were taken of all geopolymers, mostly to see the influence of the added oxides and nitrates on the matrix. However, in most cases the changes were too small to be detected by SEM. Only in the samples with 5 % addition, some interesting observations were made. Supplementary, SEM images were taken from the leached geopolymers to get an impression as to how the matrix is dissolved during leaching.

SEM images from not leached geopolymers

"ZnO" First of all a reference sample is depicted in figure 6.1. In this photograph a normal geopolymer matrix is shown with unreacted fly ash spheres, small pores and an amorphous matrix surrounding them. Some fly ash particles are partly covered with the amorphous matrix. The observed pores vary in size and can be due to preparation of the sample where fly ash particles were disconnected or are pores build by water evaporation. Looking at the sample of 5 % added ZnO, which can be seen in figure 6.3 in a high resolution of 50.000x with an in-lens detector. An edx measurement was also taken of this spot (figure 6.4) and figure 6.2 shows the matrix around this chosen edx spot.

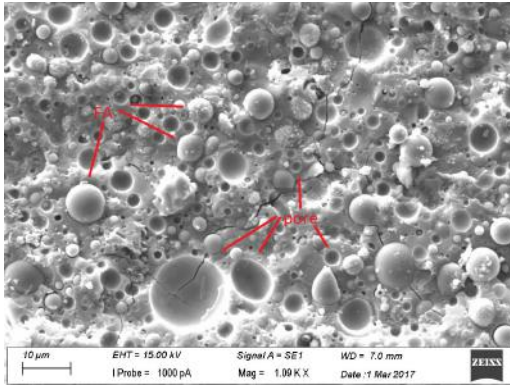


Figure 6.1: SEM image of "ZnO" 0 as reference sample showing pores and fly ash spheres

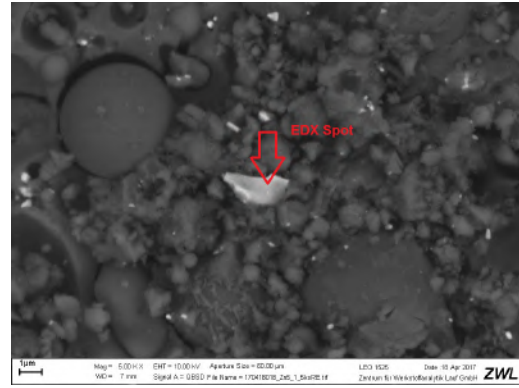


Figure 6.2: SEM image of "ZnO" 5 with the edx spot marked; magnification of 5000x

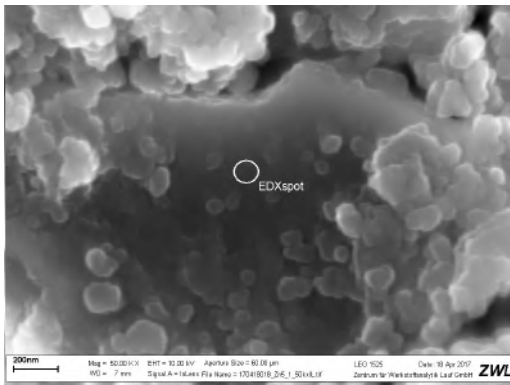


Figure 6.3: SEM image of the marked edx spot of "ZnO" 5 – high resolution (50.000x)

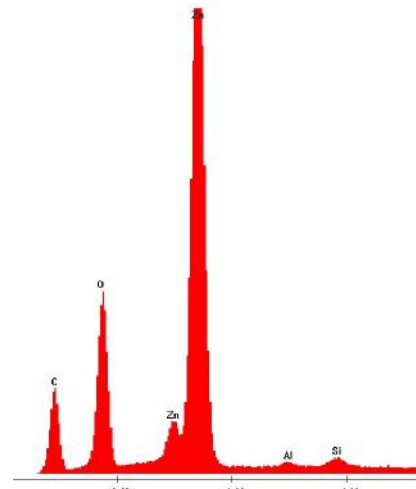


Figure 6.4: Edx spot analysis of sample "ZnO" 5

From the edx measurement it can be clearly said that this particle is a solid ZnO flake with no hint of aluminum or silicon in the particle. Moreover, no zinc signals could be detected in the surrounding geopolymer matrix. Therefore, zinc-oxide did not dissolve during the reaction but remains unchanged and physically embedded in the matrix. There is no hint to any chemical bond between the geopolymer matrix and the ZnO particle.

"PbO" Looking at the distribution of PbO in the geopolymer matrix a very different behavior is observed. An image of the in-lens detector is displayed in 6.5 and the correlating element mapping with the signals of Pb is shown in figure 6.6.

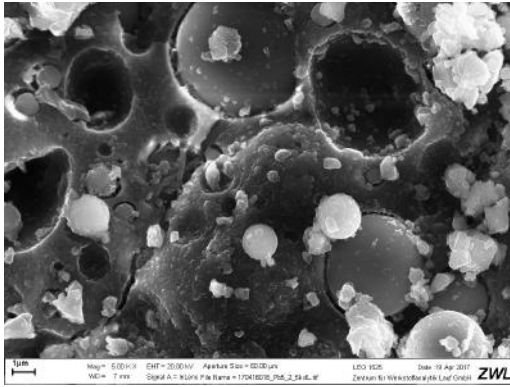


Figure 6.5: SEM image of "PbO" 5 showing geopolymeric matrix and fly ash spheres; magnification of 5000x using in-lens detector

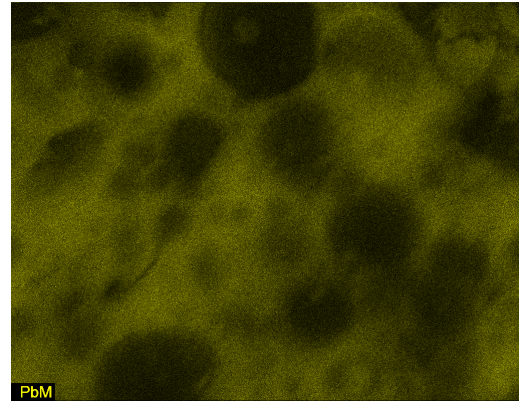


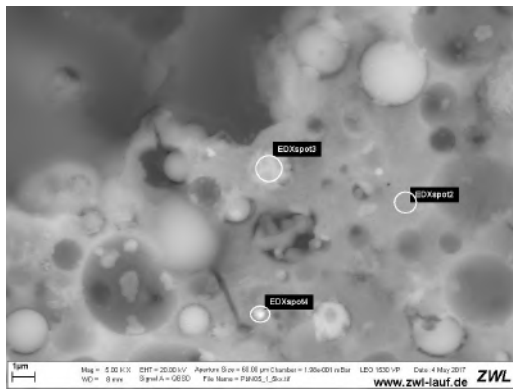
Figure 6.6: Element mapping of "PbO" 5, showing Pb signals

Looking at the element mapping it is clear that PbO is distributed throughout the whole geopolymer matrix. Only remaining fly ash particles do not show any measurable amount of Pb signals. The slightly small difference between the section of the first picture and the second one is due to the change from the normal SEM detector for the edx measurement to the in-lens detector. However pores and fly ash spheres can be matched to the parts of the element mapping where no Pb signals are detected.

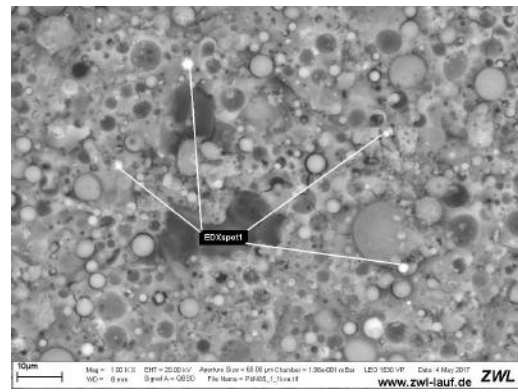
"ZnNO" The addition of $Zn(NO_3)_2$ showed no abnormalities in the SEM images at all. A taken element mapping confirms our suspicions that the Zn^{2+} -ions are completely distributed within the amorphous matrix.

"PbNO" Using the water soluble $Pb(NO_3)_2$ as supplement in the geopolymer synthesis, SEM imaging shows a mostly similar pattern as with the addition of $Zn(NO_3)_2$. However, it was possible to find small spots during the analysis where a higher concentration of Pb^{2+} was visible. The following pictures display one measured edx spots showing a higher amount of Pb-ions (figure 6.7).

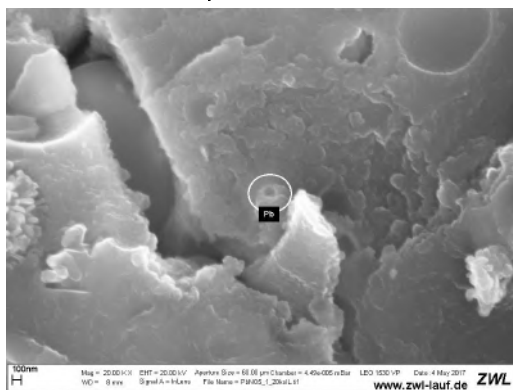
Edx spot2 and edx spot3 showed no sign of enhanced concentrations of Pb^{2+} in these areas. Only edx spot4 shows a higher amount, as displayed in the analysis in figure 6.7d. Slightly larger spots (marked with edx spot) with a similar contrast to the normal matrix showed only higher amounts of iron, see figure 6.7b). However, near the spot with higher Pb concentration, in a higher resolution, no difference in the geopolymer matrix can be determined. It seems that through the dissolving of $Pb(NO_3)_2$ in water, the lead ions get well connected with the surrounding matrix.



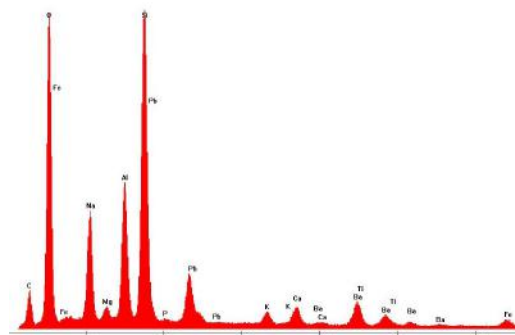
a) SEM figure of "PbNO 5" showing 3 measured edx spots



b) SEM picture of spot1; containing higher amount of iron



c) SEM image of "PbNO" 5 with marked edx spot; magnification of 20.000x using in-lens detector



d) Edx analysis of marked spot in c)

Figure 6.7: SEM analysis of "PbNO" 5; a) SEM figure of "PbNO 5" showing 3 measured edx spots, b) SEM picture of spot1; containing higher amount of iron, c) SEM image of "PbNO" 5 with marked edx spot; magnification of 20.000x using in-lens detector, d) Edx analysis of marked spot in c)

SEM images from leached geopolymers

Taking SEM images from the rest of the matrix after leaching of the geopolymers was thought to give a hint towards the dissolving of the matrix in the different leaching agents. Therefore, all samples were dried after leaching and prepared on carbon-pads for SE microscopy.

Scanning electron microscopy of the leached geopolymers, to be precisely the solid rest of the geopolymers, shows a different picture for each leaching solution. For the geopolymers leached in water (figure 6.8a), almost no difference to the former matrix is detectable. Looking at the figures of the sample leached in HCl (figure 6.8b), only fly ash particles are detectable. No geopolymeric, amorphous matrix can be seen. In figure 6.8c and d samples leached in sulfuric acid are depicted. A half destroyed matrix is visible in both figures. In the lead sample also a high amount of crystalline material can be seen, whereas in the Zn sample no such crystals are formed. In the element mappings, an interesting difference between the samples with added ZnO

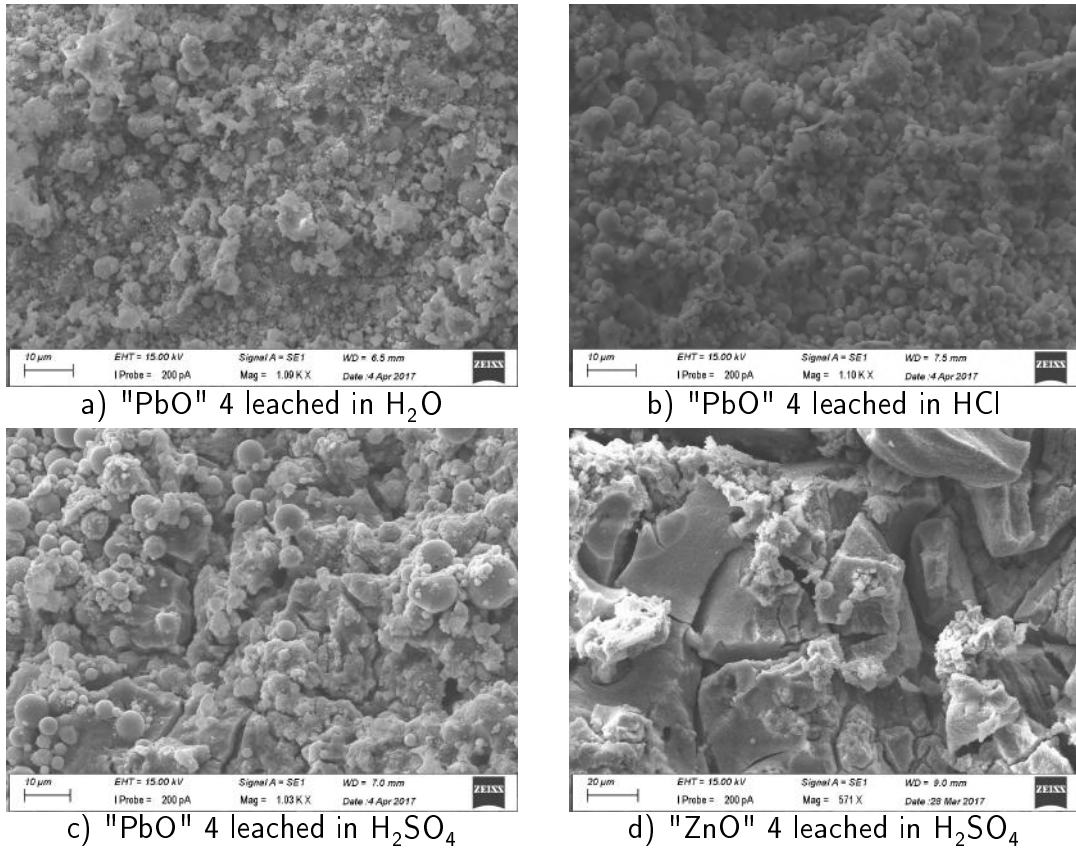


Figure 6.8: SEM analysis of "PbO" 4 and "ZnO" 4 in different leaching solutions; a) "PbO" 4 leached in H_2O , b) "PbO" 4 leached in HCl , c) "PbO" 4 leached in H_2SO_4 d) "ZnO" 4 leached in H_2SO_4

and PbO is shown (see figures 6.9 and 6.10).

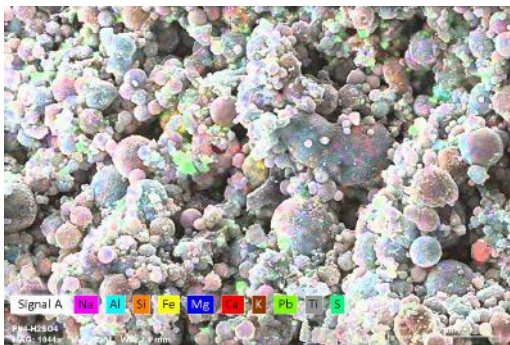


Figure 6.9: Element mapping of "PbO" 4 leached in H_2SO_4

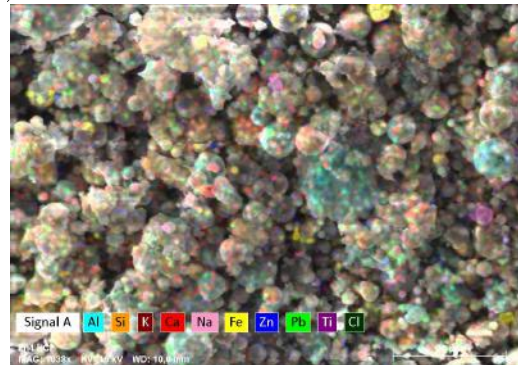


Figure 6.10: Element mapping of "ZnO" 4 leached in HCl

In the first figure with lead oxide added to the geopolymer, it is clearly visible that part of the lead stays during leaching in the solid state. It probably reacts with the sulfate-ion to build $PbSO_4$. This is indicated by the correlation between the detected sulfur ions and the lead ions. Zn cannot be detected in the rest of the geopolymer after leaching.

6.2.2 IR spectroscopy

IR spectroscopy as analytical method investigating the structural properties in geopolymers is very common and, as explained earlier, the KBr pellet method is used. All geopolymers including the leached rest of the samples were investigated by this method.

IR spectroscopy of metal oxides

Firstly, a comparison of samples with added ZnO and PbO (samples "MO" 0–5) are shown in figure 6.11 and 6.12.

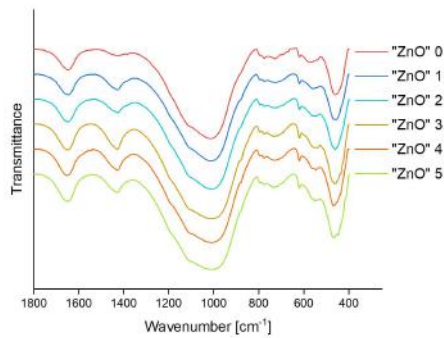


Figure 6.11: Comparison of IR spectra of "ZnO" geopolymers

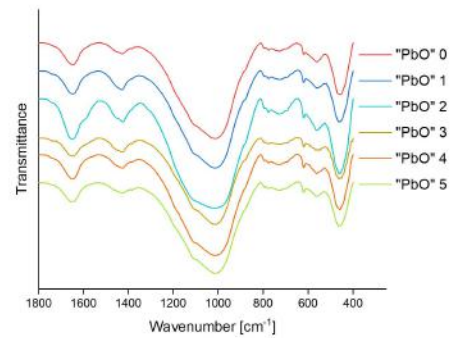


Figure 6.12: Comparison of IR spectra of "PbO"

In all samples, the expected bands of H_2O (δ -OH: 1620 cm^{-1}) and Na_2CO_3 (1410 cm^{-1}) are observed. Moreover, the Si-O-Si and Si-O-Al stretching and bending vibrations, as explained in the introduction are also apparent. However, no new signals correlating to the lead or zinc oxides are observed. Furthermore, no shift in the asymmetric stretching band of Si-O-T (1010 cm^{-1}) is observed. The samples with the addition of lead oxide, however appear rather more crystalline in their shape. This means, the signals are slightly sharper. This can be observed especially in the second signal in the peak at 1010 cm^{-1} . The small shoulder at about 1100 cm^{-1} which was suggested correlates to ν_{as} Si-O-Si vibrations, increases in intensity with the added amount of PbO. In samples with added zinc oxide no such behavior is noticed but the bands appear rather broad.

In figure 6.13 this difference in shape can be noticed better as a comparison of samples "ZnO" 0, "ZnO" 5 and "PbO" 5 is shown.

In addition to the before mentioned changes, a slight increase in the vibrations of the non-bridging-oxygen's (NBO's) at the samples "ZnO" 5 and "PbO" 5 can be detected. Also in the "ZnO" samples an increase of the band at 600 cm^{-1} , correlating to the symmetrical stretching vibrations of Si-O-Al is observed. Furthermore, an increase of the deformation vibrations at 450 cm^{-1} connects with an increase in the ZnO concentration.

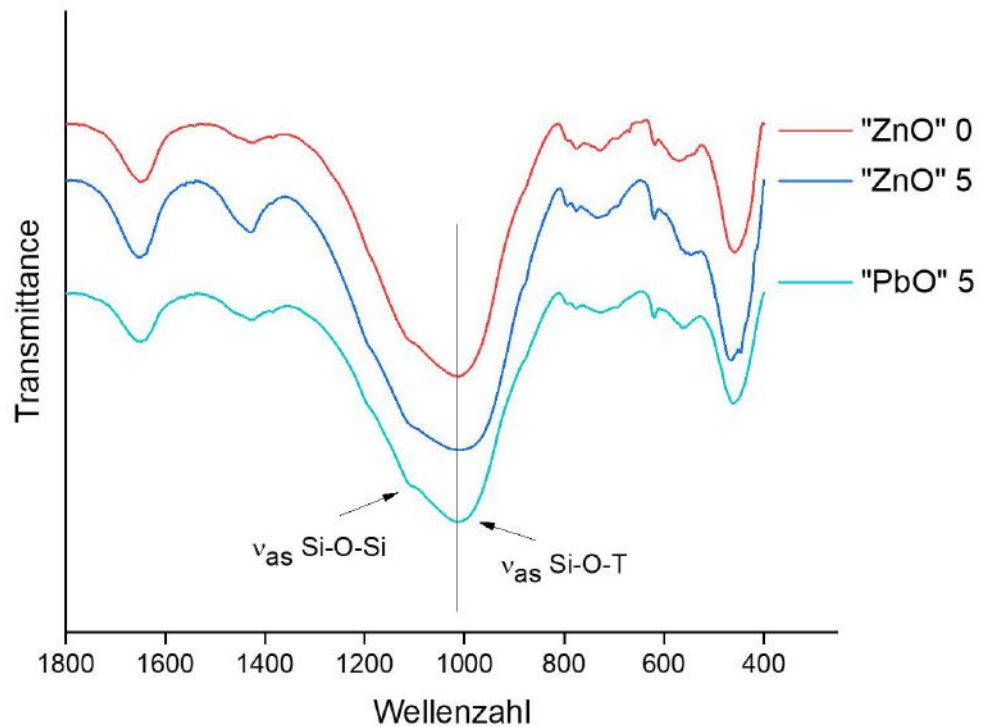


Figure 6.13: Comparison of geopolymers without any addition ("ZnO" 0), "ZnO" 5 and "PbO" 5

Looking at the same samples but in their leached state, the impact of the leaching solution is shown.

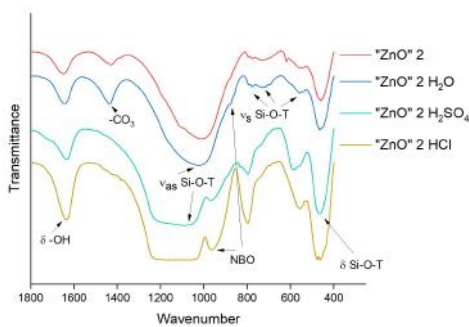


Figure 6.14: Comparison of IR spectra of "ZnO" 2 in different leaching solutions

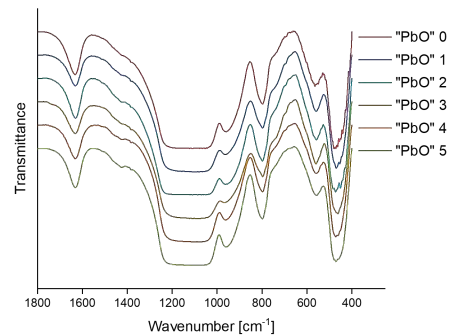


Figure 6.15: IR spectra of "PbO" leached in HCl

Water, as mentioned before, does not have any significant impact on the structure of the geopolymers. In sulfuric acid and hydrochloric acid, the asymmetrical stretching vibration of the Si-O-T bonds at 1000 cm^{-1} is shifted to higher wavenumbers but also significantly broadened. A minimum could not be determined because the transmittance detected is too close to zero. Nevertheless, no extra evolving signals in the

leached residues depending on the added amount (figure 6.15) were detected. The symmetrical stretching vibrations of Si-O-Si and Si-O-Al show a shift towards higher wavenumbers and an increase in intensity. A significant increase in the stretching band of NBO's was detected if samples were leached in acids, especially in hydrochloric acid. The difference in appearance of leached and not leached samples, suggests a destruction of the geopolymer matrix. If hydrochloric acid is used, hardly any resemblance to the spectra of the original sample is observed. These observations underline the hypothesis that hydrochloric acid is able to dissolve the amorphous matrix of geopolymers.

IR spectroscopy of metal nitrates

The IR spectra of the metal nitrates are shown in the following graphs (figures 6.16 and 6.17). Firstly, a comparison between $Zn(NO_3)_2$ and $Pb(NO_3)_2$ is drawn.

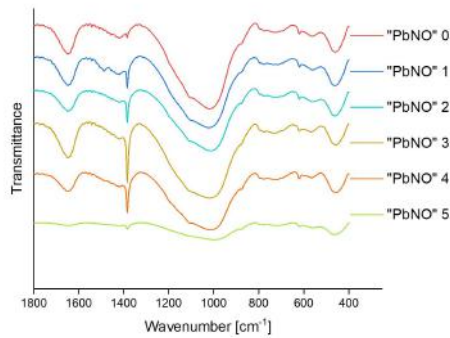


Figure 6.16: IR spectra of samples "PbNO" 0-5

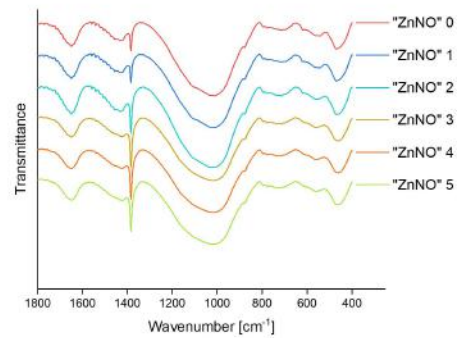


Figure 6.17: IR spectra of "ZnNO" 0-5

Comparing the two nitrates no huge differences can be detected. The lower intensities of $Pb(NO_3)_2$ 5 are due to a slightly different preparation of the KBr pellet. However, the bands show no shift, compared to the other nitrates. It is noted that the intensities of the Si-O-T vibration (1015 cm^{-1}) show a slight decrease, compared to the reference sample "PbNO" 0. A slight increase in the shoulder at 1107 cm^{-1} can be detected correlating to the asymmetrical stretching vibrations of Si-O-Si as well as an increase in the signal at 619 cm^{-1} (ν_s Si-O-Si). Comparing the spectra of the nitrates to the spectra of the oxides, a new signal, the ν_s $NaNO_3$ vibration is visible. The asymmetrical stretching vibration Si-O-T shifts from around 1005 cm^{-1} (PbO and ZnO) towards higher wavenumbers in the nitrate samples (1015 cm^{-1}).

The IR spectra of the leached samples (HCl and H_2SO_4) are shown in the following figures (figures 6.18, 6.19, 6.20 and 6.21), however no graphs of the samples leached in water are shown, as there is no difference to the reference samples.

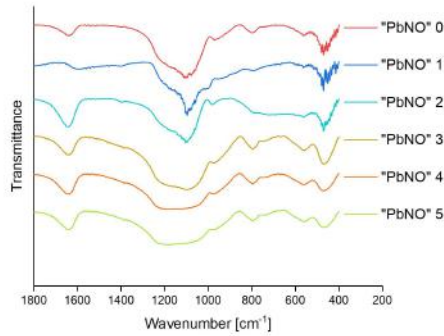
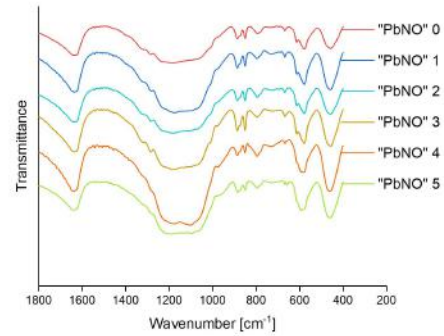


Figure 6.18: IR spectra of "PbNO" leached in HCl

Figure 6.19: IR spectra of "PbNO" leached in H_2SO_4

A comparison of $Pb(NO_3)_2$ in the two leaching solutions (figures 6.18 and 6.19) shows that in HCl the main signal, before detectable at 1015 cm^{-1} , is now shifted towards higher wavenumbers (1100 cm^{-1}). Moreover, the shape of the formerly broad band is now quite different. For the samples "PbNO" 0, "PbNO" 1, "PbNO" 2 no broad signal is detected, but a very sharp (crystalline like) signal of the ν_s Si-O-T vibration. Almost no signal of the ν_s Si-O-Si vibration (beforehand at 1105 cm^{-1}) is seen. In the spectra of the samples with a higher $Pb(NO_3)_2$ concentration, the Si-O-T band broadens significantly until in the sample "PbNO" 5 almost no difference in shape is observed. However, the shift to higher wavenumbers continues from 1015 cm^{-1} to 1100 cm^{-1} for the ν_s Si-O-T vibration and from 1105 cm^{-1} to 1190 cm^{-1} with an increasing intensity in the Si-O-Si signal. Moreover, no $NaNO_3$ band can be detected anymore. The rest of the spectra is similar to before with an increase of intensity and a shift of the shoulder at 990 cm^{-1} cm, correlating to the NBO's.

The spectra of the samples leached in sulfuric acid show a similar pattern. The shift towards higher wavenumbers is almost identical (1105 cm^{-1} and 1180 cm^{-1}) however the signal at 1180 cm^{-1} gains intensity compared to the reference samples. Another small shoulder is detectable at 1288 cm^{-1} which was not present before and is not present in the samples leached in HCl or the leached oxide samples.

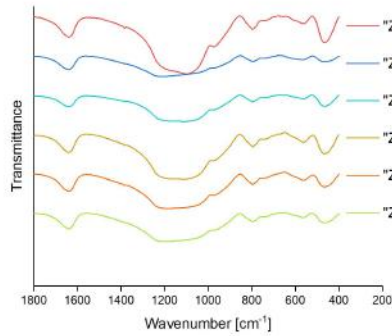
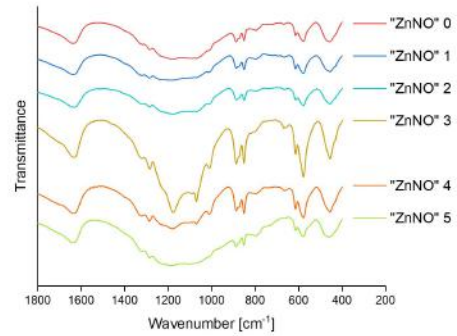


Figure 6.20: IR spectra of "ZnNO" leached in HCl

Figure 6.21: IR spectra of "ZnNO" leached in H_2SO_4

Zinc nitrates in HCl and H_2SO_4 (figures 6.20 and 6.21) do not show the same behavior as the lead nitrates. Samples with zinc nitrate leached in HCl show a smoother line than the lead nitrates. The Si-O-T band shifts to almost the same wavelength as in the other samples (1105 cm^{-1}). With increasing concentration of $Zn(NO_3)_2$ in the sample, the peak at lower wavenumbers (ν_{as} Si-O-T) decreases in intensity whereas the second signal (ν_{as} Si-O-Si) increases. Furthermore, the shoulder of the NBO's decreases in intensity with a higher concentration of added zinc nitrate. Again, no Na_2CO_3 band can be detected.

The samples leached in sulfuric acid, however, do not show a smooth line. They display sharp, crystalline like signals. The originally broad band at 1000 cm^{-1} now shows two sharp single signals of ν_s Si-O-Si (1180 cm^{-1}) and ν_s Si-O-T (1070 cm^{-1}). Again, a shoulder at 1280 cm^{-1} appears and the shoulder at 1014 cm^{-1} (NBO) remains unchanged. In sample "ZnNO" 3 interestingly, the signals are the clearest to see. The ν_s Si-O-T (890 cm^{-1} and 850 cm^{-1}) shows a high intensity compared to the not leached samples. Also, the ν_s Si-O-Al vibration, before at 540 cm^{-1} now at 580 cm^{-1} , is of a higher intensity.

For a better comparison of the direct differences of the leaching solutions, "PbNO" 4 and "ZnNO" 4 in the different solutions is shown in a separate figure (figures 6.22 and 6.23).

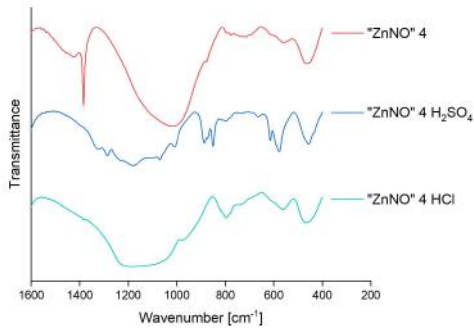


Figure 6.22: Comparison of IR spectra of leached and not leached "ZnNO" 4

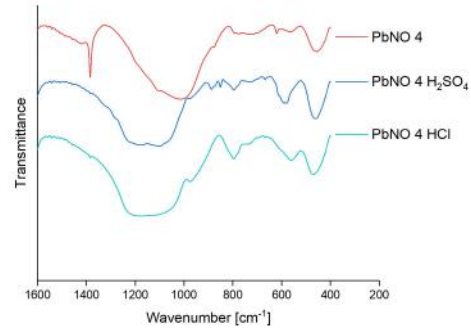


Figure 6.23: Comparison of IR spectra of leached and not leached "PbNO" 4

In the left figure, the shift of the main signal and the increase of intensity of some bands can be seen more clearly, as well as the disappearance of the $NaNO_3$ signal. In the original fly ash spectra (fig:IR-FA-1) only the expected signals of ν_{as} Si-O-T and ν_s Si-O-T are detected. When leaching the raw material in the solvents, only a shift towards slightly higher wavenumbers appears. Moreover, the wavenumbers of the ν_{as} Si-O-T are very similar to the wavenumbers detected in the leached geopolymers. Especially if HCl is used as a leaching solution, the measured spectra are almost identical. Only the shoulder at 980 cm^{-1} of the NBO vibrations is not detectable in the spectrum of fly ash. In sulfuric acid however, fly ash does not show the signals at 890 cm^{-1} , 850 cm^{-1} (both ν_s Si-O-T), 615 cm^{-1} and 580 cm^{-1} (ν_s Si-O-Al) at all. The spectra of the leached geopolymer moreover, shows small signals between 1000 cm^{-1} and 1325 cm^{-1} which the spectra of fly ash does not show. Here, only a smooth, broad band is measured.

6.2.3 X-ray diffraction spectroscopy

As mentioned in the characterization of fly ash (section 4), fly ash has an amorphous amount of about 79 %. This phase is able to react in the geopolymer reaction which leads to even higher amounts of amorphous phase in the geopolymers. Our research shows that most geopolymers in this part of the thesis possess an amorphous phase of about 90 % – 95 %. As crystalline components mullite, quartz and hematite were found, which are also apparent in fly ash. All geopolymer samples (leached and not leached) were tested using 20 % of rutile as internal standard and a solid lens applying the Rietveld method for quantification. Moreover, all samples were measured using a variable lens for qualitative testing.

The diffractograms of samples with ZnO and PbO addition are shown in figure 6.24 and figure 6.25.

The crystalline components of fly ash remain unchanged in the geopolymer samples (mullite, quartz and hematite). A clear enhancement of the ZnO signal can be

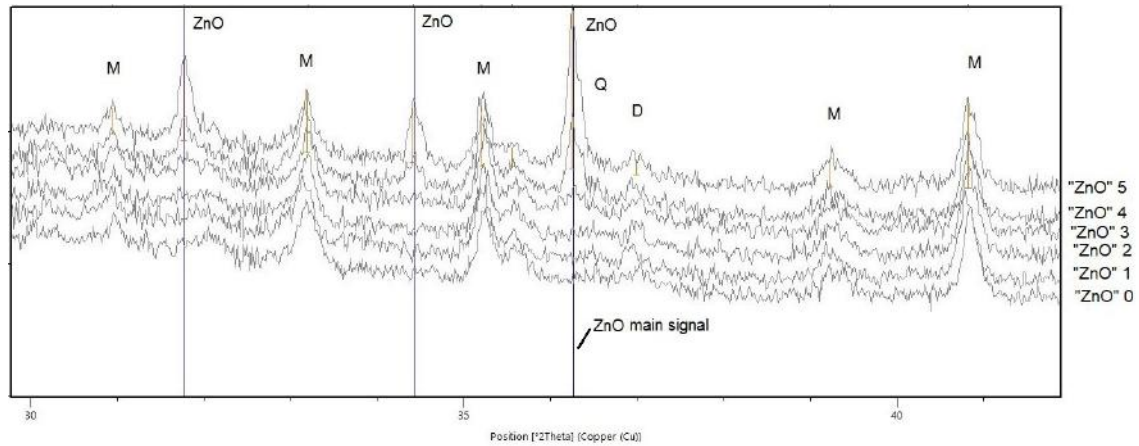


Figure 6.24: Diffractogram of samples with ZnO addition; M: mullite, Q: quartz, D: diopside

seen with increasing ZnO addition to the geopolymers. All other phases show no change. As a crystalline signal of ZnO can be seen so clearly, it is suspected that ZnO does not react in any way during the geopolymerisation reaction but remains as inert phase. Moreover, a small amount of diopside is detected.

In the diffractograms of samples with PbO addition no such enhancement of one crystalline signal can be determined. A small signal of Pb_3O_4 can be detected in samples with a relatively high amount of added PbO. All other PbO signals do not show a clear appearance in the diffractograms. Mullite, quartz and hematite signals remain unchanged. This observation leads to the conclusion that PbO is distributed in the amorphous phase and not detectable with XRD analysis anymore.

The diffractograms of the dissolved nitrates are depicted in figures 6.26 and 6.27.

In the samples with $Zn(NO_3)_2$, a zincferrate (franklinite, $ZnFe_2O_4$) can be determined in the sample with 5% addition of $Zn(NO_3)_2$, however no phases with nitrate contribution can be observed. A second, newly formed phase is found, namely $CaMgSi$ which can also be determined in the sample with 5% addition of zinc nitrate.

Adding $Pb(NO_3)_2$ to the geopolymer, phases consisting of nitrate compounds are found. Two different types ($NaNO_2$ and $NaNO_3$) are detectable. Interestingly, in the samples with a higher amount of added $Pb(NO_3)_2$, only $NaNO_3$ can be found. In samples with lower concentration ("PbNO" 1 and "PbNO" 2 only signals coming from $NaNO_2$ are measurable.

The diffractograms of the leached geopolymers were also analyzed using XRD spectroscopy. However, due to the small amounts of the solid rest material after leaching, the resolution of the diffractograms is worse than in normal geopolymers. The qualitative diffractograms are shown in figures 6.28 and 6.29.

In this part of the diffractogram, the focus is on the remaining detectable ZnO

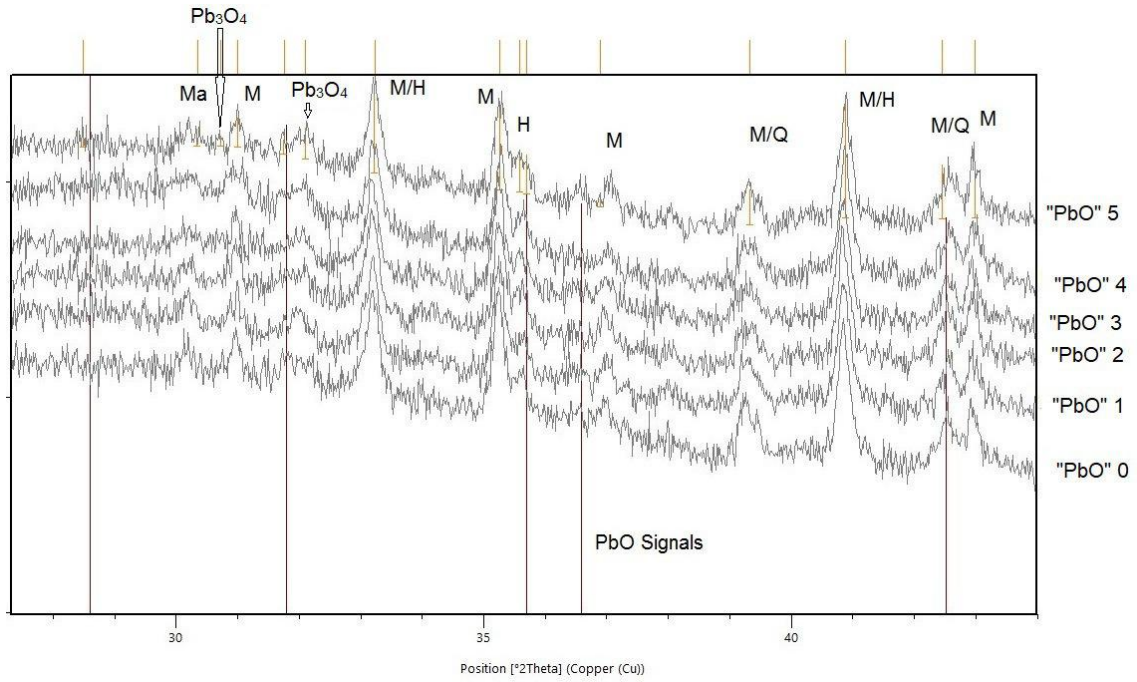


Figure 6.25: Diffractogram of samples with PbO addition; M: mullite, Q: quartz, H: hematite

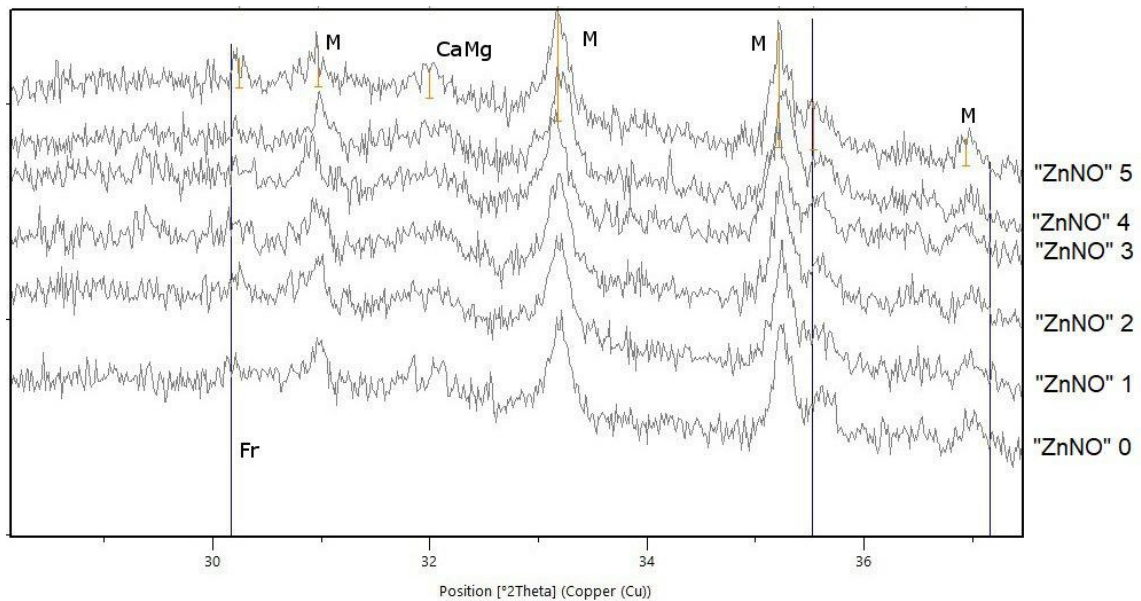


Figure 6.26: Diffractograms of samples with addition of $Zn(NO_3)_2$; Fr: franklinite, M: mullite, CaMg: calcium magnesium silicide

phases. In water as leaching solution, almost no change in the crystalline structure is detected. Moreover, the beforehand detected ZnO phases are still intact. Neither in sulfuric acid nor in hydrochloric acid are these signals apparent.

For the analysis of geopolymers with added PbO only the resulting diffractograms of the sample leached in sulfuric acid are shown (6.29). In HCl and water, similar behavior as with the samples with added ZnO was observed. With increasing concentration of PbO , a fluffy white residue was observed in the leaching solutions. This

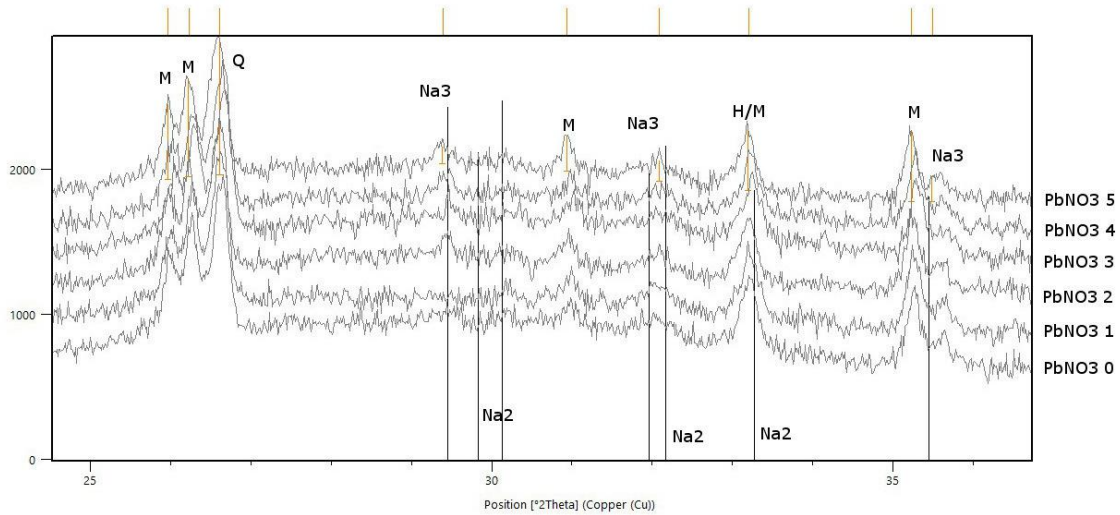


Figure 6.27: Diffractograms of samples with addition of $Pb(NO_3)_2$; Na2: $Na(NO_2)$, Na3: $Na(NO_3)$, M: mullite, Q: quartz

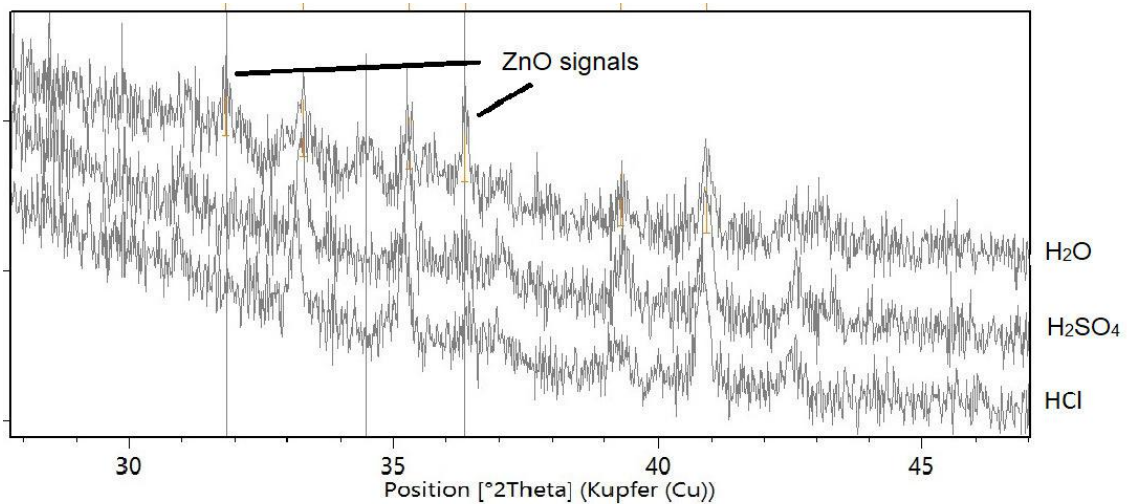


Figure 6.28: Diffractograms of "ZnO" samples leached in HCl, H_2SO_4 and H_2O

residue was analyzed with the rest of the sample and was proved to be crystalline $PbSO_4$. In samples with no ("PbO" 0) or low ("PbO" 2) addition of PbO no reflexes of lead sulfate were detected in the X-ray diffractograms.

The leached samples were compared with the leached fly ash. The resulting diffractograms of samples leached in hydrochloric acid are shown in figure 6.30.

The diffractograms of these four samples show no difference. The beforehand identified phases mullite and quartz are still apparent, no other remaining phases could be detected. In fact, the spectra are completely similar to each other.

The quantitative analysis using 20 % rutile as internal standard, showed between 89 – 94 % amorphous phase for the geopolymers, no matter if nitrates or oxides are added. The in hydrochloric acid leached samples show an amorphous phase of around 78 %.

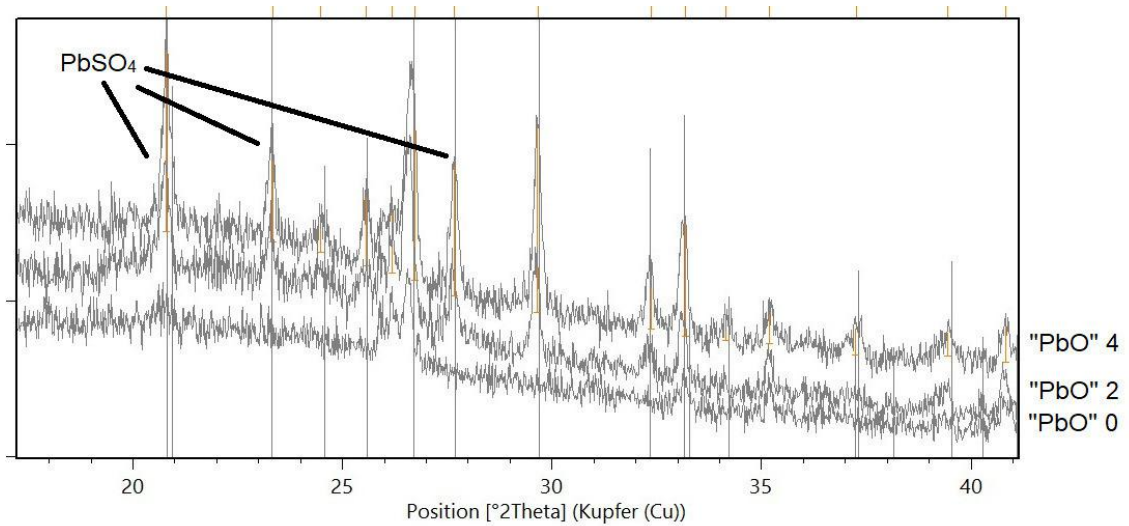


Figure 6.29: Diffractograms of samples "PbO" ("PbO" 0, "PbO" 2 and "PbO" 4) leached in the H_2SO_4

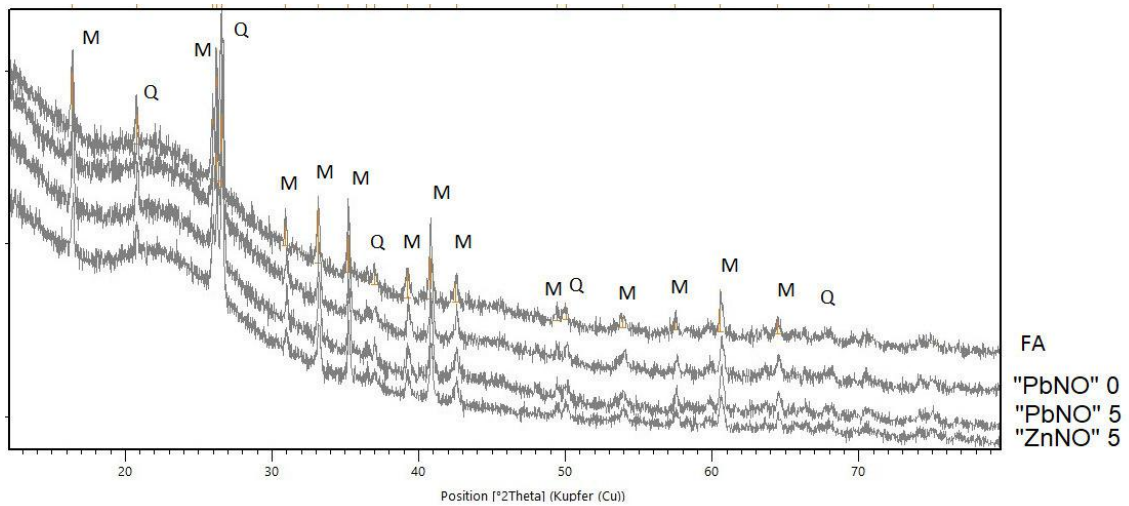


Figure 6.30: Diffractograms of leached fly ash and geopolymer samples "PbNO" 0, "PbNO" 5 and "ZnNO" 5 in HCl ; M: mullite, Q: quartz

6.2.4 Porosity

Mercury intrusion porosimetry (MIP) is used to analyze the pores in the geopolymers with a diameter ranging between $0,005 \mu m$ and $100 \mu m$. At first, the oxides and the nitrates of lead addition are compared (see figures 6.31 and 6.32).

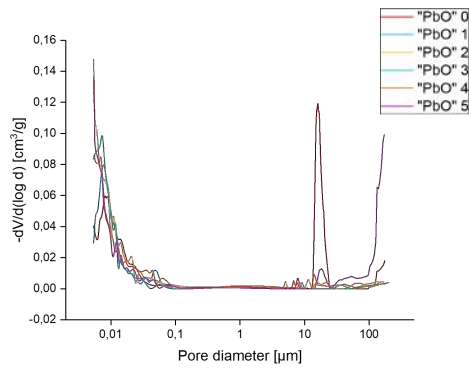


Figure 6.31: MIP of "PbO" 0–5

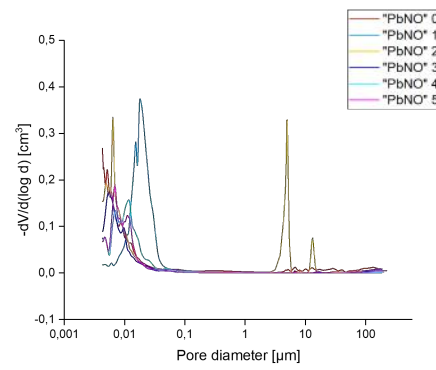


Figure 6.32: MIP of "PbNO" 0–5

All PbO samples show an increased porosity at a diameter of $0,01 \mu m$, however no pores with a higher diameter. The sample "PbO" 0, with no added lead oxide, does show pores with a diameter of over $10 \mu m$. In the nitrate samples, the pore sizes do slightly vary. In sample "PbNO" 3 a high volume is intruded at a pore diameter of $0,04 \mu m$, sample "PbNO" 2 however shows pores at $8 \mu m$ and $12 \mu m$.

To compare the intruded volume of the foamed and not foamed samples, a different representation is chosen (figures 6.33 and 6.34).

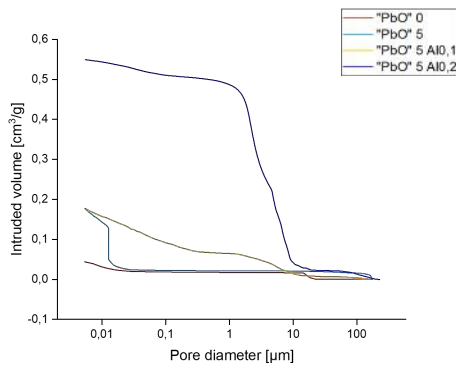


Figure 6.33: Representation of the cumulative intruded volume of sample "PbO" 5

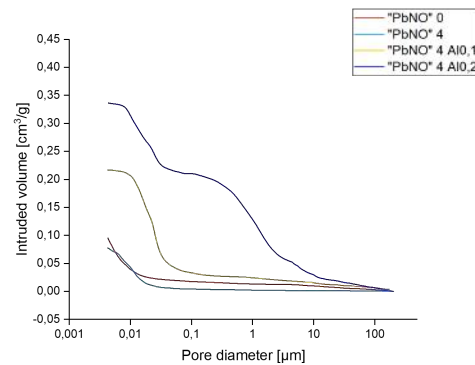


Figure 6.34: Representation of cumulative intruded volume of sample "PbNO" 4

Comparing these two graphs, it becomes clear that the oxide addition leads to a higher cumulative intruded volume, than the nitrate addition. As the preparation of the samples varies slightly, there are differences between the reference sample "PbO" 0 and "PbNO" 0. "PbNO" 0 shows an increase cumulative volume at a pore size of smaller than $0,01 \mu m$.

The cumulative intruded volume increases with the addition of Al-powder. Samples with 0,2% added aluminum powder show a higher porosity than the samples with 0,1% added Al-powder. Interestingly, the samples with lead oxide addition show a different pore size dependency. Mostly pores with a diameter of $10 \mu m$ were detected. In the samples with added lead nitrate smaller pore sizes ($3 \mu m$ and $0,1 \mu m$) are noticed. This leads to a higher totally intruded volume of the foamed

lead oxide samples, (about $0,55 \text{ cm}^3/\text{g}$ compared to $0,35 \text{ cm}^3/\text{g}$).

The resulting MIP measurements of the zinc nitrates are depicted in the following figures.

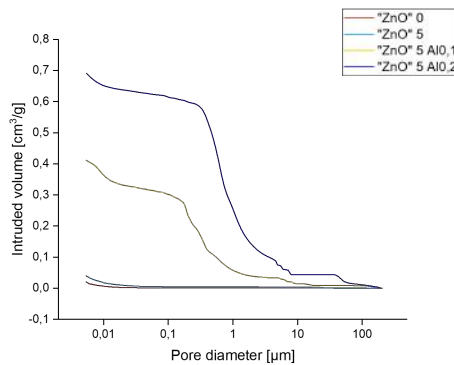


Figure 6.35: Representation of the cumulative intruded volume of sample "ZnO" 5

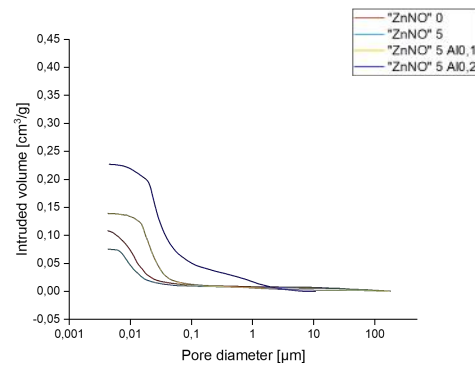


Figure 6.36: Representation of the cumulative intruded volume of sample "ZnNO" 5

Again, the cumulative intruded volume of the nitrate samples is significantly lower than the cumulative intruded volume of the zinc oxide samples. In these samples, however, the oxides show a different pore volume dependency. More pores with a smaller volume are created with the addition of Al-powder.

6.2.5 Leaching tests: Loss of weight

The geopolymers were leached in bidistilled water, sulfuric acid (10 %, 1 mol/l) and hydrochloric acid (3 mol/l). Sulfuric acid and water were chosen because of environmental studies suggest, these conditions simulate environmental procedures. Hydrochloric acid was chosen because of it's ability to dissolve the amorphous matrix in geopolymers. The geopolymers were immersed in the leaching solution in a mass ratio of 1/100 and kept in the closed containers for 28 days. After this time, the solid rest of the geopolymers was filtered through a vacuum flask and then dried at $50 \text{ }^\circ\text{C}$ for 24 hours. The filter was weighed and the mass loss calculated.

The resulting mass percentages are presented in the following tables.

In water In water all zinc oxide samples, foamed and not foamed, show a percentage of 15 % weight loss. Zinc nitrates show a slightly higher weight loss of 12 – 18 % increasing with increasing $Zn(NO_3)_2$ addition. This behavior is the same for foamed and not foamed samples.

Lead oxide addition results in a weight loss of 15 %, too. However, in the samples foamed with Al 0,2 a loss of only 9 % is measured. The nitrates show a slightly lower percentage of 12 % loss for all samples.

Sample	H ₂ SO ₄	HCl	Al 0,1	H ₂ SO ₄	HCl	Al 0,2	H ₂ SO ₄	HCl
"ZnO" 0	44.6	40.0	"ZnO" 0	33.3	64.3	"ZnO" 0	42.3	61.2
"ZnO" 1	37.5	40.9	"ZnO" 1	47.7	75.1	"ZnO" 1	50.7	57.0
"ZnO" 2	38.0	41.8	"ZnO" 2	48.0	56.7	"ZnO" 2	45.7	77.5
"ZnO" 3	35.1	42.1	"ZnO" 3	61.5	57.0	"ZnO" 3	65.1	60.3
"ZnO" 4	37.2	40.9	"ZnO" 4	51.6	57.8	"ZnO" 4	43.9	60.0
"ZnO" 5	34.6	44.4	"ZnO" 5	46.0	62.8	"ZnO" 5	48.2	58.0

Table 6.3: Weight loss of zinc oxides; [ω in %]

In sulfuric and hydrochloric acid In table 6.3 all percentages of the weight loss are given for zinc oxides. Looking at the first three columns the data for the main "ZnO" samples is given. It is apparent that the overall weight loss using HCl as leaching solution is higher than when sulfuric acid is used. However, both acids show higher results than water. In sulfuric acid a decreasing tendency of the weight loss is correlated with a higher concentration of added ZnO. In HCl a slight tendency of an increased weight loss with an increase of ZnO concentration is apparent. Looking at the foamed samples, the weight loss is significantly higher than in the not foamed samples. Again, here an increase of weight loss from ZnO 0 – ZnO 3 in sulfuric acid is observed for both amounts of added alumina. In HCl the highest weight loss of all samples (ZnO 2 Al 0,2) with 77,5% is detected. Otherwise the weight loss in HCl is again higher than in sulfuric acid.

Sample	H ₂ SO ₄	HCl	Al 0,1	H ₂ SO ₄	HCl	Al 0,2	H ₂ SO ₄	HCl
"PbO" 0	48.1	44.1	"PbO" 0	53.8	45.4	"PbO" 0	47.5	39.0
"PbO" 1	42.3	43.3	"PbO" 1	60.4	45.5	"PbO" 1	48.0	43.5
"PbO" 2	40.2	44.0	"PbO" 2	39.7	45.6	"PbO" 2	30.5	40.4
"PbO" 3	44.8	43.7	"PbO" 3	54.0	43.0	"PbO" 3	48.2	41.2
"PbO" 4	42.2	43.5	"PbO" 4	41.7	39.4	"PbO" 4	40.6	40.4
"PbO" 5	42.3	47.0	"PbO" 5	39.9	44.0	"PbO" 5	40.7	42.7

Table 6.4: Weight loss of lead oxides; [ω in %]

Looking at the lead oxide samples (table 6.4), a similar pattern can be observed, however most weight losses fall in between 40 – 50 % which is lower than in the zinc oxide samples. For the not foamed samples no increase or decrease of weight loss tendency can be observed depending on the PbO amount added. Only the reference sample ("PbO" 0) shows a slightly higher weight loss than the samples with added PbO. In the foamed samples, a similar observation can be made. Only sample "PbO" 1 Al0,1 shows a higher value than the rest of the samples.

For samples with added nitrate salts, no foamed samples were investigated. Interestingly, lead nitrate in sulfuric acid shows a negative weight loss and therefore an

Sample	H ₂ SO ₄	HCl	Sample	H ₂ SO ₄	HCl
"PbNO" 0	-17.2	40.8	"ZnNO" 0	-0.7	39.5
"PbNO" 1	-15.5	41.5	"ZnNO" 1	-15.1	45.4
"PbNO" 2	-12.8	42.0	"ZnNO" 2	-4.9	47.3
"PbNO" 3	-17.0	43.0	"ZnNO" 3	0.1	45.7
"PbNO" 4	2.3	41.8	"ZnNO" 4	10.6	45.4
"PbNO" 5	-0.5	43.5	"ZnNO" 5	17.1	43.8

Table 6.5: Weight loss of metal nitrates

increase in weight which means an increase in solid material. Only sample "PbNO" 4 shows a small weight loss and sample "PbNO" 5 a very small increase in weight. In HCl a weight loss of between 41 % and 43 % is observed. Zinc nitrate in HCl shows higher amounts of weight loss, with the highest value of 47 % in the sample "ZnNO" 2. In the samples with a higher concentration of $Zn(NO_3)_2$ the weight loss decreases again. Some samples of zinc nitrate ("ZnNO" 0 – "ZnNO" 2) in sulfuric acid show an increase in weight, like the lead samples. "ZnNO" 4 and "ZnNO" 5 however, do show a weight loss.

6.2.6 Leaching test: ICP-OES analysis

The filtrates of the different samples were analyzed by ICP-OES spectroscopy. Depending on the added salt, either zinc -or lead ions were focused on. The solutions were diluted to minimize the effects of the different matrices.

Samples in water

First of all, the samples which were eluted in water, showed no outward signs of change during the 28 days. The results from the analysis of the eluates confirm the suspected behavior. The leaching in water does not have any significant impact of the geopolymers. The element concentrations of the added ions were so minimal that our method using our ICP-OES analysis was not within the range of the concentrations.

Samples in H₂SO₄

The samples leached in sulfuric acid showed an interesting behavior. The solid samples were partly dissolved and the before colorless leaching solution turned into a bright yellow solution. Moreover, in the samples with added lead ions, a formation of a fluffy white, slightly crystalline phase was observed. The solid geopolymers turned into a colorless gel during the process. During filtration and drying of the filter cake, a gray powder was produced. The filtrates were diluted and analyzed by

ICP-OES. The resulting concentrations can be seen in the following figures.

Samples with lead addition In figure 6.37 a comparison of the foamed and not foamed samples of lead oxides can be seen, in the next figure (figure 6.38) a comparison of the not foamed samples of the lead oxides and lead nitrates can be shown.

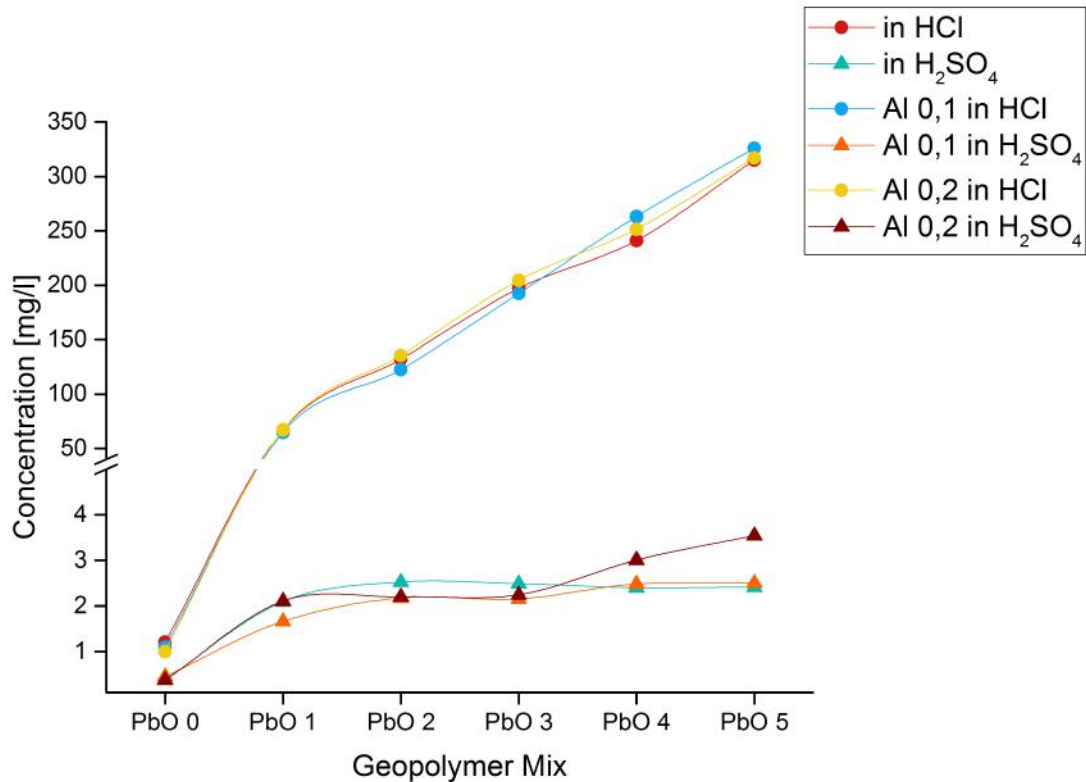


Figure 6.37: Comparison of leaching concentrations in lead samples of foamed and not foamed samples in both leaching solutions (H_2SO_4 and HCl)

It was observed that the foamed samples show the same leaching behavior as the not foamed samples. Moreover, the behavior of lead samples in H_2SO_4 is completely different than the behavior of the same samples in HCl . In sulfuric acid all samples showed a saturation from the first minimal added amount on. It was only possible to detect a leaching concentration of about 2,0 mg/l. The samples "PbO" 4 and "PbO" 5 foamed with Al 0,2 showed a slightly higher concentration of almost 3,0 mg/l.

Samples which were leached in hydrochloric acid showed always higher amounts of leached lead ions. An almost linear correlation between the added amount of lead ions and the leached concentration can be determined.

A comparison between the oxide samples and the nitrate samples shows a slightly higher leaching amount of lead ions in the nitrate samples, at least in HCl as leaching solution. However, in both experimental setups, the correlation is still almost

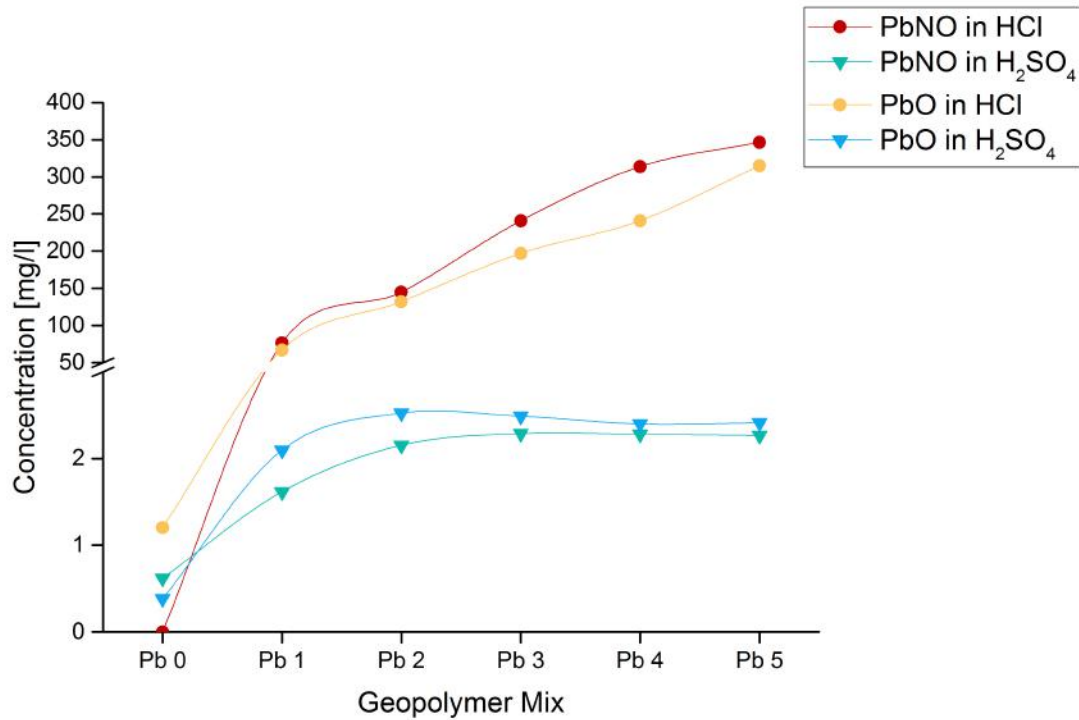


Figure 6.38: Comparison of of leaching concentrations "PbO" and "PbNO" samples

linear, resulting in maxima of 346 mg/l and 315 mg/l respectively. Using sulfuric acid, no huge differences in the leaching amounts were measured. A slightly higher amount in the oxide samples of "Pb" 1 and "Pb" 2 was observed. Calculating the actual percentage amounts of the lead ions in the geopolymer, it can be seen that in HCl about 100 % of the possible amount are leached. A complete overview of the percentage amounts is given in table 6.6.

Geopolymer	"PbNO" in HCl	"PbNO" in H ₂ SO ₄	"PbO" in HCl	"PbO" in H ₂ SO ₄
"Pb" 0	0	0	0	0
"Pb" 1	114	2.4	100	3.1
"Pb" 2	109	1.6	99	1.9
"Pb" 3	120	1.1	98	1.2
"Pb" 4	118	0.8	90	0.9
"Pb" 5	107	0.7	98	0.7

Table 6.6: Weight percentage amounts of leached lead ions; [ω in %]

A comparison of zinc nitrate and zinc oxide samples in HCl and H₂SO₄ is shown in the following figure 6.39.

All samples show a linear dependency of leached ions to the added amount of zinc nitrate or zinc oxide. However, the leached concentrations of the nitrates are considerably lower than the concentrations of the oxides, about 200 mg/l for oxide

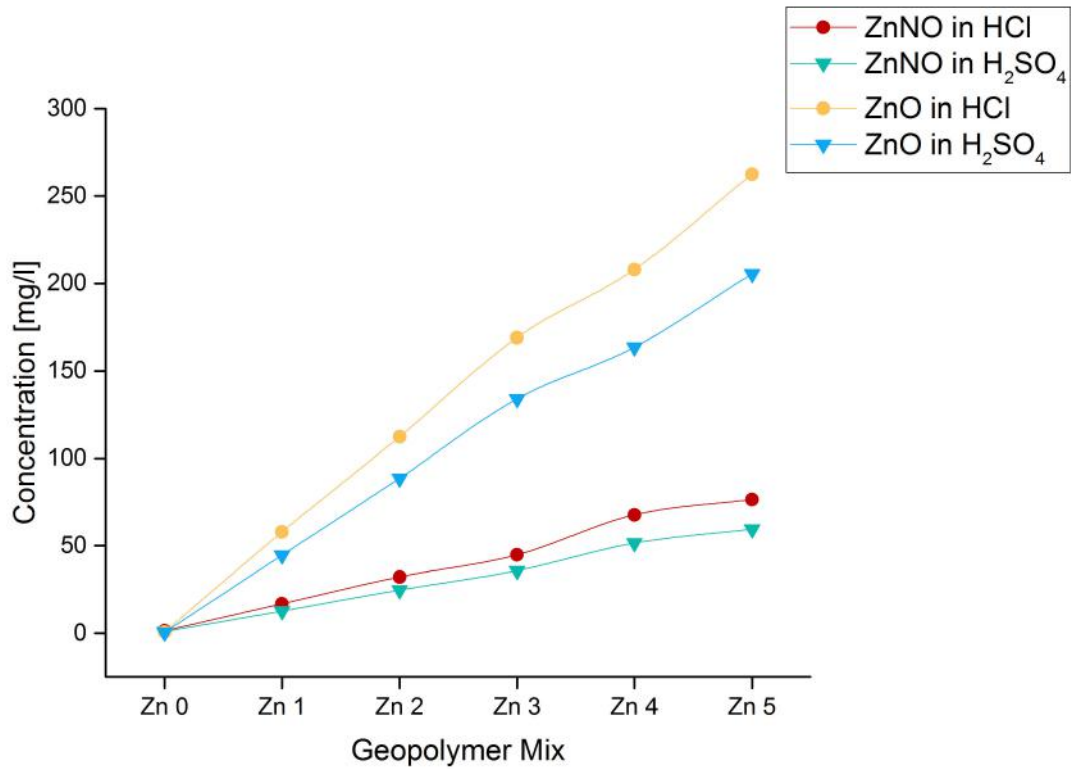


Figure 6.39: Comparison of leaching concentrations of "ZnO" and "ZnNO" samples

samples and 50 mg/l for nitrate samples. The amount of leached zinc in weight percentage is shown in table 6.7.

Geopolymer	"ZnNO" in HCl	"ZnNO" in H ₂ SO ₄	ZnO in HCl	ZnO in H ₂ SO ₄
"Zn" 0	0	0	0	0
"Zn" 1	42.1	31.7	86.7	66.9
"Zn" 2	40.3	30.8	84.2	66.4
"Zn" 3	37.3	29.8	84.5	67.0
"Zn" 4	42.3	32.2	78.0	61.3
"Zn" 5	39.6	30.7	81.8	63.7

Table 6.7: Weight percentage amounts of leached zinc ions

The amounts of zinc nitrates are lower than the amounts of zinc oxides. In HCl for zinc nitrates about 40 %, for zinc oxide 83 %, in sulfuric acid 31 % and 65 % respectively.

6.3 Discussion

6.3.1 Structural analysis

Lead addition

In our diffractograms of lead doped geopolymers no phase corresponding to Pb_3SiO_5 was observed. However, in the samples with 5% addition of lead oxide, a signal at $\approx 332\theta$ was found which was set as Pb_3O_4 . In the samples with lead nitrate addition, no signals correlating to lead were found, however sodium nitrate signals were determined. This would suggest an inclusion of the lead in the amorphous phase as it was suggested a couple of times in literature.²⁸ Moreover, apparently not all lead oxide was dissolved during the reaction but some seemed to be physically bound in the matrix and could be detected as lead oxide. In the element mappings of "PbO" samples, a homogeneous distribution of lead was found throughout the matrix, however in the samples with lead nitrate addition, some spots with a higher concentration of lead were found. Apparently, when lead is fused into the matrix, it builds up clusters which cannot be detected using XRD technique. Interestingly, no changes in the IR spectra of lead oxides could be determined.

In the samples of lead nitrate however, the lead seems to have a profound influence. A strong signal of sodium nitrate at 1380 cm^{-1} was detected underlining the findings during XRD measurements. The decreasing intensity of the Si-O-T signal at 1000 cm^{-1} and the shift to higher wavenumbers (1005 ("PbO") to 1015 ("PbNO")) would suggest an increase in the Si/Al ratio and a lesser crystalline phase.^{24,54} An increase in the Si/Al ratio correlating to a higher amount of lead ions leads to less alumina in the network which might result in a lesser compressive strength value. This was also observed in some experiments looking at the compressive strength of lead doped geopolymers.^{24,83} In our measurements of the compressive strength for lead oxides (see section 9.2.4) a clear increase was observed, for the lead nitrates however, a decrease in compressive strength was observed. The porosity of the geopolymers increased slightly when "PbO" was added but remained the same with the addition of lead nitrate. Foaming agents did increase the porosity but in the samples with added lead nitrate, the increase was less profound than in the samples of lead oxide. As lead nitrate is more involved in the geopolymer network it seems that it hinders the alumina powder to react as strongly as in not doped geopolymers.

Zinc addition

In the samples doped with "ZnO", a steadily increasing signal of ZnO was observed in the diffractograms of "ZnO" 0 – "ZnO" 5 which supports the idea of an only

physically bound ZnO particle in the geopolymer. As a ZnO particle was found in the SEM micrographs, the conclusion can be drawn that ZnO does not dissolve during the reaction and is simply immobilized in the matrix. No influence of ZnO on the porosity of the foaming behavior was observed. In the IR spectra, an increase in the NBO's vibrations and an increase in the sodium carbonate signal were observed with a higher concentration of ZnO. It seems that the addition of ZnO hinders the formation of a continuously homogenous amorphous matrix in the geopolymers by building physical barriers.

The addition of zinc nitrate into the mixture, did not lead to any signals of ZnO, however signals of a zinc iron oxide (franklinite) were found in the diffractograms. As iron is apparent in fly ash in the amount of 5 % a reaction to a zinc iron oxide is possible, however so far not mentioned in literature. The IR spectra show a strong signal of sodium nitrate at 1380 cm^{-1} and the asymmetrical stretching vibration of Si-O-T at 1015 cm^{-1} . Otherwise no shift could be detected. The intruded volume in the zinc nitrate samples is slightly decreasing with the amount of added zinc nitrate. It can be concluded that zinc nitrate is also distributed in the amorphous matrix, underlined by SEM micrographs, but does not have such a strong influence onto the structure as lead doped samples.

6.3.2 Leaching behavior

In acidic environments, the formation of monomers, dimers and trimers is kinetically favored. Moreover, a gel phase can be observed which most likely consists of silicic acid which is most stable at a pH 2–3. However, this acid can form colloidal particles or a gel. Different other reactions can take place if geopolymers are immersed in acids.

- Formation of silicic acid gel (SiOH groups form siloxane bonds)¹⁹
- Replacement of cations (Na⁺, K⁺) by H⁺²⁵
- Attack of aluminosilicate framework²⁴

The third possibility would lead to a mass loss of the geopolymers, which is observed in our research. The not foamed samples which were subjected to HCl treatment showed a mass loss of about 40 %. In the foamed samples, however an increasing weight loss with an increasing cumulative volume from MIP is observed. The addition of 0,2 % Al-powder leads to the highest observed values in weight loss, while it also shows the highest intruded volume in MIP measurements. Zinc oxide samples show a higher weight loss than lead oxide samples, where the percentage

stays at 40 %. This leads to the conclusion that the matrix is stabilized with the addition of lead oxide samples even if the surface which can be attacked (due to increased porosity through foaming agents) is higher. Almost 80 % are dissolved in the sample "ZnO" 0 Al0,2 which shows that only 20 % crystalline material and fly ash residue remain. In other words a turnover rate of almost 80 % during the geopolymerisation reaction is achieved. According to Fernández-Jiménez et al.⁴², the insoluble residue after HCl attack consists of unreacted ash (vitreous phase, mullite, and quartz).⁴² The residue was also examined using X-ray diffraction which showed mullite and quartz at exactly the same signals as in leached fly ash (see figure 4.4). Moreover, the IR spectra of in HCl leached fly ash and in HCl leached geopolymers show the same Si-O-T band at 1105 cm^{-1} . Furthermore, the topographic images taken by SEM show only loose fly ash particles in the residues of in HCl leached geopolymers (see figures 6.8b and 6.10). These results confirm the suspected dissolution of the amorphous, geopolymeric matrix leaving only unreacted fly ash phases.

Comparing the results of the mass loss in sulfuric acid, it is noticed that the percentage is lower than in HCl. However, an increase in the samples of added zinc oxide in the weight loss with increasing porosity is observed. This underlines the conclusion that the higher surface leads to a better accessibility of the built matrix. Looking at the samples with added lead oxide a slight decrease in weight loss from samples foamed with Al 0,1 to Al 0,2 is seen. However, the lead nitrates show an increase in weight which indicates the formations of a new solid material. The diffractograms of these samples show the crystalline phase of PbSO₄ which is formed by leached lead ions and the sulfate ions from the sulfuric acid. As no new crystalline phases in the samples of "ZnNO" but a weight loss is detected, a different mechanism seems to take place. As lead and sodium ions are leached from the geopolymer, it is possible that the protons of the sulfuric acid fill in for the cations, thereby stabilizing the matrix. In the SE micrographs of samples leached in sulfuric acid (see figures 6.8c and d) a broken geopolymeric matrix is observed. The photograph of "PbO" 4 shows a crystalline material on top of the matrix, in contrast the image of "ZnO" 4 shows no such crystalline (PbSO₄) material. In this sample, a matrix which looks partly intact, partly destroyed is depicted. It can be concluded that through the leaching the matrix is either partially destroyed or firstly destroyed and then partly built again using the H⁺ ions.

The analysis of the concentrations of Pb²⁺ and Zn²⁺ ions in the filtrate in the ICP-OES show first of all, no difference between foamed and not foamed samples. As in table 6.6 shown, in the case of leaching concentration in HCl already 100 % are leached. Therefore, it is not possible to get higher results in the leaching concentration of the foamed samples. In sulfuric acid, only about 2 % of the possible amount

are leached and the same results are gained for the foamed samples. In these cases however, the leached lead ions form crystalline PbSO₄. It may be concluded that at a concentration of 2 mg/l in the filtrate enough lead is apparent to crystallize.

A comparison of zinc oxide and zinc nitrate shows that zinc oxide is leached in 2 times higher concentrations than zinc nitrate, which is the case in both leaching solutions. In HCl however, the amounts are significantly higher. As ZnO is not dissolved during the geopolymerisation reaction and still detectable as ZnO in XRD and SEM, the high amounts suggest that the ZnO particles are physically bound to the geopolymer matrix and as the matrix is dissolved, the ZnO particles lose their connection, dissolve in the acidic media and can be detected in the filtrate. Interestingly, no difference between the foamed and not foamed samples can be seen, all three show a leached percentage in HCl of 82%. Zinc nitrate shows no difference in foamed and not foamed samples as well, but the leached percentage in HCl is only at 40%. With regard to this lower amount it can be theorized that the nitrates are chemically bound and located in the 60% of the geopolymer which are not affected by the acidic attack. As no crystalline phase can be seen in the X-ray diffractograms, a crystallization reaction is not probable. The SEM images of the zinc nitrates show a complete homogeneous distribution of the zinc ions in the geopolymer. Therefore, it might be concluded that the zinc nitrates remain in the amorphous matrix and stabilize this matrix through chemical bonds.

Zinc nitrates in sulfuric acid show an even lower percentage of detected zinc ions in the filtrate, 31% not depending on the added amount. As the matrix of the geopolymer is not completely dissolved as in HCl as leaching solution, the lower percentage is quite expected.

Looking at the IR spectra of the leached zinc nitrate samples, the appearance of the resulting bands in HCl look quite the same as in the original sample, only shifted towards higher frequencies. In the work of Rees⁵⁴ a shift to higher wavenumbers is connected to an increase in the vibrational force constant.^{51,54} Bakharev²⁴ observed a similar shift in leached samples and connects it to an increase in the Si/Al ratio and hence to the dealumination process during leaching.²⁴ He concludes that the size of the shift is connected to the strength of the acid in attacking the geopolymer network. In our research the shift of the Si-O-T band is quite similar in both leaching solutions. Nevertheless, there are significant differences. In sulfuric acid two signals are detected and the beforehand only as shoulder noticeable asymmetrical stretching vibration of the Si-O-Si band becomes more clearly. This is the case for all samples, especially the nitrate samples. The band of the ν_{as} Si-O-Al decreases in intensity. This underlines the theory of the dealumination in the leaching solutions. No difference in the shift depending on the amount of added lead nitrate is observed.

In the samples with added zinc nitrate, the highest intensities are observed for sample "ZnNO 3", with sample "ZnNO 5" showing almost no sign of destruction of the geopolymer matrix. In the zinc nitrate samples leached in HCl, the band of ν_{as} Si-O-Al disappears almost completely whereas the band of ν_{as} Si-O-Si increases. The spectra of the oxides show only a broad band between $1000 - 1200\text{ cm}^{-1}$. No transmission signals in this region could be measured. Therefore, it can only be speculated that the matrix in these cases was destroyed completely, not depending on the amount of added lead oxide.

In the lead nitrate samples leached in HCl, the stabilization of the matrix with the addition of lead is even more pronounced. In the samples with a low addition, a complete destruction of the amorphous matrix is observed in the IR spectra. No broad band is detected, but a sharp signal at 1100 cm^{-1} . In the samples with a higher added amount a "normal", broad amorphous band is detected. These results suggest that the nitrates are chemically bound to the matrix and stabilize the amorphous phase against the acidic attack.

6.4 Conclusion

From our structural analysis (SEM, IR spectroscopy and XRD) we conclude the following:

- The addition of lead oxide leads to the formation of Pb_3O_4 .
- Lead -and zinc oxide do not dissolve completely within the reaction but are still detectable in the geopolymer.
- Sodium nitrate is formed with the addition of metal nitrates.
- Increase in the Si/Al ratio is correlating with increase in lead nitrate addition.
- Metal nitrates hinder the reaction with aluminum powder which results in a lesser porosity. Lead nitrate hinders the reaction to a greater extent.
- The addition of zinc nitrate leads to the formation of zinc iron oxides which are detectable in XRD.

Our leaching experiments and the analysis of the residues of the geopolymers including the weight loss analysis lead us to the following conclusions:

- Geopolymers without foaming agents show a weight loss of 40 % in hydrochloric acid for both metals in sulfuric -and hydrochloric acid.

- If the geopolymers, doped with metal oxides, are foamed with aluminum powder a weight loss of 80 % in hydrochloric acid can be achieved. Hence, the maximal turnover rate in this reaction is 80 %.
- The analyzed residues after leaching show exactly the same XRD and IR signals as the residue of leached fly ash.
- The geopolymer samples with added lead nitrate and then leached in sulfuric acid form $PbSO_4$ if a concentration higher than 2,0 mg/l is apparent in the leaching solution
- The concentration of leached zinc is 2 times higher from samples with added zinc oxide than zinc nitrate. Zinc oxide is only physically imbedded in the matrix, zinc nitrate however is chemically bound.
- During leaching a dealumination of the geopolymer is detected in both leaching solutions.
- A stronger Si-O-Si signal is detected in leached samples with added metal nitrates
- Lead oxide shows a lesser stabilization of the geopolymer matrix than lead nitrate if the geopolymer is exposed to acidic attack.

Leaching experiments have proven very helpful in understanding the chemical behavior of geopolymers. In our further research, we will focus on the variation of the Si/Al ratio and the influences this ratio has on the inclusion of lead and zinc nitrates in geopolymers.

7 Variation of the Si/Al ratio and addition of Pb^{2+} and Zn^{2+}

In this fourth part of the thesis, a varying Si/Al ratio is investigated. In addition of this variation, lead nitrate salts and zinc nitrate salts are added to the geopolymer during the synthesis. Focus will be laid onto the structural differences of the geopolymers with and without addition of metal nitrates. Moreover, the acidic resistance of the samples will be measured using the described static leaching tests. Differences of the stability of the matrix can be assumed, depending on the Si/Al ratio and the added metal nitrate salt.

7.1 Materials and Methods

Geopolymer synthesis

Geopolymers were synthesized with a varying Si/Al ratio but a steady l/s ratio of 0.5 and a Si/Na ratio of 0.6. As dry component fly ash and SIKALON were used, activating solution and water were added as liquid components to the mixture. The composition of the samples can be seen in table 7.1.

Activating Solution

The activating solutions were prepared using 39T and a specific amount of NaOH pellets which were dissolved in the sodium silicate solution (see table 7.2). The

Sample	Si/Al ratio	SIKALON [ω in %]	fly ash [ω in %]	H ₂ O [ω in %]
F10	2.0	16	100	4
F15	2.2	18	100	9
F20	2.4	25	100	12
F25	2.6	33	100	18
F30	2.8	43	100	22
F35	3.0	54	100	28

Table 7.1: Composition of geopolymers, the amount of fly ash is set as 100 %; AL:activating solution

Sample	F10	F15	F20	F25	F30	F35
NaOH [ω in %]	25	20	15	10	5	0

Table 7.2: NaOH added to 39 T

Sample	Si/Al ratio	SIKALON [ω in %]	H ₂ O [ω in %]	MNO _{aq} [ω in %]
F10 "MNO"	2.0	16	1	9
F15 "MNO"	2.2	18	1	9
F20 "MNO"	2.4	25	5	9
F25 "MNO"	2.6	33	11	9
F30 "MNO"	2.8	43	15	9
F35 "MNO"	3.0	54	22	9

Table 7.3: Composition of geopolymers with added metal nitrates, the amount of fly ash is set as 100 %; AL:activating solution, M: Pb or Zn

activating solutions were stirred for 24 h. SIKALON was added directly to the geopolymer mix as a dry component.

Geopolymers with metal nitrates

The synthesis of the geopolymer with the addition of metal nitrate salts was slightly different. The same Si/Al ratios were used and the l/s ratio was set to 0.51 due to preparation problems. 250 g of metals nitrate powder were dissolved in 300 ml water. These solutions were added to the mixture. The composition of the activating solutions did not change but the amount of added water was adjusted. A water free lead nitrate was used, however $Zn(NO_3)_2 \cdot 6H_2O$ was used as zinc nitrate. The exact compositions can be seen in table 7.3.

7.2 Results and Discussion

7.2.1 Structural analysis

Geopolymer samples were analyzed using XRD, IR and SEM after the setting time was completed.

X-ray diffraction

The original samples were analyzed using X-ray diffraction spectroscopy as a qualitative and a quantitative method. Therefore, different procedures were used, as explained in the introduction. Rietveld quantification was used to determine quantitatively the amorphous phase.

The not leached samples showed the phases mullite and quartz as main phases, as was expected. Moreover, in some samples, starting with F25 (Si/Al ratio = 2.1) more crystalline components were found. The diffractograms of samples F25 – F35 are shown in the following figure (see figure 7.1).

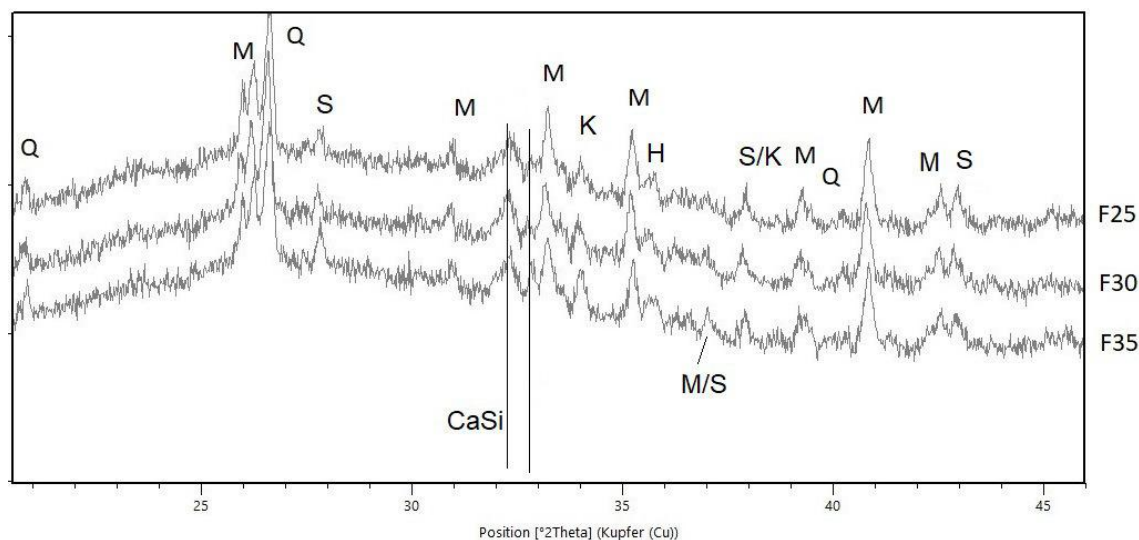


Figure 7.1: XRD of samples F25, F30 and F35; M: mullite, Q: quartz, S: aluminum silicate (Al_2SiO_5) K: potassium magnesium silicate ($K_2(MgSi_5O_{12})$), CaSi: calcium silicate

The mullite and quartz signals are also apparent in fly ash as raw material. These crystalline phases do not take part in the geopolymer reaction and are still present in the geopolymers. In samples starting with F25 other phase were found, namely aluminum silicate, potassium magnesium silicate and calcium silicate. These phases start appearing when the $n(Si)/n(Al)$ ratio is higher than 2.6. The signal of the CaSi phase enhances in higher ratios with the formation of a second, less intense signal (peak at $32.85^\circ 2\theta$). It seems, these phases are connected with the geopolymer reaction and are build as crystalline components. This would also explain why the highest amorphous amount was observed for F20 with 95 %. The lowest value was found for F35 (89 %). With the addition of zinc nitrate, the amorphous amounts were in between 89 % and 93 % and for samples with addition of lead nitrate between 92 % and 94 %. However, these changes are so small that there cannot be a trend concluded from these values. The lesser values for samples with added nitrate salts are simply due to the formation of $NaNO_3$. Only sample F35 shows a "significant" increase of 5 % (4 %) in the amorphous phase if lead nitrate (resp. zinc nitrate) is added. Therefore, it seems in this case the addition of nitrate salts leads to a slight increase of the amorphous phase.

Figure 7.2 shows a comparison of F25, F25 "PbNO" and F25 "ZnNO". Hereby, the influences of the added nitrates are shown. It can be seen that the mullite and

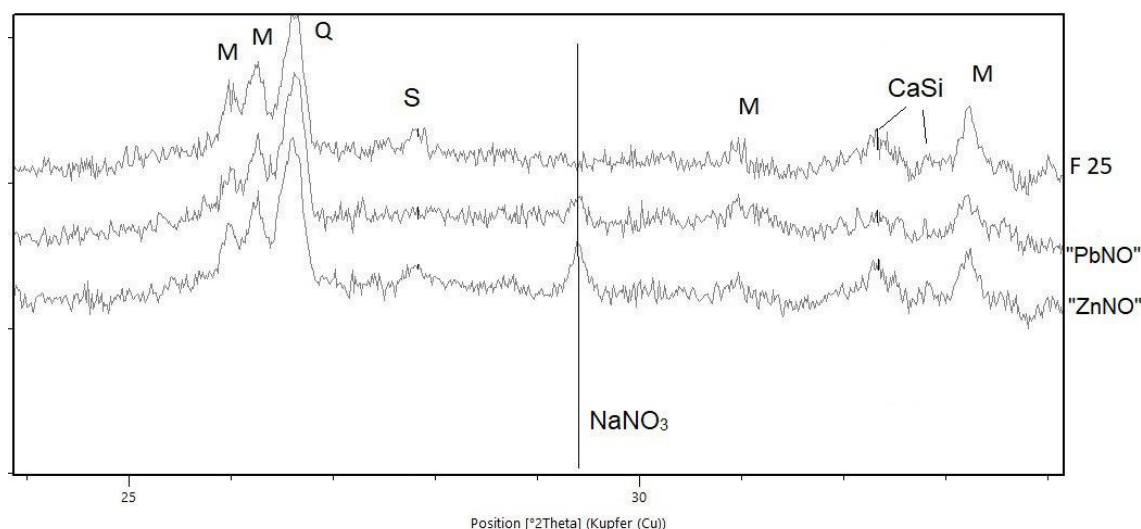


Figure 7.2: XRD of F25, F25 "PbNO" and F25 "ZnNO"; M: mullite, Q: quartz, S: aluminum silicate (Al_2SiO_5), CaSi: calcium silicate, $NaNO_3$: sodium nitrate

the quartz phase do not change. The aluminum silicate phase, however, disappears in samples with added lead nitrate. With the added amount of nitrates, sodium nitrate is also found as crystalline component. This suggests, that the building of the aluminum silicate and the phase, which takes place during the geopolymer reaction, is disturbed by the presence of the lead ions. As lead and zinc influence the geopolymer matrix and the reaction in different ways, it is our suggestion that the inclusion of lead into the amorphous matrix influences the Si/Al ratio and therefore hinders the formation of the aluminum silicate phase.

IR Spectroscopy

First of all, samples F10 – F35 are depicted in the following figure 7.3. In the right figure (figure 7.3b)) a comparison of F10 – F35 with the addition of $Pb(NO_3)_2$ can be seen.

Both figures show only the range between 1800 cm^{-1} and 250 cm^{-1} . Other signals detected in the IR spectra, at 3250 cm^{-1} and 2350 cm^{-1} are due to $-OH$ and CO_2 vibrations.^{51,52} The here observed signals can be matched to stretching bending vibrations of Si-O-Si and Si-O-Al according to table 2.2.

Not connected to the Si-O-T vibrations is the signal 1620 cm^{-1} ($\delta - OH$), at 1380 cm^{-1} which is due to NO_3 stretching vibrations and the bands at 1450 cm^{-1} and 1410 cm^{-1} which come from Na_2CO_3 and $NaHCO_3$ respectively forming on the surface of the geopolymer.⁸⁴

The nitrate band is only apparent in samples with the addition of zinc or lead nitrate. In these samples, however the carbonate band decreases. A comparison of the samples F25, F25 "ZnNO" and F25 "PbNO" is shown in figure 7.3c. The

observed shifts of the asymmetric stretching vibrations of Si-O-T are shown in figure 7.3d.

It is to keep in mind that a shift to a higher wavenumber of the asymmetric stretching band of Si-O-T is connected to a dealumination process in the sample. A shift towards lower wavenumbers is therefore a sign for the inclusion of alumina into the lattice. This behavior can be explained by a higher force constant which is the case in Si-O bindings rather than in Al-O bindings. A higher force constant always implies higher wavenumber and thus a lower wavelength.^{50,54}

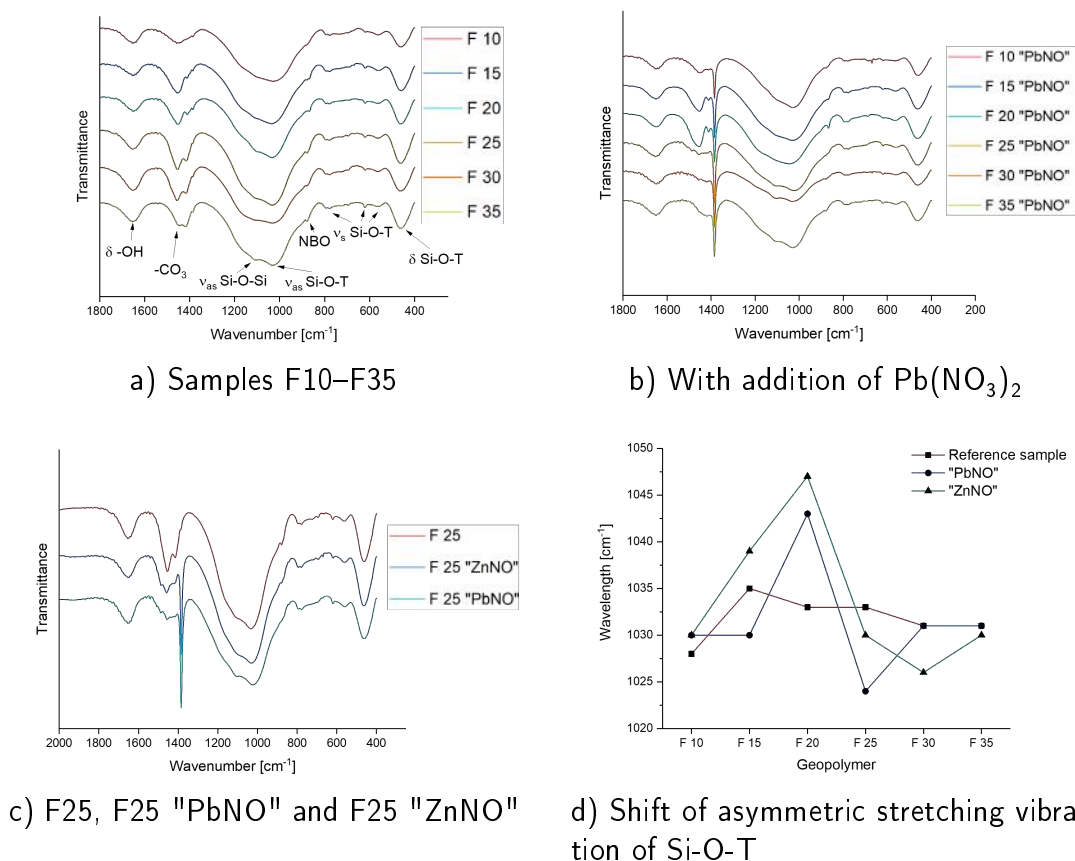


Figure 7.3: IR spectra of F10-F25; a) Samples F10-F35, b) With addition of $Pb(NO_3)_2$, c) F25, F25 "PbNO" and F25 "ZnNO", d) Shift of asymmetric stretching vibration of Si-O-T

A comparison of sample F25 shows that with the addition of the nitrates no specific new bands, which connect to the geopolymer structure, are created. However, the appearance of the band at 1100 cm^{-1} changes slightly in the means that the signal of ν_{as} Si-O-Si increases slightly. At the same time, the shoulder at 880 cm^{-1} becomes less sharp. This may lead to the conclusion that the presence of the lead -and zinc nitrate changes the structural behavior depending on the Si/Al ratio. It increases the Si-O-Si bonds which would suggest a decrease in the non-bridging-oxygens.

The shift of the asymmetrical stretching vibration of Si-O-Al is also strongly de-

pendent on the Si/Al ratio. In the samples without addition of metal nitrates, a shift from sample F10 to sample F15 from 1028 cm^{-1} to 1035 cm^{-1} is observed. Afterward, the samples show a decreasing wavenumber down to 1031 cm^{-1} for sample F35. This behavior suggests firstly a lesser inclusion of aluminum ions into the matrix (Si/Al = 2.0 to 2.2), followed by a slight increase of inclusion. However, it can be said that sample F10 with a Si/Al ratio of 2.0 shows the highest amount of alumina in the geopolymer matrix. Furthermore, sample F10 shows the smoothest line in the IR spectra with increase in sharpness with an increasing Si/Al ratio. These findings correlate well with the observed trends in the XRD diffractograms, showing an increase in crystalline phases from sample F25 to sample F35. Furthermore, in the spectra of sample F35 a second small signal at 1111 cm^{-1} is observed, signaling the formation of more Si-O-Si bonds.

For samples F10 and F35 only a shift of two, respectively 1 cm^{-1} is observed with the addition of metal nitrates. A shift in this ratio might be due to the experimental error in IR spectroscopy. However, for zinc nitrate, it fits well into the observed behavior of the following ratios, in which an increase in wavenumber up to 1047 cm^{-1} for sample F25 is observed. In these ratios of 2.0, 2.2 and 2.4 it seems zinc nitrate facilitates the formation of Si-O bonds. In samples with a higher ratio, F25 – F35 it apparently facilitates the formation of Al-O bonds as the wavelength of the peak shifts to frequencies below the reference sample. For zinc nitrate addition a minimum in frequency is achieved in sample F30 with a value of 1026 cm^{-1} .

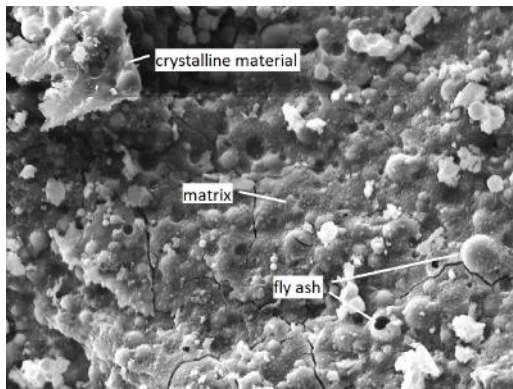
Only in sample F20 lead nitrate facilitates the formation of Si-O bonds as in this sample the only shift to higher frequencies (up to 1043 cm^{-1}) is observed. In all other samples, lead nitrate promotes the formation of Si-O-Al bonds. The minimum frequency of 1024 cm^{-1} observed for sample F25 with a Si/Al ratio of 2.6.

We can conclude, that in samples with a high Si/Al ratio (2.6, 2.8 and 3.0) the addition of metal nitrates leads to a better inclusion of aluminum into the geopolymer matrix. This behavior is observed to a greater extent in samples doped with zinc nitrate. Moreover, it can be said that the built structure in sample F20 is strongly influenced by the presence of metal nitrates.

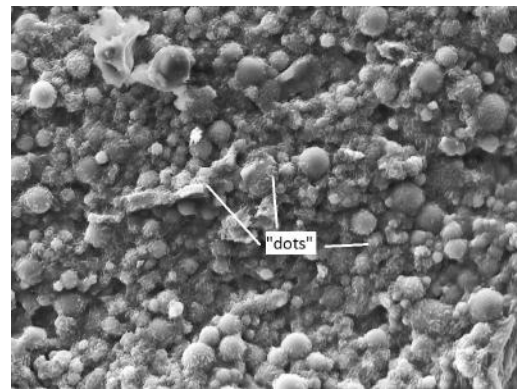
Scanning Electron Microscopy

Samples were analyzed using SEM technology. To get an impression as to how the Si/Al ratio influences the topography of the geopolymer all samples in a resolution of 2000 x are shown in the following figure 7.4.

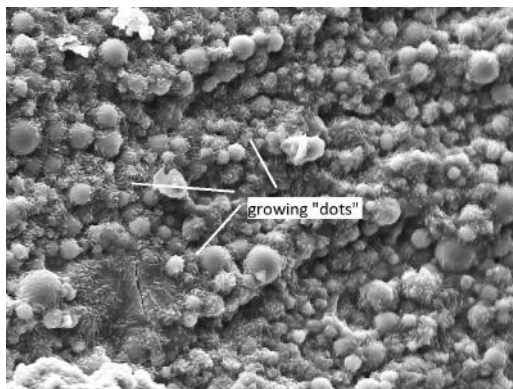
These are exemplary photographs of the samples, however the topography of these samples was very homogenous. Between the samples a change in the topography is visible. In all samples, the not reacted fly ash particle spheres are visible. In figure



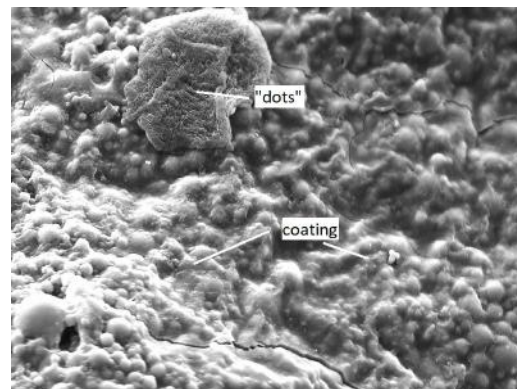
a) F10 showing fly ash spheres and geopolymer matrix



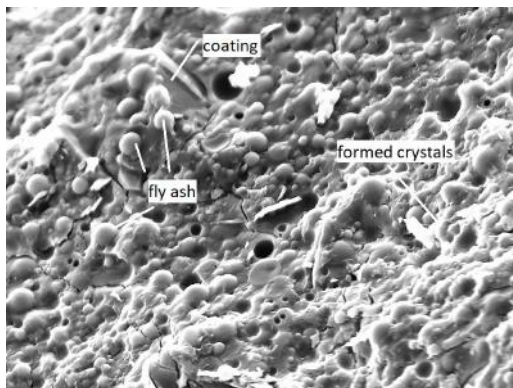
b) F15 showing small "dots" on top of the matrix and fly ash residues



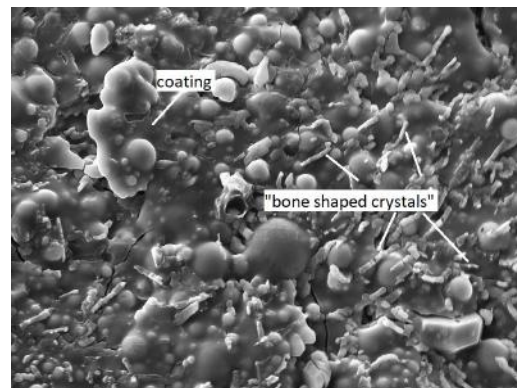
c) F20 showing growing "dots"



d) F25 showing "dots" and a growing coating



e) F30 showing formed coating and growing crystals



f) F35 showing "bone like crystals" and broke down coating

Figure 7.4: SEM images of samples F10–F35, Magnification of 2 kx

7.4a, the sample with the lowest Si/Al ratio, small dots on top of the matrix are visible. These dots increase in size in samples F15 and F20. In sample F25 (figure 7.4d) it looks like these dots form a connected coating, which is also apparent in figure 7.4e. In the SE micrograph of sample F35, however, the coating seems to have broken down and instead bone formed crystals are observed.

Looking at the element mappings taken of samples with the addition of $Zn(NO_3)_2$

and $Pb(NO_3)_2$, a similar pattern to previous research is detected. Both metal nitrates show a homogenous distribution throughout the matrix. No metal signals however, can be detected from the residues of the fly ash spheres. In figures 7.5 and 7.6 the taken images of samples F15 and F30 are shown.

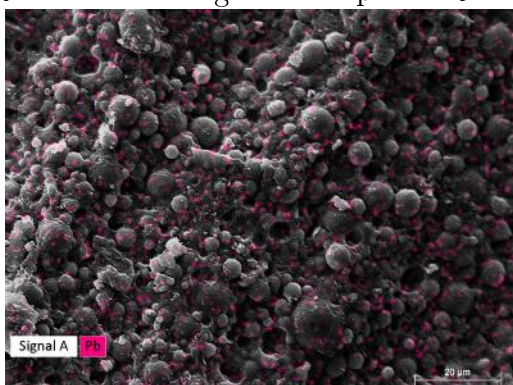


Figure 7.5: F15 "PbNO", red shows lead included and distributed throughout the matrix

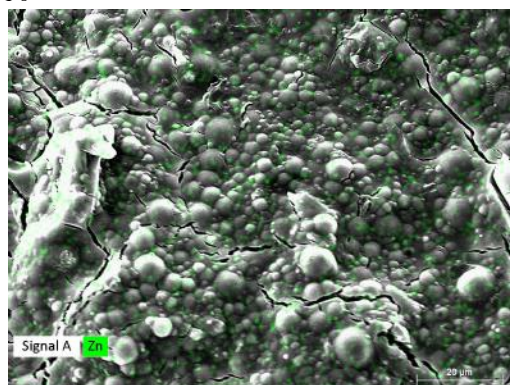


Figure 7.6: F30 "ZnNO", green shows zinc distributed throughout the matrix

7.2.2 Leaching tests

Leaching tests were conducted using the static leaching method. Thereby, the sample is left in the leaching solution (HCL and H_2SO_4) for a specific time (28 days) and is then analyzed. In our case, leaching solution and sample were filtered and then the residue was dried and prepared for analysis (XRD, IR and SEM). The filtrate was examined using ICP-OES.

ICP-OES

For ICP-OES analysis, the filtrates were diluted and HNO_3 was added, thus minimizing the effects of the different leaching solutions. The percentage of the leached metals (Pb^{2+} or Zn^{2+}) was determined and is shown in figure 7.7.

Samples with added lead nitrate show the highest leaching percentages in hydrochloric acid. A maximum of almost 120 % was calculated, however slight mistakes in preparation and measurement can explain this too high ratio. Samples F15, F20, F30 and F35 show a complete leaching of the added lead ions. Sample F25 shows only a percentage of 66 % and sample F10 only 7 %. As previous research showed, HCl has the ability to destroy the amorphous matrix in geopolymers^{24,37,42}. However, in contrast to previous experiments, no silica gel was found to precipitate during leaching time. The samples in HCl stayed outwardly intact. Sample F10 with a Si/Al ratio of 2.0 and, as we have shown previously, the highest amount of bound alumina seemed to be most stable against the acidic attack. Also, sample F25 which shows a minimum in the Si-O-T asymmetric stretching vibration and

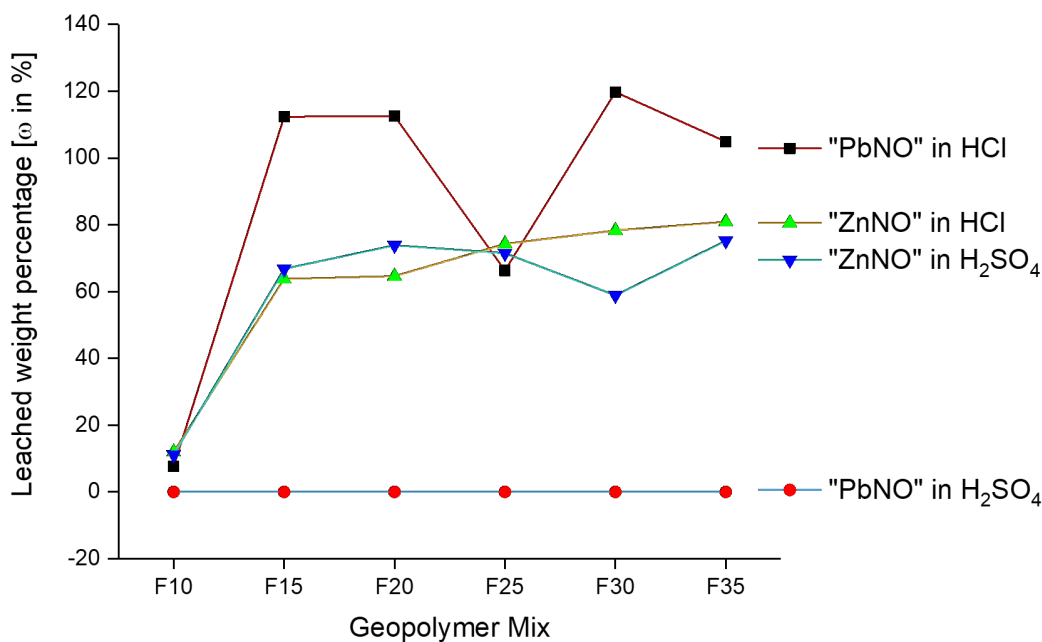


Figure 7.7: Comparison of resulting leached weight percentages of F10–F35 using ICP-OES

therefore, a high amount of bound alumina if the sample is doped with lead nitrate, shows a high stability.

Looking at the amounts of zinc leached in HCl, an even lower percentage was calculated. A maximum leaching amount of 80 % was found. Almost the same behavior is observed in the sulfuric acid environment. Hereby, a maximum of 75 % for sample F35 was found. Only sample F30 shows a lower leaching value of 59 % which is out of line. Sample F10, however shows again the by far lowest value of about 11 %. Furthermore, zinc is bound more strongly than lead in the geopolymer matrix.

Lead nitrate samples leached in sulfuric acid did not show any measurable concentration of lead in the ICP-OES analysis. However, this is due to the formation of lead sulfate leading to a maximum concentration of lead in the filtrate of 2,0 mg/l, which was proven in previous experiments.

In this study, we also examined the leaching behavior of other elements, namely: Ca^{2+} , K^+ , Fe^{2+} and Mg^{2+} . These elements are already apparent in the fly ash component of the geopolymer. The resulting weight percentages can be seen in figures 7.8 and 7.9.

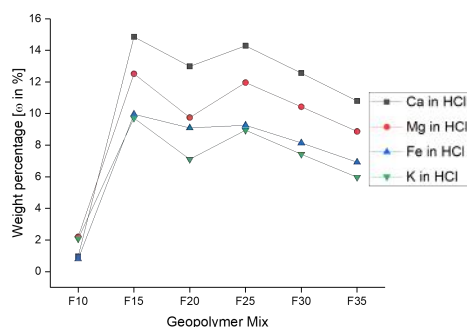


Figure 7.8: ICP-OES results of leached Ca^{2+} , K^+ , Fe^{2+} and Mg^{2+} in HCl

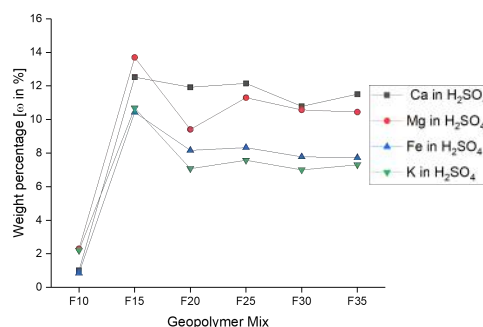


Figure 7.9: ICP-OES results of leached Ca^{2+} , K^+ , Fe^{2+} and Mg^{2+} in H_2SO_4

In both leaching solutions calcium shows the highest leached values which are about 14%. In sample F10 the lowest values are calculated. This was already the case in the observed lead and zinc values. It leads to the conclusion that geopolymers with a Si/Al ratio of 2.0 are the most stable against acidic attack. If we accept that HCl dissolves the amorphous matrix to a high or complete level, we conclude that about 85% of the remaining examined elements are located in the remaining fly ash particles or the surrounding, not dissolving material. For calcium and iron, some phases with a higher level could be determined by SEM. These phases seem to be stable against the acidic attack.

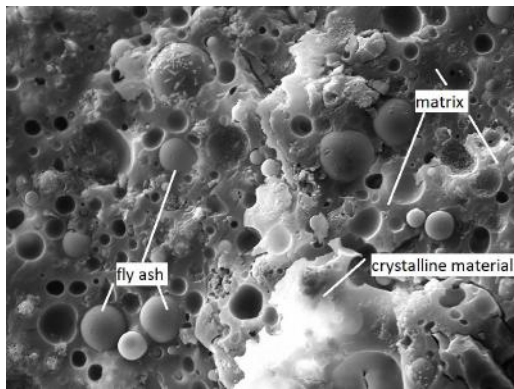
In samples F25–F35 leached in hydrochloric acid, the values of all analyzed elements sinks continuously, after reaching a maximum at F15. This behavior is not dependent on the element but rather highly influenced by the Si/Al ratio. In samples leached in sulfuric acid, the level stays constant from samples F20 – F35. Again, the highest values are detected for F15.

From the leaching experiments we can conclude that sample F10 with a Si/Al ratio of 2.0 is the most stable against hydrochloric attack, not depending on the doping with lead or zinc nitrate. Furthermore, we can see a correlation of the amount of aluminum bound in the geopolymer matrix to the acidic resistance. The reference sample show a decreasing leached amount of ions Ca^{2+} , K^+ , Fe^{2+} and Mg^{2+} with an increase in aluminum, as concluded by IR spectroscopy.

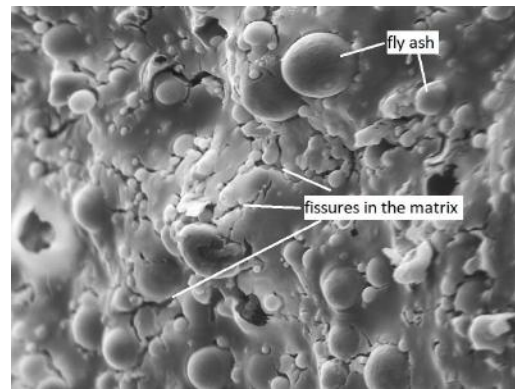
Structural Analysis of residues after leaching

SEM was used to get an impression as to how the geopolymer samples changed during leaching.

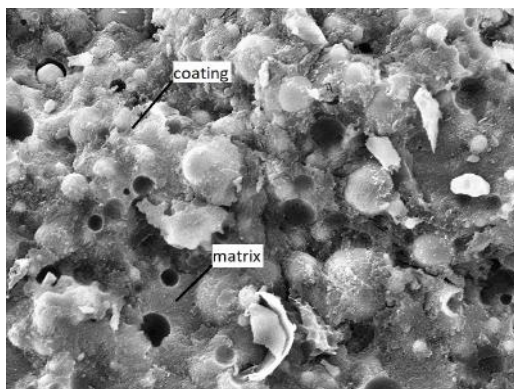
Figure 7.10a shows a mostly intact matrix of sample F10, although the sample was leached in HCl for 28 d. Sample F35 in HCl shows a not completely unchanged matrix, compared to the not leached sample, however the matrix is not completely destroyed. Looking at figures 7.10c and 7.10d one can see that the addition of



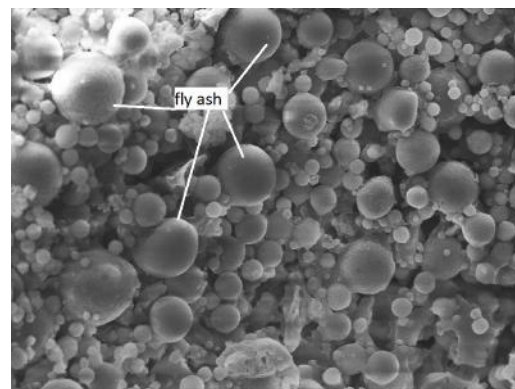
a) F10 in HCl, still showing fly ash spheres, geopolymer matrix and crystalline material



b) F35 in HCl, showing fissures in the matrix and fly ash spheres



c) F20 "ZnNO" in H_2SO_4 still showing coating and matrix but partly destroyed



d) F20 "PbNO" in HCl, showing only fly ash spheres and no matrix

Figure 7.10: SEM images of leached samples F10, F35 and F20; a) F10 in HCl, b) F35 in HCl, c) F20 "ZnNO" in H_2SO_4 , d) F20 "PbNO" in HCl

the metals influences the behavior in the leaching solution. Especially the addition of lead forms a geopolymer in which only the residues of the not reacted fly ash particles are detectable. No matrix, as described beforehand is still visible. The sample with zinc nitrate addition leached in sulfuric acid, shows a partly destroyed matrix. However, the coating as in the original sample is still apparent.

IR spectra were used to confirm the structural changes in the leached residues. In figures 7.11 and 7.12 comparisons of the spectra of samples F10 and F20 are displayed. Only the part between 1800 cm^{-1} and 200 cm^{-1} is shown, the band from the sodium carbonate and sodiumhydrogencarbonate, beforehand observed, disappear during the leaching of the geopolymer samples.

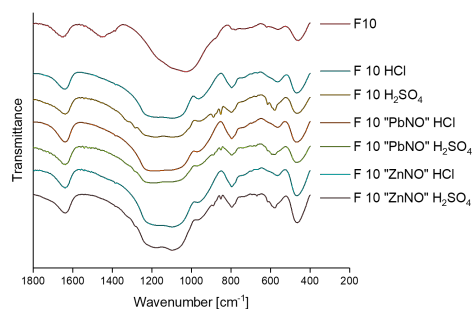


Figure 7.11: IR spectra of F10 in all leaching solutions and with addition of metal nitrates

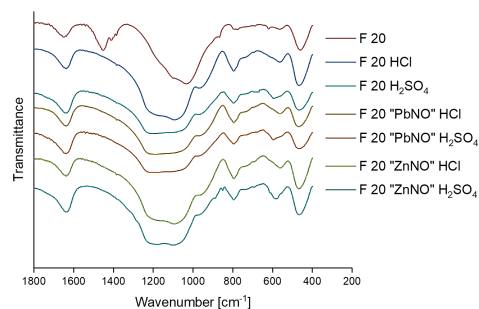


Figure 7.12: IR spectra of F20 in all leaching solutions and with addition of metal nitrates

A comparison of sample F10 with and without the addition of metal nitrates shows a shift in the main stretching vibration from 1000 cm^{-1} to 1100 cm^{-1} as was detected in previous research. No difference in the shift between each individual leaching solution is detected. However, in all leached samples the signal of ν_{as} Si-O-Si is more enhanced than before. Not one single broad band is observed, but a combination of two bands. For samples leached in HCl the signal of Si-O-Si (1180 cm^{-1}) becomes stronger pronounced than the beforehand dominating band of Si-O-Al (1105 cm^{-1}). This proves the dealumination and destruction process of the amorphous geopolymer matrix through the acidic attack. Bakharev²⁴ observed a similar behavior, however in his research the Si-O-Si signal did not show such a strong enhancement. The Si-O and Al-O stretching vibration at 880 cm^{-1} (labeled NBO in figure 7.13) show an increase in strength and a shift to higher wavenumbers. The ν_s Si-O-T vibrations also show an increase in strength in the leached samples, especially if hydrochloric acid is used as eluate.

In figure 7.13 a comparison of samples F10 – F35 leached in sulfuric acid is displayed. Hereby, the influence of the Si/Al ratio is detectable, as the signals at 1180 cm^{-1} and 1090 cm^{-1} corresponding to ν_{as} Si-O-Si and ν_{as} Si-O-T respectively change in intensity. Moreover, a shift from 1030 cm^{-1} to 1090 cm^{-1} is observed. Sample F20 shows a strong enhancement of the Si-O-Si signal and a decrease in the Si-O-T signal, so not two peaks are visible in the IR spectra but only one broad band. This behavior is also apparent in samples F20 "PbNO" and F35 "PbNO" leached in sulfuric acid and for sample F20 "PbNO" also when leached in hydrochloric acid. This broad "hump" is the same "hump" that appears when fly ash is leached in hydrochloric acid (see figure 4.5). In the sample with zinc nitrate addition no such behavior is observed (see figure 7.12).

The analysis of the residues using XRD revealed that mullite and quartz remained unchanged during the acidic attack. Figure 7.14 shows a comparison of sample F35 with and without added metal nitrates leached in both leaching solutions.

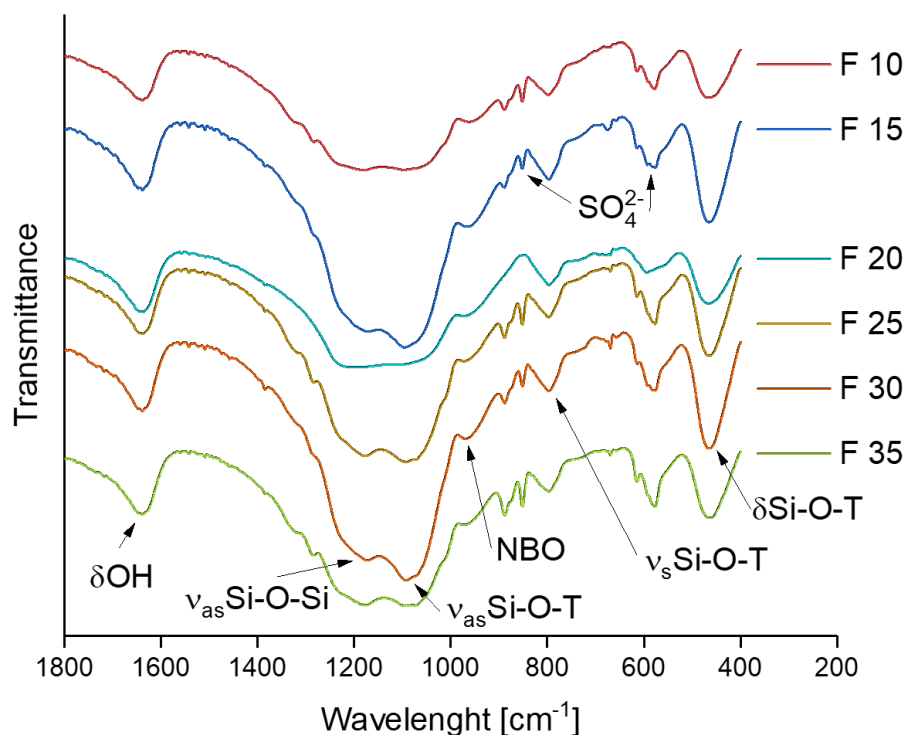


Figure 7.13: IR spectra of samples F10 – F35 leached in H_2SO_4

No remaining crystalline phase of aluminum silicate, potassium magnesium silicate or of calcium silicate remained in the residue. However, in sample F35 "PbNO" leached in sulfuric acid, signals of lead sulfate are appearing. This crystalline phase forms when lead is leached from the geopolymer and confirms our previous research. Other samples (F10 – F30) show the same signals of mullite and quartz. Moreover, it was proven that fly ash shows the same residue signals as geopolymers leached in sulfuric -and hydrochloric acid.

7.3 Conclusion

The increasing Si/Al ratio leads to the formation of new crystalline silicate phases in the geopolymer, namely aluminum silicate, potassium magnesium silicate and calcium silicate. Moreover, a change in the topography of the geopolymers was noticed. This underlines the different behavior we have noticed, during preparation. The highest synthesized value, 3.0 did not harden completely, that is why our suggestion is that it is possible to produce geopolymers (with acceptable consistency) up to a Si/Al ratio of 2.6. The most stable ratio in our experiments was sample F10 with a ratio of 2.0 which also showed the highest amount of aluminum bound into the

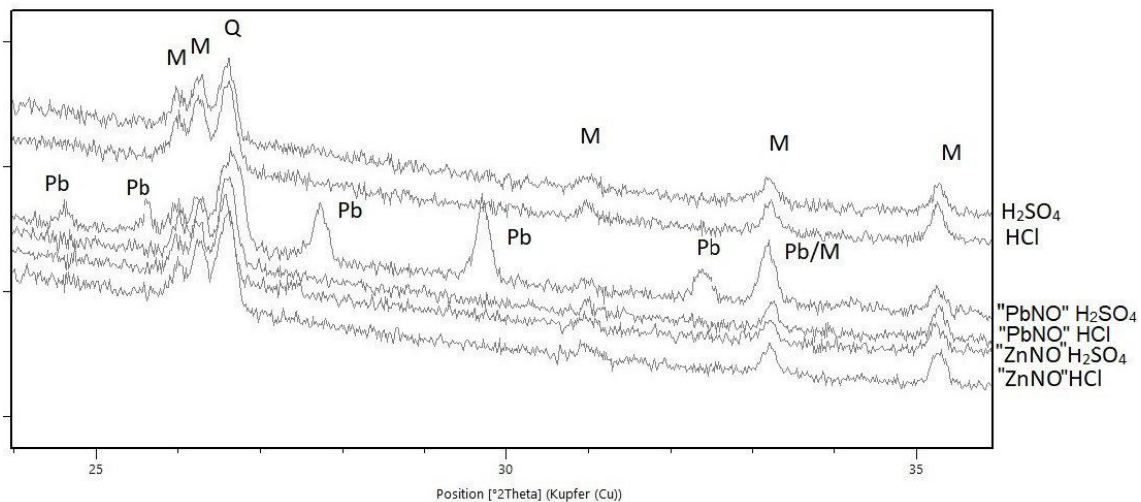


Figure 7.14: XRD diffractograms of F35, F35 "PbNO" and F35 "ZnNO" in different leaching solutions; M: mullite; Q: quartz, Pb: $PbSO_4$

geopolymer matrix.

To summarize our leaching experiments, we prove that the resistance of geopolymers to acidic attack is strongly dependent on the Si/Al ratio. F10 shows the lowest leached values, not dependent on the metal ion. F15, F20, F30 and F35 show a lead leaching percentage of 100 % suggesting a complete destruction of the amorphous matrix. This conclusion is underlined by the taken SEM images in which the matrix of samples with lead addition appears completely destroyed. Zinc is leached up to a percentage of 80 %, not regarding sample F10, not depending on the Si/Al ratio (F15–F35).

The addition of lead nitrate leads to a less stable matrix against acidic attack. With the addition of zinc nitrate, we see either a dealumination process for samples with a relatively low Si/Al ratio, however if the ratio increases, zinc ions facilitate the formation of aluminum inclusion. Moreover, zinc stabilizes the geopolymer matrix against acidic attacks.

8 Summary and Conclusion

In this thesis a thorough investigation of the possible influences of the Na/Al and the Si/Al ratios in geopolymers was made. Moreover, we showed the influences of porosity and ratios onto the ability to immobilize the heavy metal ions Pb^{2+} and Zn^{2+} . For this investigation we used a variety of analytical tools, including acidic resistance tests.

First of all, the used fly ash (Microsit 10) was shown to possess an amorphous amount of 79 % with an even higher value of reactive silicon and aluminum. Only 3 % of silicon and 6.4 % of aluminum are bound in the crystalline phases mullite and quartz. Moreover, fly ash was leached in hydrochloric and sulfuric acid as well as in water. Therefore, we were able to compare these results with the leaching results of our synthesized geopolymers.

In the investigation of the Na/Al ratio in geopolymers, we found that a ratio of 0.6 is the most stable ratio against acidic attack. Furthermore, a high amorphous amount of 90 % was found for these geopolymers. The addition of metal powders as foaming agents reduced this amorphous amount to 80 %. Moreover, Zn-powder showed the highest porosity values, followed by aluminum powder added in a percentage of 0.2 %. We used these results as a foundation for our further investigations. Therefore, all following geopolymer samples showed a Na/Al ratio of 0.6.

Using this ratio as basis for the next experimental setup, lead and zinc ions were added to the samples. As salts, water insoluble oxides as well as water soluble nitrates were used. We found that an amount below 3 % does not show in any XRD diffractograms, however when higher amounts are added, traces of Pb_3O_4 were observed. As expected, ZnO and PbO do not take part in the reaction, but lie physically embedded in the geopolymer matrix. Leaching tests confirm that ZnO and PbO are leached at a significantly higher ratio than $\text{Pb}(\text{NO}_3)_2$ and $\text{Zn}(\text{NO}_3)_2$ and are therefore possibly bound chemically into the amorphous matrix. Another fact supporting this conclusion, is that the addition of zinc nitrates leads to the formation of small amounts of zinc oxides which are detectable in XRD. Furthermore, a dealumination process, confirmed by shifts in IR spectra, is correlating with an increase in lead nitrate addition to the pure geopolymer. Moreover, an addition of nitrates leads to a lesser reaction with aluminum powder, and therefore to a lesser porosity. The porosity influences the weight loss to a great extent, proving that a

higher surface is more exposed to acidic attack, hence the foamed geopolymers are less stable.

An increasing Si/Al ratio, with a stable sodium ion amount, leads to the formation of new crystalline phases, aluminum silicate, potassium magnesium silicate and calcium silicate, in geopolymers which are detectable in XRD. This proves that the potassium and calcium ions can take part in the reaction and cannot be disregarded in the reaction process. From our samples, the geopolymer with a Si/Al ratio of 2.0 showed the best stability against acidic attack and the highest aluminum values bound into the geopolymer matrix. This samples leads only to a leaching percentage of about 10 % for lead nitrate as well as zinc nitrate.

To summarize, this thesis brings new knowledge to the mechanisms included in geopolymer synthesis and their behavior when heavy metals are added to the slurry. It supports the theory that geopolymers can be used as cement substitutes, however more research, especially more dynamic leaching tests are necessary before environmental consequences can be predicted. Foamed geopolymers can be used as light weight materials for example, as filling material in brick industry. The inclusion of zinc ions can lead to a better stability against acidic attack, although further research is necessary to understand the included mechanisms.

Bibliography

- [1] Commission, E. 2050 low-carbon economy. 2017; https://ec.europa.eu/clima/policies/strategies/2050_en.
- [2] (VDZ), V. D. Z. Zementindustrie im Überblick 2016/2017. 2017; https://www.vdz-online.de/fileadmin/gruppen/vdz/3LiteraturRecherche/Zementindustrie_im_Ueberblick/VDZ_Zementindustrie_im_Ueberblick_2016_2017.pdf.
- [3] Komnitsas, K. et al. *Minerals Engineering* **2007**, *20*, 1261–1277.
- [4] Shi, C. et al. *Cement and Concrete Research* **2011**, *41*, 750–763.
- [5] Glukhovskiy, V. *Budivelnyk Publisher* **1967**, 156 pp.
- [6] Krivenko, P. Alkaline cements: terminology, classification, aspects of durability. 1997.
- [7] van Deventer, J. et al. *Journal of Hazardous Materials* **2007**, *139*, 506–513.
- [8] Palomo, A. et al. *British ceramic. Transactions and journal* **1992**, *91*, 107–112.
- [9] Davidovits, J. *Journal of Thermal Analysis* **1991**, *37*, 1633–1656.
- [10] Ikeda, K. et al. *Chem Pap* **1998**, *52*, 214–7.
- [11] Joseph Davidovits, *Geopolymer Chemistry and Applications*, 4th ed.; Institut Géopolymère, 2015.
- [12] Khale, D. et al. *Journal of Materials Science* **2007**, *42*, 729–746.
- [13] J.G.S. van Jaarsveld, J.S.J. van Deventer, *Minerals Engineering* **1996**, *10*, 659–669.
- [14] A. Fernández-Jiménez, A. Palomo, M.M. Alonso, Alkali activation of fly ashes: mechanisms of reaction. 2005.
- [15] Swaddle, T. W. et al. *Chem. Soc. Rev.* **1994**, *23*, 319–325.
- [16] Provis, J. L. et al. *Chemistry of Materials* **2005**, *17*, 3075–3085.
- [17] Fernández-Jiménez, A. et al. *Microporous and Mesoporous Materials* **2005**, *86*, 207–214.
- [18] Fernández-Jiménez, A. et al. **2006**, *91*, 111–119.

- [19] Iler, R. *The colloid chemistry of silica and silicates*; George Fisher Baker non-resident lectureship in chemistry at Cornell University; Cornell University Press, 1955.
- [20] Madras, G. et al. *The Journal of Chemical Physics* **2001**, *115*, 6699–6706.
- [21] García, I. Compatibilidad de geles cementantes CSH y NASH. Estudios en muestras reales y en polvos sintéticos. Ph.D. thesis, Thesis, 2008.
- [22] Zheng, L. et al. *Frontiers of Environmental Science & Engineering* **2015**, *9*, 642–648.
- [23] Nikoli, V. et al. *Ceramics International* **2014**, *40*, 8479–8488.
- [24] Bakharev, T. *Cement and Concrete Research* **2005**, *35*, 658–670.
- [25] Breck, D. W. *Zeolite molecular sieves: Structure, chemistry*; Wiley: New York, 1973.
- [26] A. Palomo, J. L. d. l. F. *Cement and Concrete Research* **2003**, *33*, 281–288.
- [27] A. Palomo, M. P. *Cement and Concrete Research* **2003**, *33*, 289–295.
- [28] Zhang, J. et al. *Journal of Hazardous Materials* **2008**, *157*, 587–598.
- [29] Perera, D. S. et al. *Journal of the American Ceramic Society* **2005**, *88*, 2586–2588.
- [30] Martina Minaščíková, F. š. *Ceramics - Silikaty* **2006**, *50*, 200–207.
- [31] Phair, J. et al. *Applied Geochemistry* **2004**, *19*, 423–434.
- [32] Guo, X. et al. *Journal of Wuhan University of Technology-Mater. Sci. Ed.* **2013**, *28*, 938–943.
- [33] X. J. Song, M. Marosszcky, M. Brungs, R. Munn, Durability of fly ash based Geopolymer concrete against sulphuric acid attack. 2005.
- [34] John A. Redner, Randolph P. Hsi, Edward J. Esfandi, Roger Sydney, Robin M. Jones, Donna Won, James Andraska, Evaluation of protective coatings for concrete.
- [35] Ali Allahverdi, F. Š. *Ceramics - Silikaty* **2001**, 143–149.
- [36] Arioz, E. et al. *Procedia Engineering* **2012**, *42*, 1114–1120.
- [37] Lloyd, R. R. et al. *Materials and Structures* **2012**, *45*, 1–14.
- [38] Mehta, A. et al. *Construction and Building Materials* **2017**, *146*, 136–143.
- [39] Temuujin, J. et al. *Cement and Concrete Composites* **2011**, *33*, 1086–1091.
- [40] Granizo, M. L. et al. *Journal of the American Ceramic Society* **2002**, *85*, 225–231.

- [41] Fernández-Jiménez, A. et al. *Fuel* **2006**, *85*, 625–634.
- [42] Fernández-Jiménez, A. et al. *Fuel* **2006**, *85*, 1960–1969.
- [43] Haha, M. B. et al. *Cement and Concrete Research* **2010**, *40*, 1620–1629.
- [44] Ohsawa, S. et al. **1985**, *15*, 357–366.
- [45] Suprenant, B. A. et al. *Journal of Materials in Civil Engineering* **1991**, *3*, 48–59.
- [46] Lumley, J. et al. *Cement and Concrete Research* **1996**, *26*, 139–151.
- [47] Luke, K. et al. *Cement and Concrete Research* **1987**, *17*, 273–282.
- [48] Li, S. et al. *Cement and Concrete Research* **1985**, *15*, 1079–1086.
- [49] Palomo, A. et al. *Journal of the American Ceramic Society* **2004**, *87*, 1141–1145.
- [50] Bell, R. J. et al. Atomic Vibrations in Vitreous Silica: Discussions of the Faraday Society, 1970. 50: p. 55-61. 1970.
- [51] Roy, B. N. *J. Am. Ceram. Soc.* **1990**, *73*, 846–855.
- [52] Keresztury, G. et al. *Spectrochimica Acta Part A: Molecular Spectroscopy* **1980**, *36*, 1007 – 1008.
- [53] Lee, W. K. W. et al. *Langmuir* **2003**, *19*, 8726–8734.
- [54] Rees, C. A. Mechanisms and kinetics of gel formation in geopolymers. PhD thesis, The University of Melbourne, Melbourne, Australia, 2007.
- [55] Plinio Innocenzi, *Journal of Non-Crystalline Solids* **2003**, 309–319.
- [56] Agarwal, A. et al. *Journal of Non-Crystalline Solids* **1997**, *209*, 166–174.
- [57] Henderson, C. et al. *Spectrochimica Acta Part A: Molecular Spectroscopy* **1979**, *35*, 929–935.
- [58] Tuddenham, W. et al. *Analytical Chemistry* **1959**, *31*, 377–380.
- [59] Stubičan, V. et al. *Journal of the American Ceramic Society* **1961**, *44*, 625–627.
- [60] Voll, D. et al. *Vibrational Spectroscopy* **2002**, *30*, 237–243.
- [61] Tarte, P. *Spectrochimica Acta Part A: Molecular Spectroscopy* **1967**, *23*, 2127–2143.
- [62] Flanigen, E. M. et al. *Molecular Sieve Zeolites-I*; Chapter 16, pp 201–229.
- [63] Shigemoto, N. et al. *Journal of materials science* **1995**, *30*, 5777–5783.
- [64] Sweet, J. et al. *Physics and Chemistry of Glasses* **1969**, *10*, 246.

- [65] Rees, C. A. et al. *Langmuir : the ACS journal of surfaces and colloids* **2007**, *23*, 8170–8179.
- [66] Narayanan, N. et al. *Cement and Concrete Composites* **2000**, *22*, 321–329.
- [67] Abdullah, Mohd Mustafa Al Bakri, et al. *International Journal of Molecular Sciences* **2012**, *13*, 7186–7198.
- [68] Masi, G. et al. *Ceramics International* **2014**, *40*, 13891–13902.
- [69] Nyale, S. M. et al. *Procedia Environmental Sciences* **2013**, *18*, 722–730.
- [70] Prud'homme, E. et al. *Applied Clay Science* **2011**, *51*, 15–22.
- [71] Strozi Cilla, M. et al. *Ceramics International* **2014**, *40*, 5723–5730.
- [72] Bell, J. et al. Preparation of ceramic foams from metakaolin-based geopolymer gels. *Ceram Eng Sci Proc.* 2009; pp 97–112.
- [73] Hajimohammadi, A. et al. *Cement and Concrete Composites* **2017**, *80*, 277–286.
- [74] Butt, H. et al. *Physics and Chemistry of Interfaces*; Wiley, 2006.
- [75] James Goldberg & Martin Thomas, *PoreMaster & PoreMaster GT Manual.* 2009.
- [76] Schüth, F., Ed. *Handbook of porous solids*; Wiley-VCH: Weinheim, 2002.
- [77] Abell, et al. *Journal of colloid and interface science* **1999**, *211*, 39–44.
- [78] Tolk, F. Microsit10: Feinstflugasche für Hochleistungsbeton. <http://www.baumineral.de/downloads/file/385/Infoblatt%20Microsit%20Stand%2011.2014.pdf>.
- [79] Provis, J. L. et al. *Annual Review of Materials Research* **2014**, *44*, 299–327.
- [80] Sathyanarayana, D. *Vibrational Spectroscopy: Theory and Applications*; New Age International (P) Limited, 2015.
- [81] Tognonvi, M. T. et al. *Journal of Non-Crystalline Solids* **2011**, *357*, 43–49.
- [82] Prud'homme, E. et al. *Journal of Sol-Gel Science and Technology* **2012**, *61*, 436–448.
- [83] Zheng, L. et al. *Chemosphere* **2010**, *79*, 665–671.
- [84] Barbosa, V. F. et al. *International Journal of Inorganic Materials* **2000**, *2*, 309–317.

List of Figures

2.1	Schematic illustration of a geopolymer structure	3
2.2	The six steps to form a geopolymer network	4
2.3	Polycondensation reaction involved in geopolymer reaction mechanism	5
2.4	Corrosion rates of samples exposed to nitric and sulfuric acid ³⁷	10
2.5	IR spectra of Na X (b), Na A zeolite (d) and their amorphous precursors ((a) for Na-X, (c) for Na-A). ⁶³	16
2.6	Shift in position of aluminosilicates with different Al contents. (a) asymmetric stretch T-O bonds, (b) symmetric stretch of Si-O-T, (c) double 6-ring vibrations, (d) T-O bending, (e) pore opening. ⁶³	16
2.7	FTIR spectra showing geopolymer development over 200 days ⁶⁵	17
2.8	Shift in the position of main Si-O-T asymmetric stretch bond in the FTIR spectra of sample A (with added aluminum) and Sample B (no added aluminum). ⁷³	19
4.1	SEM image of Microsit 10; Magnification of 5,92 kx ⁷⁸	25
4.2	XRD diffractogram of fly ash; M: mullite, Q: quartz, A: anhydrite, H: hematite, Fe: magnetite	27
4.3	IR spectra of fly ash Microsit 10	28
4.4	Comparison of fly ash (FA), fly ash leached in water (H ₂ O), in sulfuric acid (H ₂ SO ₄) and hydrochloric acid (HCl); A: anhydrite, H: hematite	29
4.5	Comparison of IR spectra of leached and not leached fly ash; 1800 – 250 <i>cm</i> ⁻¹	30
5.1	Compressive strength values of samples F04–F08	32
5.2	Material properties (thermoconductivity, density, compressive strength) of foamed samples F04–F08	33
5.3	Mass loss determined in hydrochloric and sulfuric acid of geopolymer samples F04–F08	34
5.4	Microscopy images of geopolymers F08 using different foaming agents	34
5.5	SEM image of F06 foamed with 0,2% Al-powder; Magnification: 1 kx	35
5.6	Element mapping of F06 foamed with 0,1% Al-powder showing Na crystals, fly ash spheres and geopolymer matrix; Magnification: 1 kx	35
5.7	High resolution (6 kx) SEM images of samples with different Na/Al ratio.	37
5.8	IR spectra of geopolymers; a) IR spectra of F04–F08, b) IR bands 1600–250 <i>cm</i> , c) Shift of wavelength of Si-O-T bond, d) Shift of wavelengths of ν_{as} Si-O-T vibrations in foamed geopolymers	38
5.9	Qualitative XRD spectra of geopolymers F04-F08; Q: quartz; M: mullite; A: anhydrite, H: hematite, Fe: magnetite	39

5.10	Mercury Intrusion porosimetry of samples F04–F08: a) Overview of all not foamed geopolymers, b) Comparison of geopolymers foamed using Zn–powder, c) Comparison of F06 using all foaming agents . . .	41
5.11	Intruded volume, recorded by MIP, of samples F04–F08	42
6.1	SEM image of "ZnO" 0 as reference sample showing pores and fly ash spheres	46
6.2	SEM image of "ZnO" 5 with the edx spot marked; magnification of 5000x	46
6.3	SEM image of the marked edx spot of "ZnO" 5 – high resolution (50.000x)	46
6.4	Edx spot analysis of sample "ZnO" 5	46
6.5	SEM image of "PbO" 5 showing geopolymeric matrix and fly ash spheres; magnification of 5000x using in-lens detector	47
6.6	Element mapping of "PbO" 5, showing Pb signals	47
6.7	SEM analysis of "PbNO" 5; a) SEM figure of "PbNO 5" showing 3 measured edx spots, b) SEM picture of spot1; containing higher amount of iron, c) SEM image of "PbNO" 5 with marked edx spot; magnification of 20.000x using in-lens detector, d) Edx analysis of marked spot in c)	48
6.8	SEM analysis of "PbO" 4 and "ZnO" 4 in different leaching solutions; a) "PbO" 4 leached in H ₂ O, b) "PbO" 4 leached in HCl, c) "PbO" 4 leached in H ₂ SO ₄ d) "ZnO" 4 leached in H ₂ SO ₄	49
6.9	Element mapping of "PbO" 4 leached in H ₂ SO ₄	49
6.10	Element mapping of "ZnO" 4 leached in HCl	49
6.11	Comparison of IR spectra of "ZnO" geopolymers	50
6.12	Comparison of IR spectra of "PbO"	50
6.13	Comparison of geopolymers without any addition ("ZnO" 0), "ZnO" 5 and "PbO" 5	51
6.14	Comparison of IR spectra of "ZnO" 2 in different leaching solutions	51
6.15	IR spectra of "PbO" leached in HCl	51
6.16	IR spectra of samples "PbNO" 0–5	52
6.17	IR spectra of "ZnNO" 0–5	52
6.18	IR spectra of "PbNO" leached in HCl	53
6.19	IR spectra of "PbNO" leached in H ₂ SO ₄	53
6.20	IR spectra of "ZnNO" leached in HCl	54
6.21	IR spectra of "ZnNO" leached in H ₂ SO ₄	54
6.22	Comparison of IR spectra of leached and not leached "ZnNO" 4	55
6.23	Comparison of IR spectra of leached and not leached "PbNO" 4	55
6.24	Diffractiongram of samples with ZnO addition; M: mullite, Q: quartz, D: diopside	56
6.25	Diffractiongram of samples with PbO addition; M: mullite, Q: quartz, H: hematite	57
6.26	Diffractiongrams of samples with addition of Zn(NO ₃) ₂ ; Fr: franklinite, M: mullite, CaMg: calcium magnesium silicide	57
6.27	Diffractiongrams of samples with addition of Pb(NO ₃) ₂ ; Na2: Na(NO ₂), Na3: Na(NO ₃), M: mullite, Q: quartz	58
6.28	Diffractiongrams of "ZnO" samples leached in HCl, H ₂ SO ₄ and H ₂ O	58

6.29	Diffractograms of samples "PbO" ("PbO" 0, "PbO" 2 and "PbO" 4) leached in the H_2SO_4	59
6.30	Diffractograms of leached fly ash and geopolymer samples "PbNO" 0, "PbNO" 5 and "ZnNO" 5 in HCl; M: mullite, Q: quartz	59
6.31	MIP of "PbO" 0–5	60
6.32	MIP of "PbNO" 0–5	60
6.33	Representation of the cumulative intruded volume of sample "PbO" 5	60
6.34	Representation of cumulative intruded volume of sample "PbNO" 4	60
6.35	Representation of the cumulative intruded volume of sample "ZnO" 5	61
6.36	Representation of the cumulative intruded volume of sample "ZnNO" 5	61
6.37	Comparison of leaching concentrations in lead samples of foamed and not foamed samples in both leaching solutions (H_2SO_4 and HCl)	64
6.38	Comparison of of leaching concentrations "PbO" and "PbNO" samples	65
6.39	Comparison of leaching concentrations of "ZnO" and "ZnNO" samples	66
7.1	XRD of samples F25, F30 and F35; M: mullite, Q: quartz, S: aluminum silicate (Al_2SiO_5) K: potassium magnesium silicate ($K_2(MgSi_5O_{12})$), CaSi: calcium silicate	75
7.2	XRD of F25, F25 "PbNO" and F25 "ZnNO"; M: mullite, Q: quartz, S: aluminum silicate (Al_2SiO_5), CaSi: calcium silicate, $NaNO_3$: sodium nitrate	76
7.3	IR spectra of F10–F25; a) Samples F10–F35, b) With addition of $Pb(NO_3)_2$, c) F25, F25 "PbNO" and F25 "ZnNO", d) Shift of asymmetric stretching vibration of Si-O-T	77
7.4	SEM images of samples F10–F35, Magnification of 2 kx	79
7.5	F15 "PbNO", red shows lead included and distributed throughout the matrix	80
7.6	F30 "ZnNO", green shows zinc distributed throughout the matrix	80
7.7	Comparison of resulting leached weight percentages of F10–F35 using ICP-OES	81
7.8	ICP-OES results of leached Ca^{2+} , K^+ , Fe^{2+} and Mg^{2+} in HCl	82
7.9	ICP-OES results of leached Ca^{2+} , K^+ , Fe^{2+} and Mg^{2+} in H_2SO_4	82
7.10	SEM images of leached samples F10, F35 and F20; a) F10 in HCl, b) F35 in HCl, c) F20 "ZnNO" in H_2SO_4 , d) F20 "PbNO" in HCl	83
7.11	IR spectra of F10 in all leaching solutions and with addition of metal nitrates	84
7.12	IR spectra of F20 in all leaching solutions and with addition of metal nitrates	84
7.13	IR spectra of samples F10 – F35 leached in H_2SO_4	85
7.14	XRD diffractograms of F35, F35 "PbNO" and F35 "ZnNO" in different leaching solutions; M: mullite; Q: quartz, Pb: $PbSO_4$	86
9.1	F04–F08 foamed with Al0,1	98
9.2	F04–F08 foamed with Al0,2	98
9.3	F04–F08 foamed with Al0,1	98
9.4	XRD of F06 foamed and not foamed sample	99
9.5	F04–F08 foamed with Al0,1	99
9.6	F04–F08 foamed with Al0,2	99

9.7	"PbO" 0-5 leached in H ₂ O	99
9.8	"PbO" 0-5 leached in HCl	99
9.9	"PbO" 0-5 with 0,1 % Al leached in H ₂ O	100
9.10	"PbO" 0-5 with 0,1% Al leached in H ₂ SO ₄	100
9.11	"PbO" 0-5 with 0,1 % Al leached in HCl	100
9.12	"PbO" 0-5 with 0,2% Al leached in H ₂ O	100
9.13	"PbO" 0-5 with 0,2 % Al leached in HCl	100
9.14	"PbO" 0-5 with 0,2% Al leached in H ₂ SO ₄	100
9.15	"ZnO" 0-5 leached in H ₂ O	100
9.16	"ZnO" 0-5 leached in HCl	100
9.17	"ZnO" 0-5 leached in H ₂ SO ₄	101
9.18	"ZnO" 0-5 with 0,1 % Al leached in H ₂ O	101
9.19	"ZnO" 0-5 with 0,1% Al leached in H ₂ SO ₄	101
9.20	"ZnO" 0-5 with 0,1 % Al leached in HCl	101
9.21	"ZnO" 0-5 with 0,2% Al leached in H ₂ O	101
9.22	"ZnO" 0-5 with 0,2 % Al leached in HCl	101
9.23	"ZnO" 0-5 with 0,2% Al leached in H ₂ SO ₄	101
9.24	XRD of "PbNO" 0-5 leached in H ₂ O	102
9.25	XRD of "PbNO" 0-5 leached in HCl	102
9.26	XRD of "PbNO" 0-5 leached in H ₂ SO ₄	102
9.27	XRD of "ZnNO" 0-5 leached in H ₂ O	103
9.28	XRD of "ZnNO" 0-5 leached in HCl	103
9.29	XRD of "ZnNO" 0-5 leached in H ₂ SO ₄	103
9.30	MIP of "PbO" 0-5	104
9.31	MIP of "PbO" 0-5 foamed with 0,1 % Al	104
9.32	MIP of "PbO" 0-5 foamed with 0,2 % Al	104
9.33	MIP of "ZnO" 0-5	104
9.34	MIP of "ZnO" 0-5 foamed with 0,1 % Al	104
9.35	MIP of "ZnO" 0-5 foamed with 0,2 % Al	104
9.36	MIP of "PbNO" 0-5 foamed with 0,1 % Al	105
9.37	MIP of "PbNO" 0-5 foamed with 0,2 % Al	105
9.38	MIP of "ZnNO" 0-5	105
9.39	MIP of "ZnNO" 0-5 foamed with 0,1 % Al	105
9.40	MIP of "ZnNO" 0-5 foamed with 0,2 % Al	105
9.41	IR spectra of F10-F35 "ZnNO"	106
9.42	IR spectra of F10-F35 leached in HCl	106
9.43	IR spectra of F10-F35 "PbNO" leached in H ₂ SO ₄	106
9.44	IR spectra of F10-F35 "PbNO" leached in HCl	106
9.45	IR spectra of F10-F35 "ZnNO" leached in H ₂ SO ₄	107
9.46	IR spectra of F10-F35 "ZnNO" leached in HCl	107
9.47	XRD of F10-F35	107
9.48	XRD of F10-F35 "PbNO"	107
9.49	XRD of F10-F35 "ZnNO"	108
9.50	XRD of F10 leached in HCl and H ₂ SO ₄	108
9.51	XRD of F15 leached in HCl and H ₂ SO ₄	108
9.52	XRD of F20 leached in HCl and H ₂ SO ₄	109
9.53	XRD of F25 leached in HCl and H ₂ SO ₄	109
9.54	XRD of F30 leached in HCl and H ₂ SO ₄	109

List of Tables

2.1	Methods of selective chemical dissolution of fly ash based cementitious systems; *Rinse solution	12
2.2	Overview of IR active vibrations in geopolymers ⁵³ ; T = Si, Al; sh: shoulder, s: strong, m: medium, w: weak	13
3.1	Specifications of sodium silicate solution	24
3.2	Used Chemicals	24
4.1	XRF Analysis of Composition; in %	26
4.2	ICP-OES analysis of acid fusion; in ppm	26
4.3	Quantification of determined phases in fly ash by Rietveld refinement	27
4.4	Mass loss of fly ash after leaching experiments	28
5.1	Composition of Geopolymers	32
5.2	Quantitative data obtained from XRD measurements; [ω in %]	39
5.3	Quantitative data obtained from XRD measurements, a comparison of foamed samples; [ω in %]	40
6.1	Composition of geopolymers with metal oxide addition	44
6.2	Composition of geopolymers with metal nitrate addition	44
6.3	Weight loss of zinc oxides	62
6.4	Weight loss of lead oxides	62
6.5	Weight loss of metal nitrates	63
6.6	Weight percentage amounts of leached lead ions	65
6.7	Weight percentage amounts of leached zinc ions	66
7.1	Composition of geopolymers, the amount of fly ash is set as 100 %; AL:activating solution	73
7.2	NaOH added to 39 T	74
7.3	Composition of geopolymers with added metal nitrates, the amount of fly ash is set as 100 %; AL:activating solution, M: Pb or Zn	74
9.1	Compressive strength values [N/mm ²] of samples "ZnO", "PbO", "ZnNO" and "PbNO" 0-5	106

9 Appendix

9.1 Chapter 5: Variation of the Na/Al ratio with addition of metal powders

9.1.1 IR spectroscopy

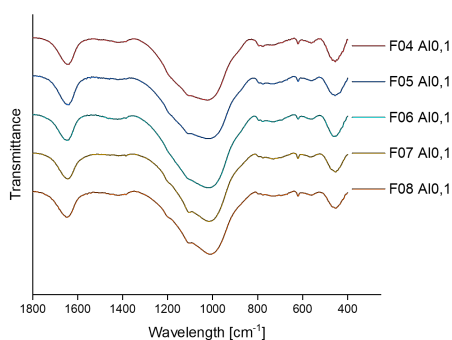


Figure 9.1: F04–F08 foamed with Al_{0,1}

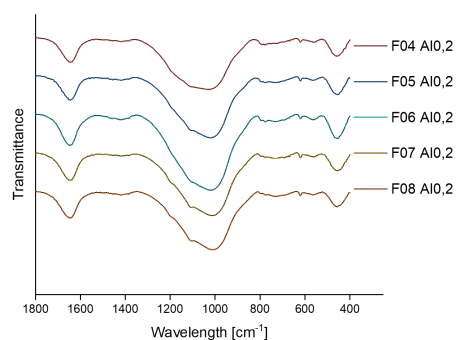


Figure 9.2: F04–F08 foamed with Al_{0,2}

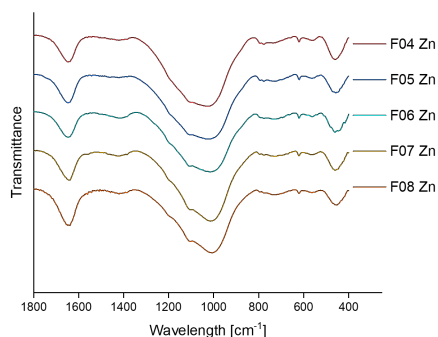


Figure 9.3: F04–F08 foamed with Al_{0,1}

9.1.2 XRD

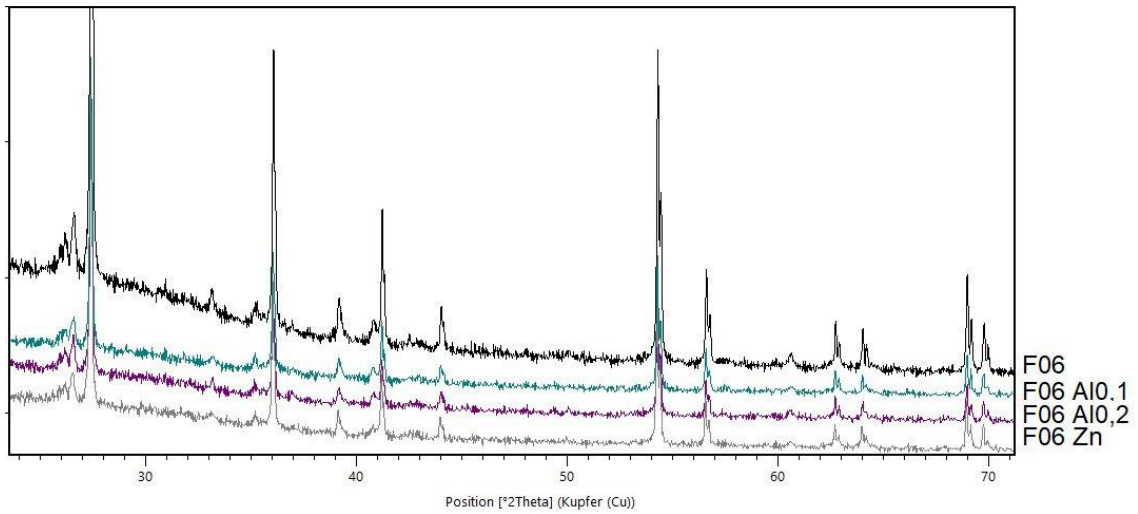


Figure 9.4: XRD of F06 foamed and not foamed sample

9.1.3 MIP

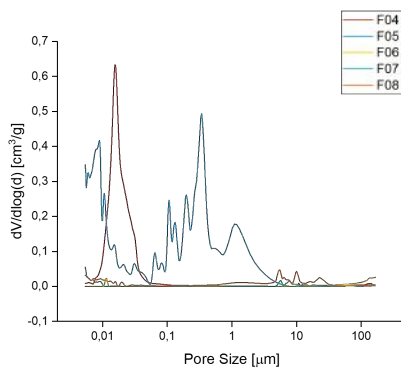


Figure 9.5: F04–F08 foamed with Al_{0,1}

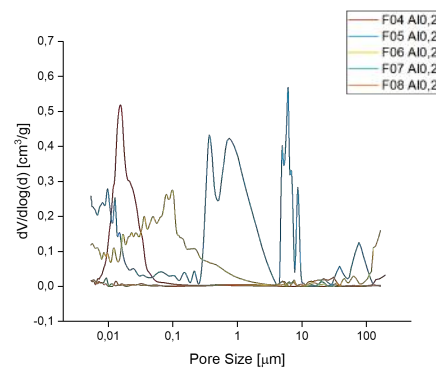


Figure 9.6: F04–F08 foamed with Al_{0,2}

9.2 Chapter 6: Addition of PbO, Pb(NO₃)₂, ZnO and Zn(NO₃)₂

9.2.1 IR spectroscopy

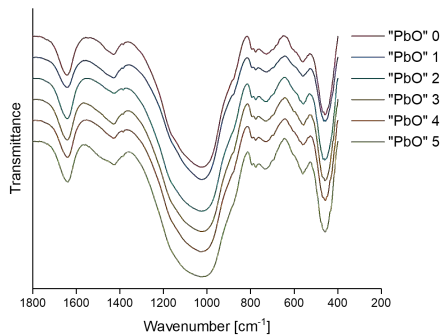


Figure 9.7: "PbO" 0–5 leached in H₂O

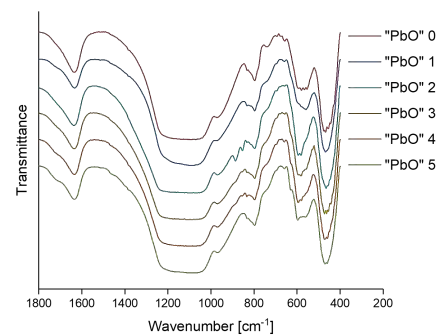


Figure 9.8: "PbO" 0–5 leached in HCl

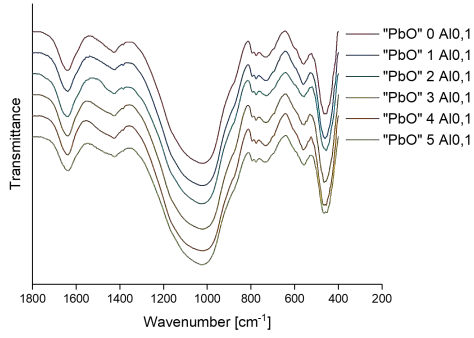


Figure 9.9: "PbO" 0–5 with 0,1% Al leached in H₂O

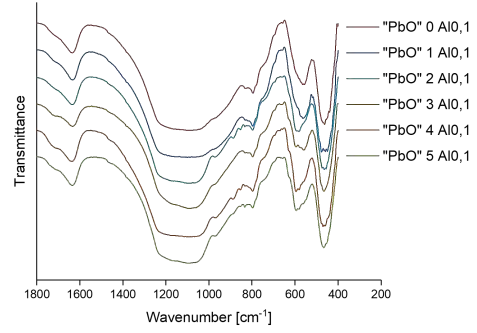


Figure 9.10: "PbO" 0–5 with 0,1% Al leached in H₂SO₄

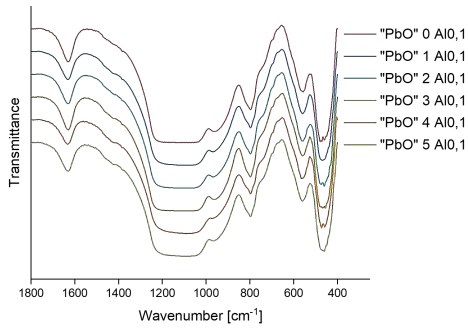


Figure 9.11: "PbO" 0–5 with 0,1% Al leached in HCl

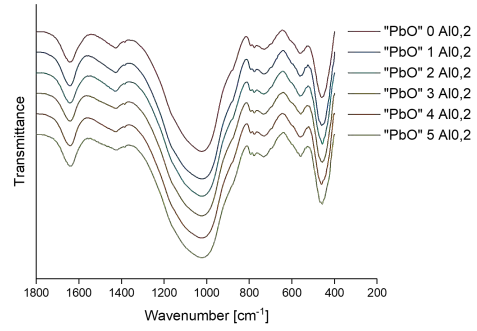


Figure 9.12: "PbO" 0–5 with 0,2% Al leached in H₂O

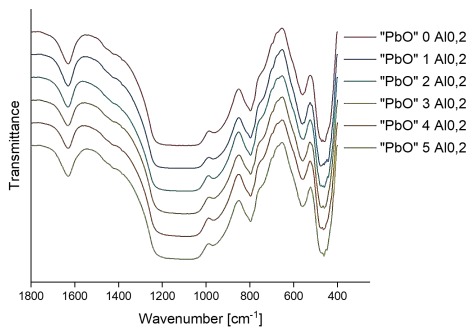


Figure 9.13: "PbO" 0–5 with 0,2% Al leached in HCl

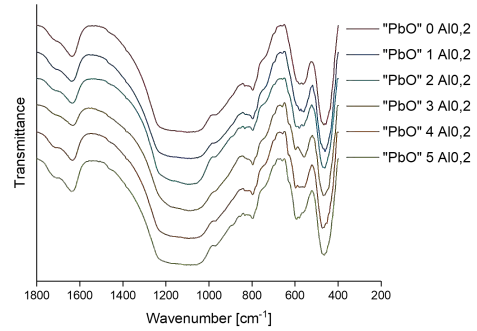


Figure 9.14: "PbO" 0–5 with 0,2% Al leached in H₂SO₄

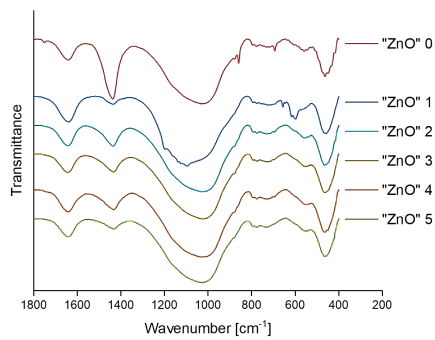


Figure 9.15: "ZnO" 0–5 leached in H₂O

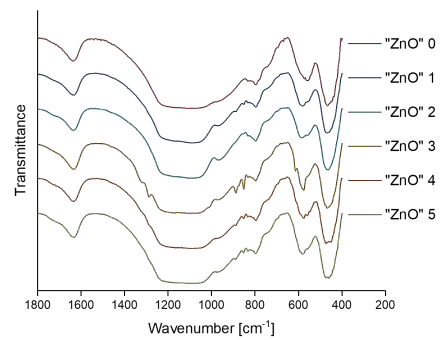


Figure 9.16: "ZnO" 0–5 leached in HCl

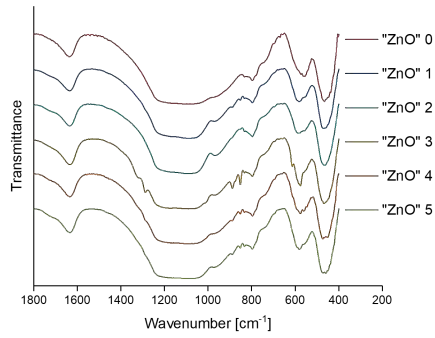


Figure 9.17: "ZnO" 0–5 leached in H_2SO_4

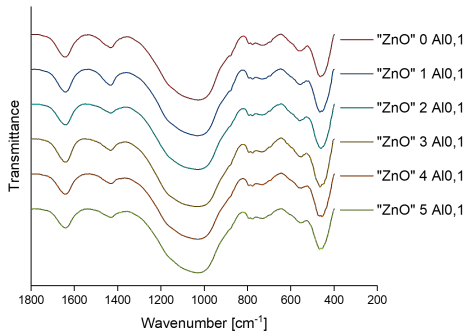


Figure 9.18: "ZnO" 0–5 with 0,1 % Al leached in H_2O

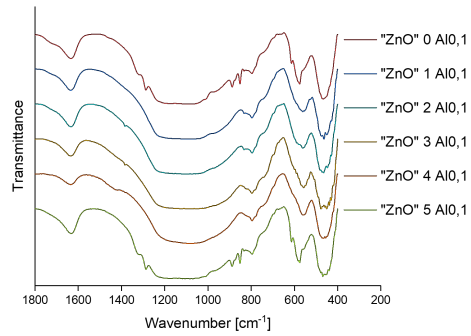


Figure 9.19: "ZnO" 0–5 with 0,1% Al leached in H_2SO_4

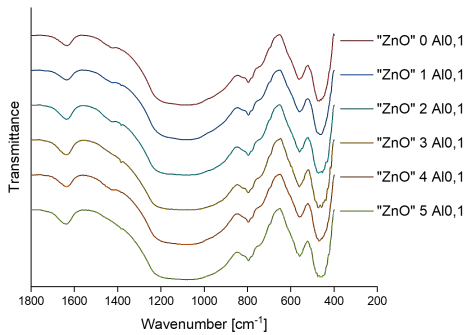


Figure 9.20: "ZnO" 0–5 with 0,1 % Al leached in HCl

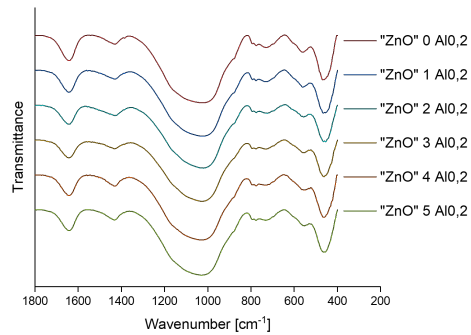


Figure 9.21: "ZnO" 0–5 with 0,2% Al leached in H_2O

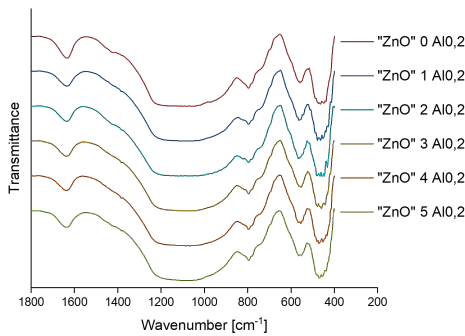


Figure 9.22: "ZnO" 0–5 with 0,2 % Al leached in HCl

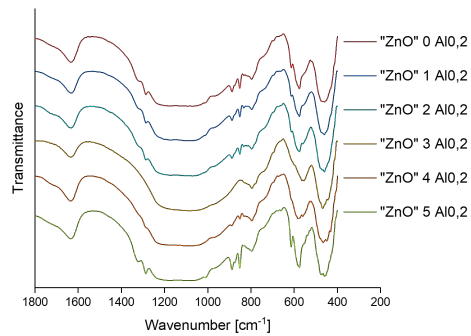


Figure 9.23: "ZnO" 0–5 with 0,2% Al leached in H_2SO_4

9.2.2 XRD

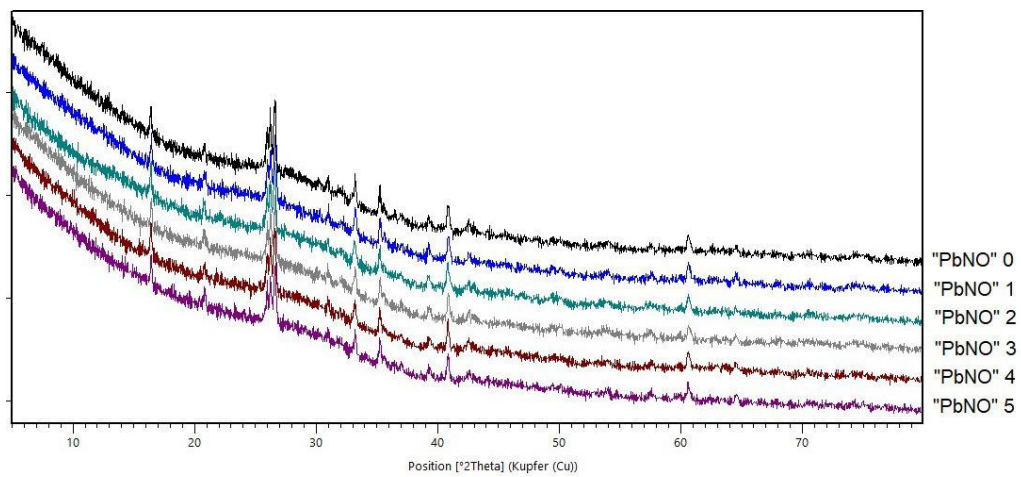
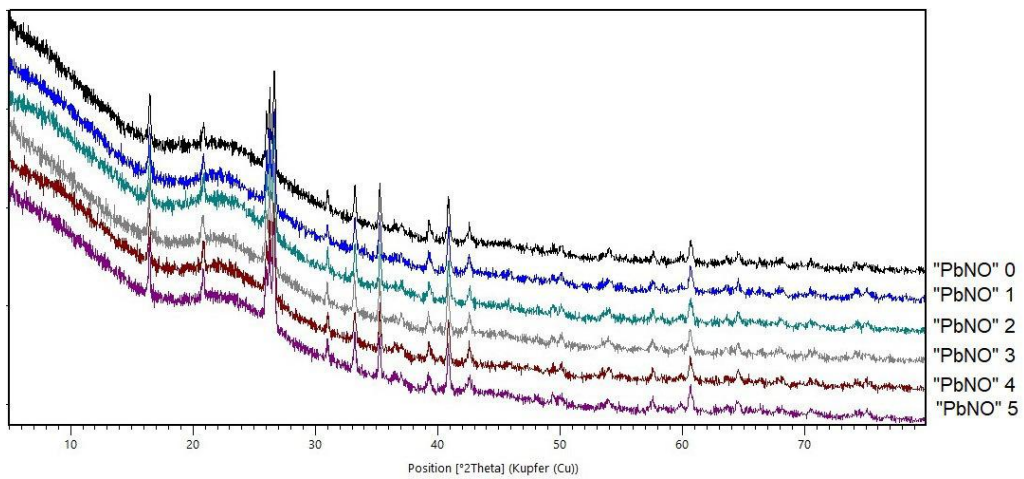
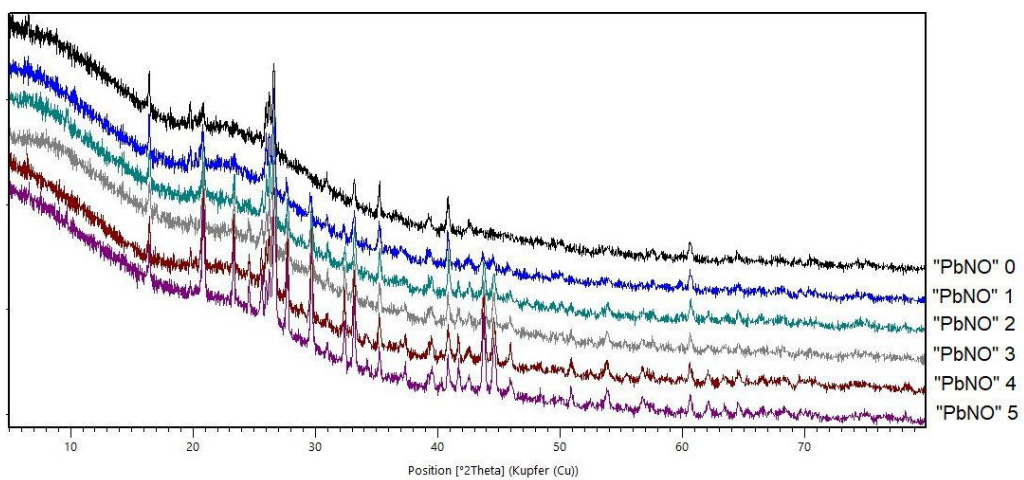
Figure 9.24: XRD of "PbNO" 0-5 leached in H₂O

Figure 9.25: XRD of "PbNO" 0-5 leached in HCl

Figure 9.26: XRD of "PbNO" 0-5 leached in H₂SO₄

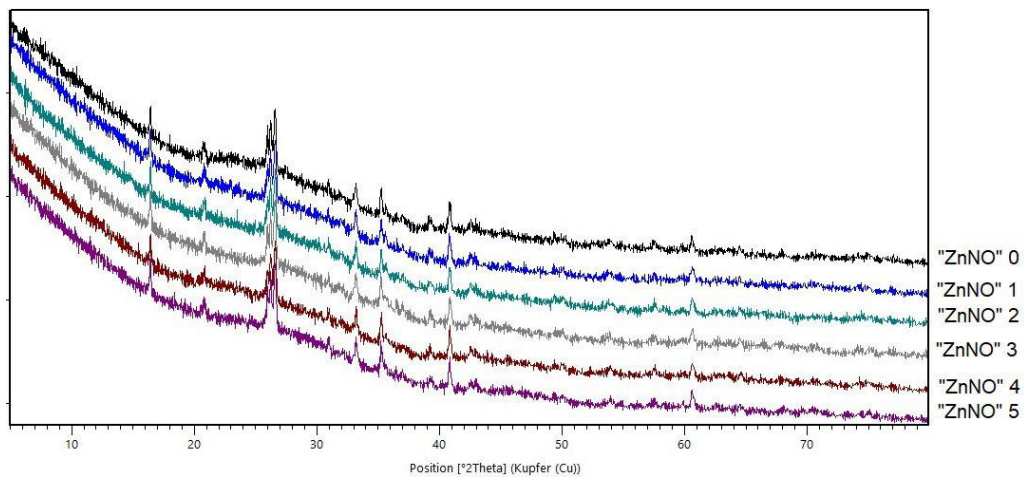


Figure 9.27: XRD of "ZnNO" 0-5 leached in H₂O

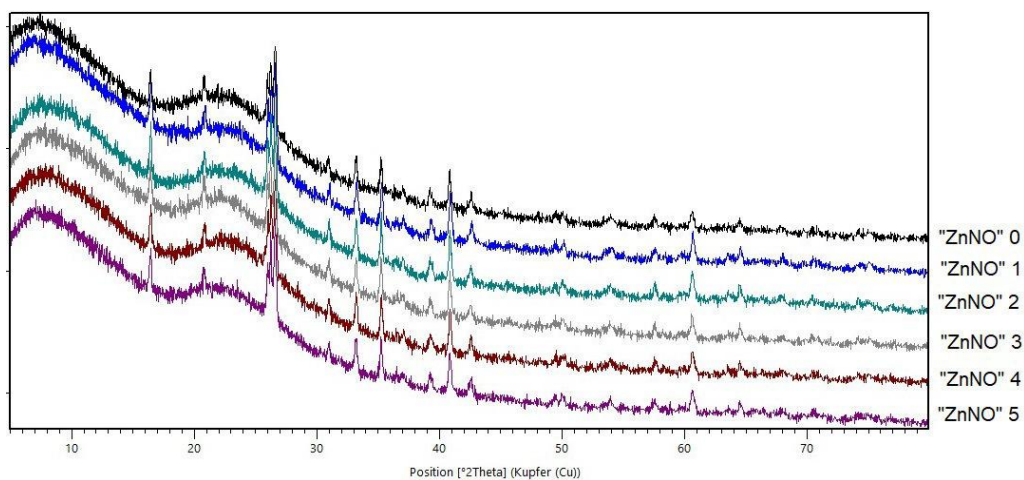


Figure 9.28: XRD of "ZnNO" 0-5 leached in HCl

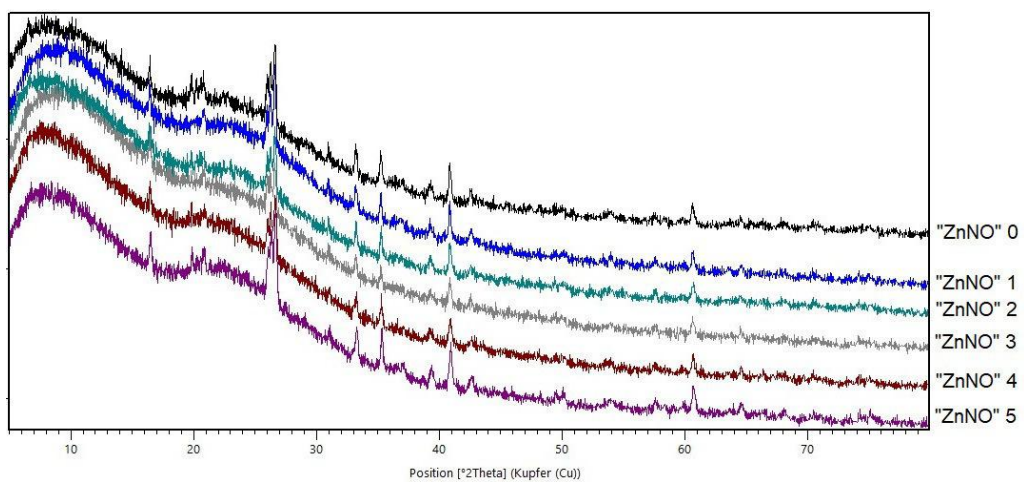


Figure 9.29: XRD of "ZnNO" 0-5 leached in H₂SO₄

9.2.3 MIP

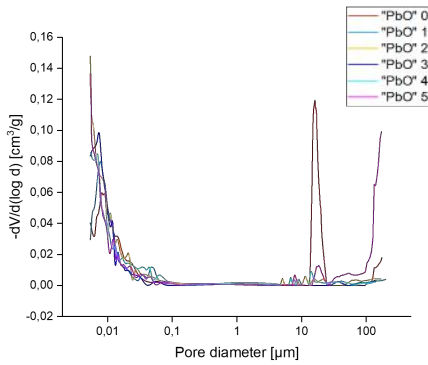


Figure 9.30: MIP of "PbO" 0-5

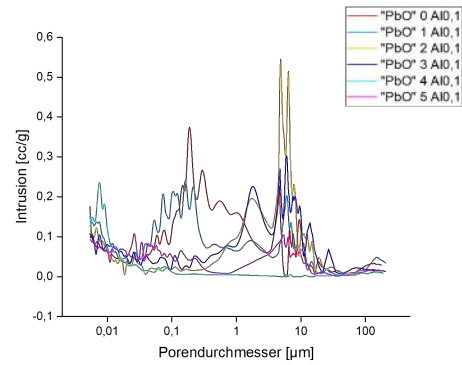


Figure 9.31: MIP of "PbO" 0-5 foamed with 0,1 % Al

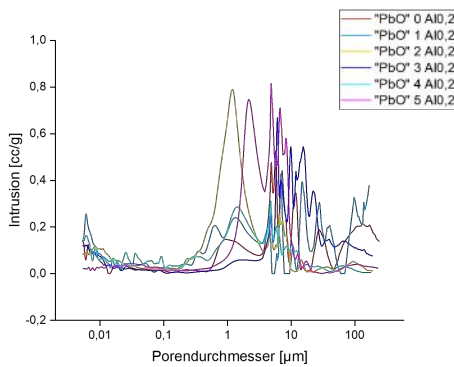


Figure 9.32: MIP of "PbO" 0-5 foamed with 0,2 % Al

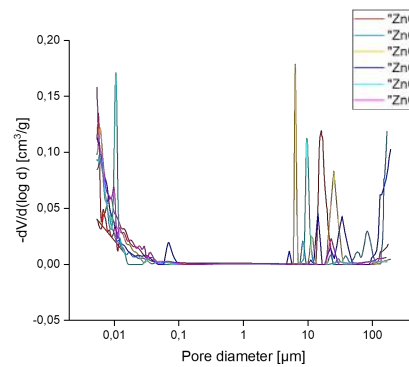


Figure 9.33: MIP of "ZnO" 0-5

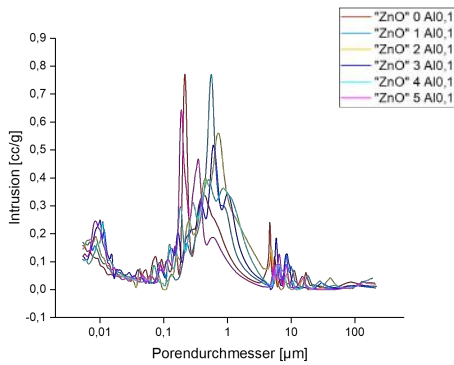


Figure 9.34: MIP of "ZnO" 0-5 foamed with 0,1 % Al

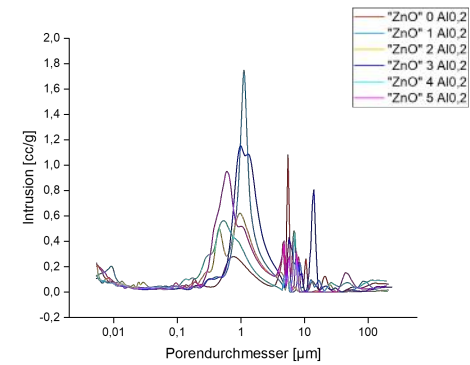


Figure 9.35: MIP of "ZnO" 0-5 foamed with 0,2 % Al

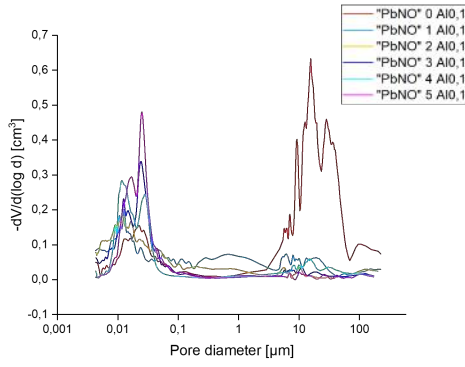


Figure 9.36: MIP of "PbNO" 0-5 foamed with 0,1 % Al

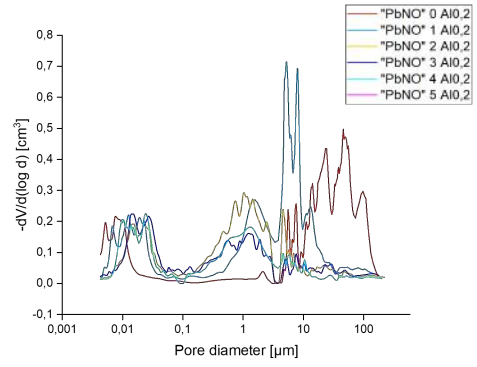


Figure 9.37: MIP of "PbNO" 0-5 foamed with 0,2 % Al

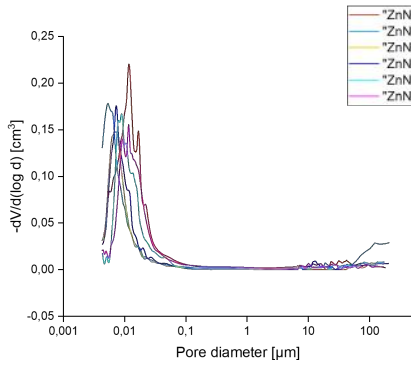


Figure 9.38: MIP of "ZnNO" 0-5

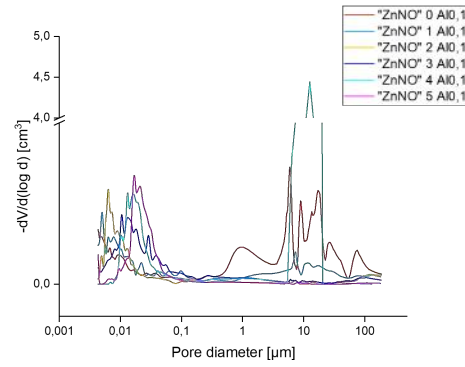


Figure 9.39: MIP of "ZnNO" 0-5 foamed with 0,1 % Al

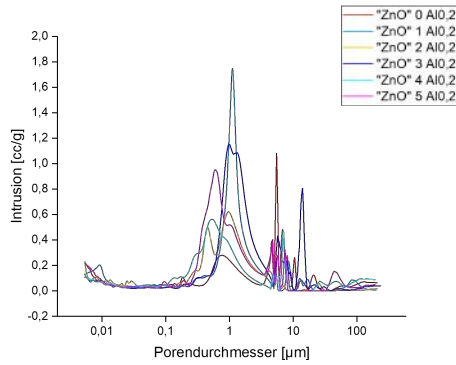


Figure 9.40: MIP of "ZnNO" 0-5 foamed with 0,2 % Al

Added percentage	ZnO	PbO	Zn(NO ₃) ₂	Pb(NO ₃) ₂
0	6,21	16,3	26,2	28,7
1	23,1	7,75	15,8	14,8
2	26,8	14,2	13,3	11,6
3	24,7	32,2	18,5	14,3
4	14,8	12,5	13,8	13,5
5	16,1	38,6	22,2	13,6

Table 9.1: Compressive strength values [N/mm²] of samples "ZnO", "PbO", "ZnNO" and "PbNO" 0–5

9.2.4 Compressive strength

9.3 Chapter 7: Variation of the Si/Al ratio and addition of Pb²⁺ and Zn²⁺

9.3.1 IR spectroscopy

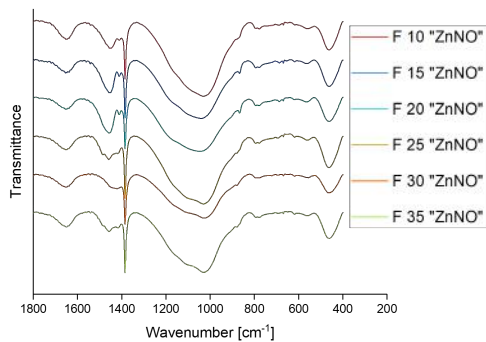


Figure 9.41: IR spectra of F10–F35 "ZnNO"

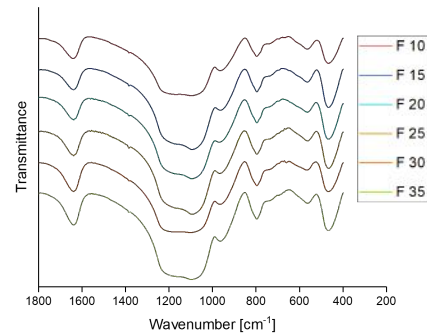


Figure 9.42: IR spectra of F10–F35 leached in HCl

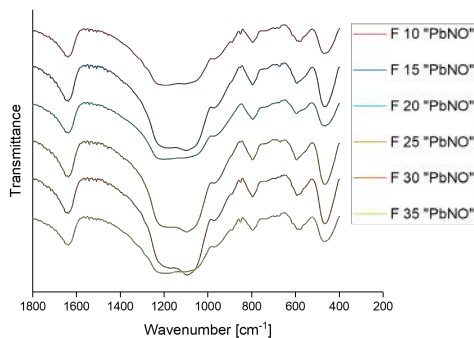


Figure 9.43: IR spectra of F10–F35 "PbNO" leached in H₂SO₄

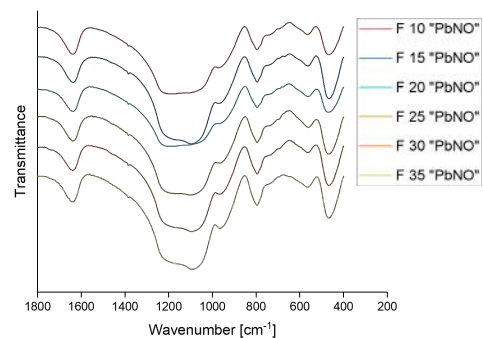


Figure 9.44: IR spectra of F10–F35 "PbNO" leached in HCl

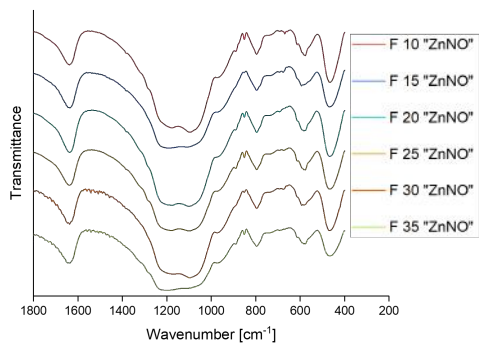


Figure 9.45: IR spectra of F10–F35 "ZnNO" leached in H_2SO_4

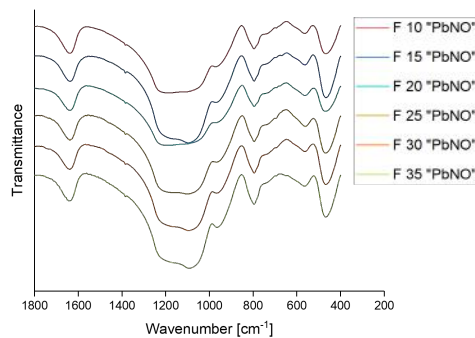


Figure 9.46: IR spectra of F10–F35 "ZnNO" leached in HCl

9.3.2 XRD

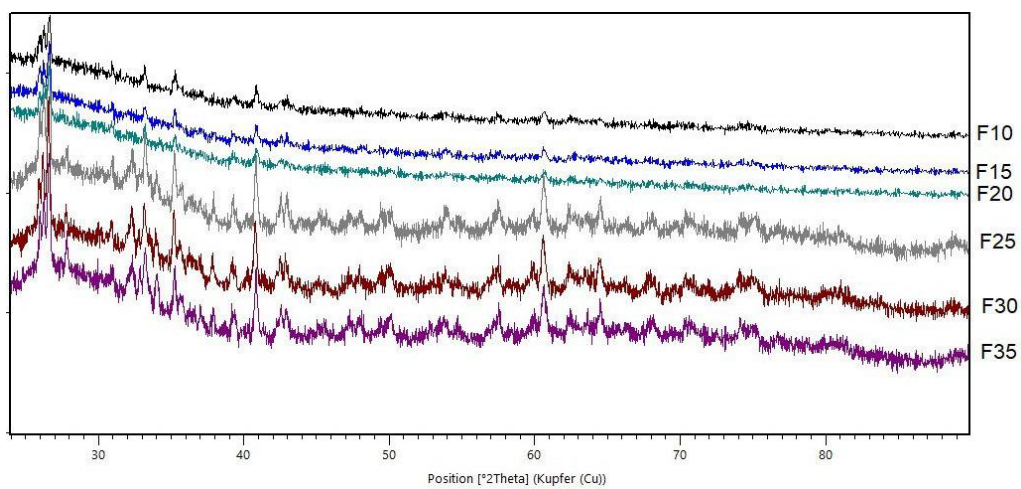


Figure 9.47: XRD of F10–F35

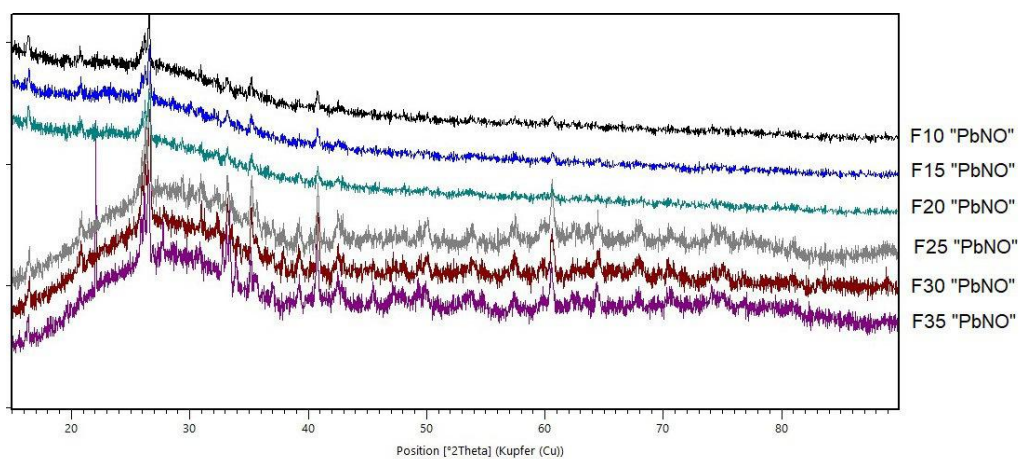


Figure 9.48: XRD of F10–F35 "PbNO"

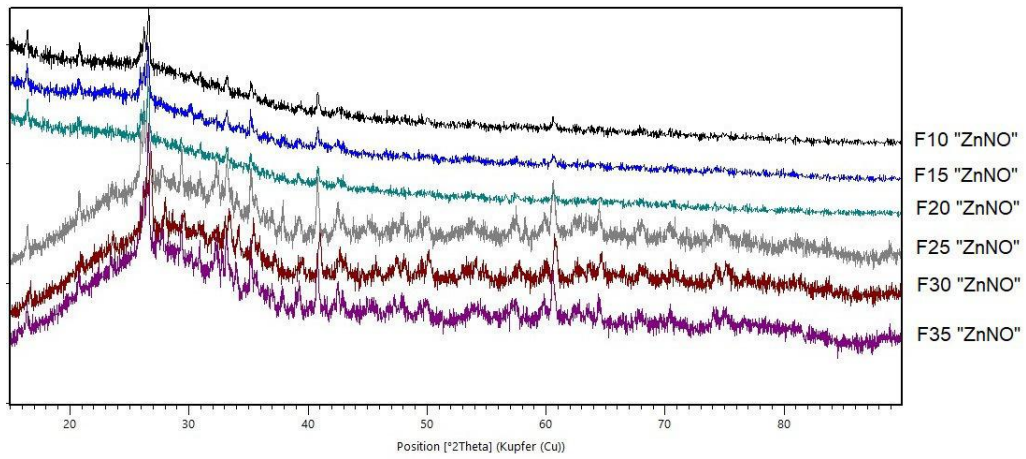


Figure 9.49: XRD of F10–F35 "ZnNO"

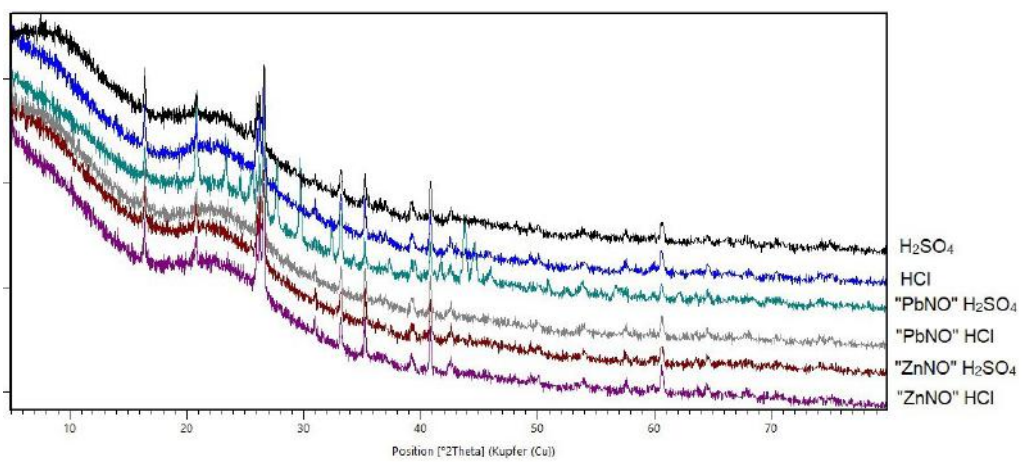


Figure 9.50: XRD of F10 leached in HCl and H₂SO₄

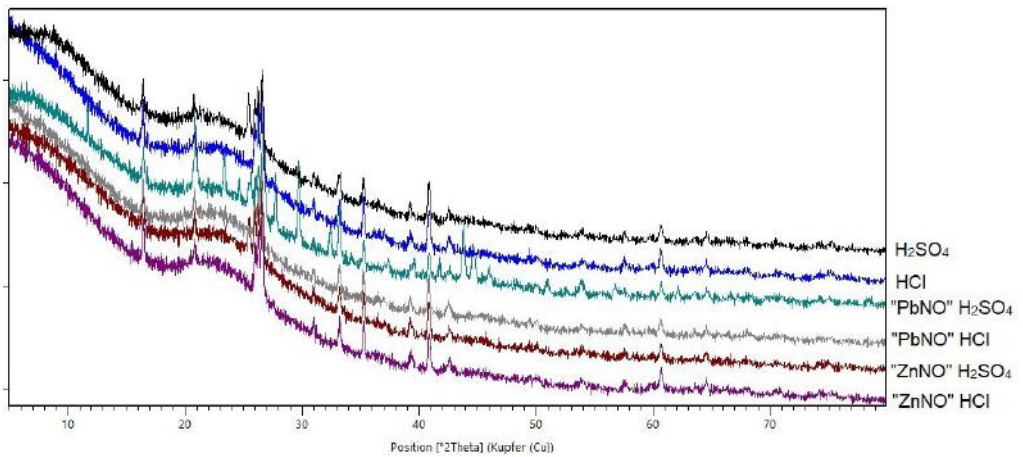
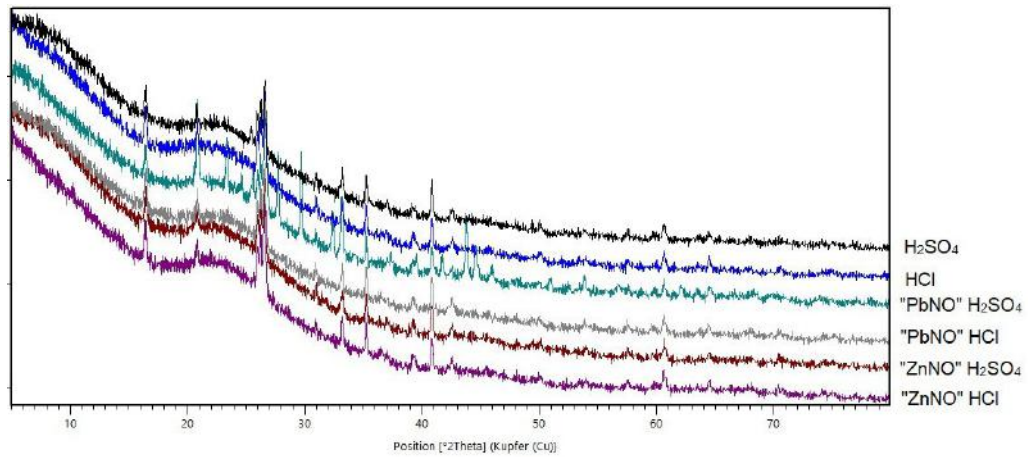
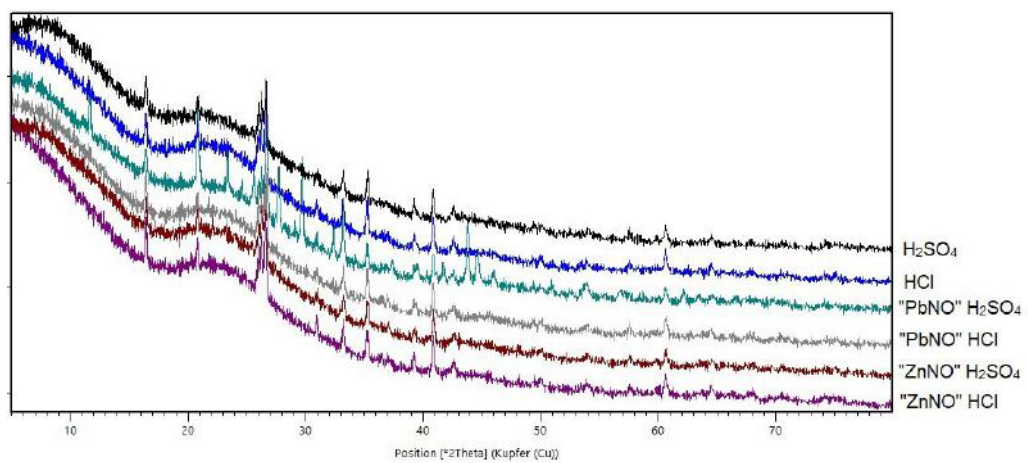
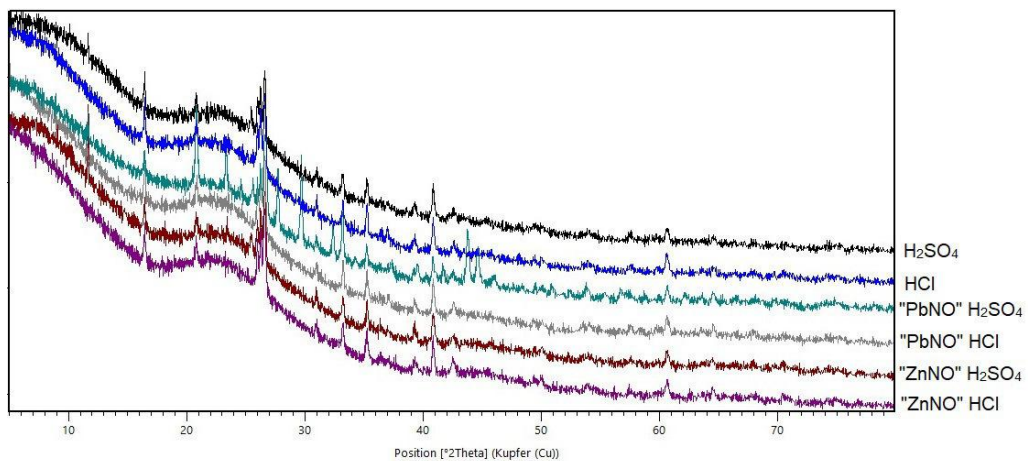


Figure 9.51: XRD of F15 leached in HCl and H₂SO₄

Figure 9.52: XRD of F20 leached in HCl and H₂SO₄Figure 9.53: XRD of F25 leached in HCl and H₂SO₄Figure 9.54: XRD of F30 leached in HCl and H₂SO₄

Declaration

I hereby declare that I have written this thesis on my own without any help, using only the quoted references and due acknowledgments have been made in the text to all other materials used.

Eva Kränzlein

Curriculum Vitae

Personal

Name:	Eva Kränzlein
Date of birth:	16.07.1989
Birthplace:	Nürnberg
Family Status:	Single

Work experience

06/2014 – 07/2017	Research Assistant	Nuremberg Tech, Nuremberg
-------------------	--------------------	------------------------------

Education

03/2015 – today	PhD candidate	MLU Halle–Wittenberg Faculty of Natural Sciences III Geology and Mineralogy
03/2016 – 09/2016	Economics, Business Manager	Nuremberg Tech Ohm Professional School
10/2011 – 03/2014	Chemistry, M.Sc.	FAU Erlangen Nuremberg
10/2008 – 09/2011	Chemistry, B.Sc.	FAU Erlangen Nuremberg
1999 – 2008	Abitur	Hans-Sachs Gymnasium Nuremberg
1995 – 1999	Elementary School	Hegelschule, Nuremberg

Nuremberg, February 21, 2018, Eva Kränzlein